QUANTUM STATE PREPARATION USING CHIRPED LASER PULSES IN SEMICONDUCTOR QUANTUM DOTS

by

Ajan Ramachandran

Submitted in partial fulfillment of the requirements
for the degree of Doctor of Philosophy

at

Dalhousie University
Halifax, Nova Scotia
May 2020

Table of Contents

List of Tables

List of Figures

Abstract

A quantum emitter (QE) is a physical system that can be used to encode a quantum state via some internal degree of freedom (e.g. exciton, electron spin, valley) and is coupled to light via a dipolar transition that enables the conversion of that quantum state into the state of a photon and vice versa. Such QEs can be applied to sources of single and entangled photons for applications in quantum cryptography or quantum imaging and a collection of coupled QEs can be used to realize a small quantum simulator or quantum memory node in a distributed quantum network. Among solid state QE systems, semiconductor quantum dots (QD) are particularly attractive due to their high radiative quantum efficiencies, their strong optical coupling, enabling fast and arbitrary qubit rotations, and their tunable emission in the range of standard telecommunication wavelengths. Adiabatic rapid passage (ARP) is a state preparation scheme that enables the excitation and de-excitation of a QE with a high fidelity even in the presence of fluctuations in experimental parameters such as intensity and frequency of the control laser pulse. This excitation scheme may be used for quantum state initialization in quantum information platforms and for triggering quantum light sources.

This thesis work concerns an exploration of the efficacy of ARP for the quantum control of excitons in semiconductor QDs. The experiments carried out in this work show that the impact of phonons may be suppressed for ARP, pointing to the possibility of high-fidelity inversion at elevated temperatures. We also investigate the dependence of the threshold for decoherence suppression on the size and shape of the QD. The experiments performed in this thesis work also quantify the detuning tolerance of ARP. ARP was also used to demonstrate parallel quantum state initialization in two different QDs with different transition energies and dipole moments.

List of Abbreviations and Symbols Used

AlGaAs aluminum gallium arsenide

ARP adiabatic rapid passage

BBO β barium borate

C-NOT controlled-NOT

C-ROT controlled-rotation

CCD charge-coupled device

CWPL continuous wave photoluminescence

FWHM full-width at half maximum

FWM four wave mixing

GaAs gallium arsenide

InAs indium arsenide

InP indium phosphide

LA longitudinal acoustic

LO longitudinal optical

MIIPS multiphoton intrapulse interference phase scan

NV Nitrogen-Vacancy

OBE optical Bloch equation

OPO optical parametric oscillator

PLE photoluminescence excitation

QD quantum dot

QIP Quantum information processing

SHG second-harmonic generation

SK Stranski-Krastanov

SLM spatial light modulator

SPDC spontaneous parametric down-conversion

STED Stimulated Emission Depletion Microscopy

TA transverse acoustic

TL transform limited

TO transverse optical

Acknowledgements

During the last seven years I spend at Dalhousie, I had the opportunity to meet and work with a lot of wonderful people. This thesis work would not have been possible without their help.

First and foremost I would like to thank my supervisor Kimberley Hall for her support, guidance, and teaching me all the physics I know. You have been a mentor to me beyond physics.

Thank you to Dennis Deppe at the University of Central Florida for providing the quantum dot samples.

I am extremely grateful to the members of Hall group: Reuble Mathew, Dan Webber, Sam March, Seth Todd, Drew Riley, Luke Hacquebard, Hong Yi Shi Yang, Allister Mason, Ali Binai-motlagh, Luke Fraser-Leach, Owen Bennet-Gibbs, and Grant Wilbur. This thesis is yours as much as it is mine. Thank you for the wonderful time, all the help in the lab, and troubleshooting my terrible code. To all the friends I made during my time at Dal: Charlotte Clegg, Chris Sutherland, Dave Kalliecharan, Eric Bergmann, Stephen Payne, Tolson Winters, and the Dal Judo club, to list a few. Thank you very much for all the beers, board games, movies, potlucks, and judo. They were instrumental in keeping me sane.

Thank you to the physics office staff: Heather Ann Jennex, Jennifer Currie, Valerie O'Neill, and especially Tanya Timmins for helping with all the administrative work and your overall love and care for graduate students. Thanks to Kevin Borgel, John Noddin, and Jim Chrisholm. No science is possible in the Dunn without your help.

Last but not least, I would like to thank everyone back home for your love and support. There are too many of you to list, but a special mention to my father Ramachandran, I wouldn't have made this far without your encouragement and sage advice.

Chapter 1

Introduction

1.1 Introduction to Quantum Technology

The twentieth century witnessed the world being transformed by the first quantum revolution, where certain aspects of the quantum mechanical nature of energy and matter became applicable to useful technologies. For example, the existence of discrete energy levels and the wave nature of matter for electrons have been used to develop applications ranging from transistors to lasers. The world right now is at the cusp of a second quantum revolution where previously unexplored aspects of quantum mechanics, in particular superposition and entanglement, have the potential to give rise to a new wave of devices with increased capabilities. Quantum information processing (QIP) is the branch of technology that uses quantum mechanical phenomena such as superposition and entanglement to process information.

The most fundamental unit that makes up a QIP system is a qubit. A qubit, analogous to a classical bit, consists of two quantum mechanical states $|0\rangle$ and $|1\rangle$. Unlike a classical bit of information, a qubit can be in a coherent superposition of the two states. Furthermore one qubit can be entangled with other qubits generating strong correlations between them such that measurement of the state of one qubit can influence the state of its entangled partners. In general, the state of a single qubit can be written as $|\Psi\rangle = C_0 |0\rangle + C_1 |1\rangle$, where the coefficients C_0 and C_1 are complex probability amplitudes. The full parameter space of the wavefunction of a qubit can be represented geometrically on a Bloch sphere by writing the state as $|\Psi\rangle = \cos(\theta/2) |0\rangle + \sin(\theta/2)e^{-i\phi} |1\rangle$, where the polar angle θ dictates the relative occupation of states $|0\rangle$ and $|1\rangle$ and the azimuthal angle ϕ represents the relative phase between the two basis states. The Bloch sphere representation of a qubit is shown in Fig 1.1(b).

A system of n qubits can exist in a superposition of 2^n states. This ability to be in multiple states at once allows for parallel processing of information. For example,

certain classes of problems called Bounded Error Quantum Polynomial Time problems can be solved by quantum computers in a time that grows with the complexity of the problem in the form of a polynomial. This is referred to as "polynomial time" where the running time is given by $t(n) = O(n^k)$. Here k is a positive integer and n is a measure of the complexity of the problem. In contrast, an equivalent classical algorithm would scale with "exponential time", $t(n) = O(2^{n^k})$ [1]. Shor's algorithm developed for factoring integers [2] and Grover's algorithm developed for searching through unsorted lists are examples of quantum algorithms [3]. Shor's algorithm may be applied to decoding standard RSA encryption schemes, with massive implications for both economic and national security. Grover's algorithm may aid in the managing and processing of big data. For physicists, one of the most exciting potential applications of a quantum computer is the simulation of complex quantum systems as envisioned by Richard Feynman [4]. Such complex systems could include molecules used for biosensing or solid-state systems used for energy storage, enabling crucial advances in materials science. Experimental demonstrations of quantum algorithms are still in their infancy, however advances are occurring at an ever increasing pace. For example, Shor's algorithm was used to factorize the number 21 on a photonic qubit platform [5].

There are a variety of approaches to manipulating qubits for carrying out calculations. In circuit model quantum computation [6], an algorithm is decomposed into a series of single and two-qubit gates. The algorithms are designed in such a manner that, at the end of the prescribed operations, the measurement of the state of the multi-qubit system would yield the solution to the problem at hand. There are also other approaches to QIP such as adiabatic quantum computing [7], complex instruction set quantum computing [8] and measurement based quantum computing [9]. In adiabatic quantum computing, qubits are prepared in the ground state of a known Hamiltonian and this Hamiltonian is adiabatically varied to a final Hamiltonian whose ground state encodes the solution to the problem. In complex instruction set quantum computing, several single and multi-qubit gates are replaced by a single composite gate, thereby significantly reducing the number of

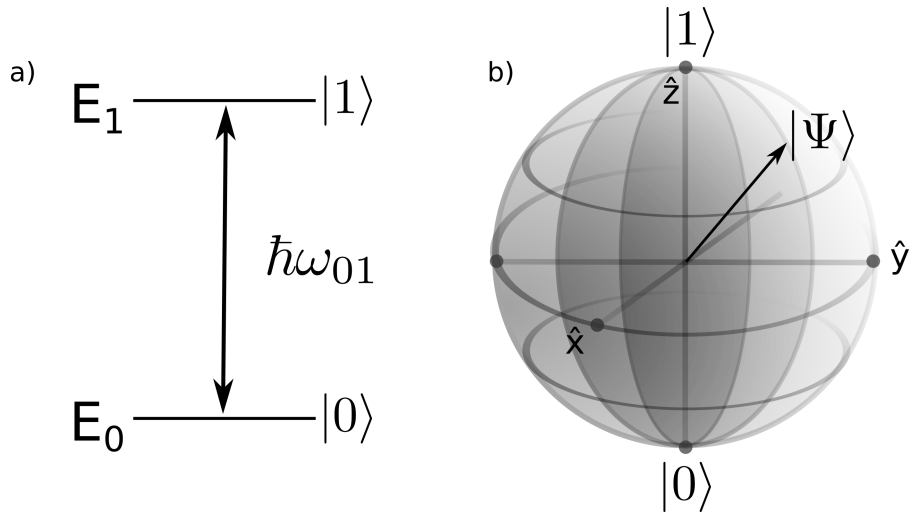

Figure 1.1: (a) Energy level diagram of a qubit represented by states $|0\rangle$ and $|1\rangle$. For this chosen representation, the qubits basis states have energies E_o and E_1, with $E_1 - E_0 = \hbar\omega_{01}$. (b) Bloch sphere representation of a qubit. The state $|\Psi\rangle$ is represented as a unit vector on the surface of the Bloch sphere. The pure states $|0\rangle$ and $|1\rangle$ representing unit occupancy of each of the basis states, are mapped to the south and north pole respectively, while every other point on the Bloch sphere represent a distinct superposition of the states $|0\rangle$ and $|1\rangle$.

steps required to implement an algorithm. This approach was used with femtosecond pulse shaping to implement a multiple input AND gate involving 6 qubits encoded in the rovibrational eigenstates of a Li_2 molecule [10]. In measurement based (or one-way) quantum computation, the system of qubits are prepared in a highly entangled state. Individual qubits are then measured in a certain order and basis as specified by an algorithm.

The requirements for a physical implementation of a QIP system depend on the model of computation. For example, for circuit model quantum computation these requirements were laid out by DiVincenzo [11] and include the following:

1. Any quantum algorithm must be decomposable into a universal set of quantum gates.

2. The physical system must have well characterized qubits and be scalable to a large number of qubits.

3. It must be possible to initialize the state of the qubits.

4. The coherence time of the qubits must be substantially longer than the time for a single operation (*i.e* the gate time).

5. The state of each qubit must be measurable.

The requirements for other models of quantum computation are not as clearly established, but the ability to initialize and measure qubits, along with the need for precise control of the physical system of qubits would be essential for any implementation of QIP.

A number of candidate platforms for QIP are under active development [12], each with their own strengths and weaknesses. A future quantum computer will very likely be a hybrid, combining the strengths of multiple candidate platforms. Competing qubit candidates can be broadly classified into four categories: (i) atomic and molecular systems, (ii) superconducting systems, (iii) solid-state systems and (iv) photonic systems. Atomic and molecular systems have the advantage of an early start and hence are one of the most advanced [13]. In these systems, neutral atoms or ions are laser-cooled and held in a trap formed using counter propagating laser beams along with a combination of electric and magnetic fields. Qubits are defined by two stable electronic levels within each atom and are manipulated optically to implement quantum gates [14]. Qubit-qubit interactions can be implemented using Rydberg or Coloumb interactions between atoms by bringing them closer together [12]. Superconducting qubits are loops of superconductors with Josephson junctions in between. The qubit can be encoded in the charge, flux or phase of the Cooper pairs across the junction. These qubits are manipulated using magnetic biases [15]. Coupling between qubits may be achieved in a variety of ways. The simplest mechanism involving flux qubits is to couple adjacent qubits through mutual inductance. More complex methods also exist, including those involving d.c. squids, transformers, LC oscillators etc [16]. A variety of solid-state platforms have been proposed, including Nitrogen-Vacancy (NV) centers in diamonds, dopants in silicon and semiconductor quantum dots (QD). An NV center is a substitutional nitrogen atom adjacent to a vacancy defect in a diamond crystal. A qubit can be encoded in the spin states of the electrons bound to this defect. The qubit state can be manipulated with microwave fields [17]. In silicon dopant based systems, a qubit can be encoded in the nuclear spin of the donor atom or the electron spin of

its outermost bound electron. These spin states can be manipulated using pulsed ac magnetic fields and read out through a single-electron transistor [18]. Two-qubit gates between solid-state qubits may be implemented by coupling the qubits using optical links [12, 19]. For example, one of the proposals for two-qubit operations in QD systems in which the qubit is defined using the spin state of a single electron in the conduction band of a QD makes use of an optical cavity mode that both QDs are coupled to [20]. In this method, fully controllable spin-spin interactions between distant QD spins can be achieved via Raman coupling using the common cavity mode. Photonic qubit systems use single photons as qubits. These photons must be emitted by a deterministic source. Qubits can be encoded in the photon's polarization state or time bin. The path degrees of freedom of the photon may also be used for encoding. Photonic qubits can be manipulated by optical elements like waveplates [21]. Two-qubit gates may be implemented using non-linear optical elements. An example of a two-qubit operation is a controlled-NOT (C-NOT) gate in which the state of a target qubit is flipped if and only if the control qubit is in state 1. One of the proposals for implementing a C-NOT gate in photonic systems uses a non-linear optical interaction between the photon encoding the control qubit and the photon encoding the target qubit to induce a π phase shift to the target qubit. The target qubit is subject to a Hadamard gate operation both before and after its interaction with the control qubit. If the control qubit is absent, the second Hadamard gate reverses the operation of the first Hadamard gate leaving the target unchanged. If the control qubit is present, a π phase shift is applied to the target qubit and it undergoes a bit-flip at the second Hadamard gate [21].

The above discussion was focused on quantum computing but quantum technology applications are expected to encompass a variety of other areas, including quantum imaging [22, 23, 24], sensing [25, 26, 27, 28] and quantum networks [19, 29, 30]. For instance, Fig 1.2 shows a proposal for quantum network from Ref [19]. Each node in such a network has a quantum memory with several qubits with capabilities for fast and efficient single and two-qubit operations. If at least one qubit in each node is coupled to qubits in other nodes through an optical channel, multiple nodes can be entangled with high fidelity through heralded optical measurements. Each node then acts as a small quantum simulator that can be used for

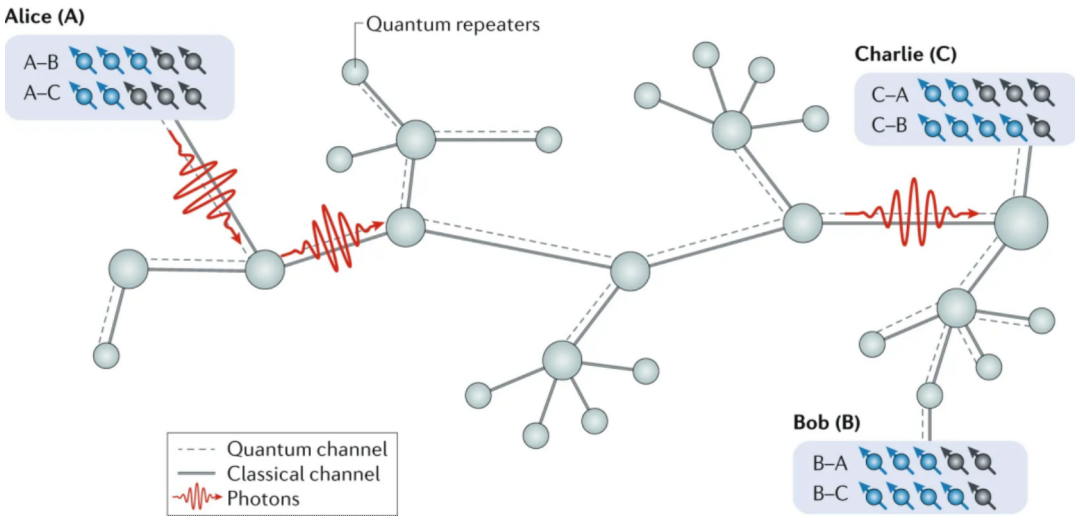

Figure 1.2: A quantum network comprises of several nodes with each node containing a collection of qubits. These nodes may be entangled with each other using an optical channel. The qubits of a node can act as a small quantum simulator, while other qubits operate as a quantum repeater distributing entanglement between nodes. Figure adapted with permission from Ref [19].

applications such as quantum-state teleportation or distributed quantum computing. Defects in diamond such as NV centers, artificial atoms in 2D materials like transition metal dichalcogenides, and semiconductor QDs are potential platforms for this type of network architecture. In quantum imaging, most proposals make use of correlations between entangled photons for applications such as high resolution imaging, noiseless amplification of images and efficient imaging in extreme spectral windows [31, 32]. Implementations of quantum sensing include magnetic field sensors based on the Zeeman effect on atomic vapors with a resolution on the order of femto Teslas [33]. Single NV centers have also been used as sensitive magnetometers [34], pressure sensors [35] and nano-scale thermometers [36]. A recent experiment demonstrated two-photon interference between a single photon emitted by a QD and sunlight [37]. Such experiments probing the second-order coherence of photons from astronomical sources could reveal information about the photon sources such as changes in the solar magnetic field patterns.

The research done in this thesis aims to advance semiconductor QD based platforms which could act as a host for confined charge or spin qubits, while also being

a robust single photon source for a photonic QIP system. Experiments that constitute this thesis work helped in developing robust methods for initializing qubits in QD systems.

1.2 Semiconductor Quantum Dots as Quantum Emitters and Qubits

1.2.1 Electronic Structure

Semiconductor crystals have a regular arrangement of atoms creating a periodic potential for the electrons. This periodic potential results in bands of allowed energies. At 0 K, the fully occupied bands are called valance bands and the unoccupied bands are called conduction bands. The energy difference between the highest occupied valance band and the lowest conduction band is called the band gap (E_g) of the crystal. The absorption of a photon with an energy higher than E_g will excite an electron to the conduction band, leaving an absence of an electron - called a hole - in the valence band. The band gap energy E_g is determined by the constituent elements that form the semiconductor and the crystal structure. For example the QDs used in this work are made of indium arsenide (InAs) and gallium arsenide (GaAs). InAs has a band gap of 0.35 eV while GaAs has a band gap of 1.42 eV at 300 K.

A semiconductor QD is formed by a local confining potential superimposed onto the periodic crystal potential of the semiconductor. For a QD, this confining potential exists in all three crystallographic dimensions. The result is a physical realization of the quantum mechanical problem of a "particle in a box". This confining potential is called a QD provided that it extends over a length scale that is comparable to the de Broglie wavelength of the electron.

There are several ways to realize a spatially varying potential in a semiconductor to create a QD. For example, one can make use of the change in potential that occurs at the interface between dissimilar semiconductors. For conduction band electrons the potential is higher in AlGaAs than in GaAs. This conduction band potential is also higher in GaAs than in InAs. When a layered structure is created, the presence of a potential step on either side results in the confinement of electrons in that layer. Monolayer flat layers of dissimilar semiconductors may be grown using molecular

beam epitaxy. The case of confinement in two-dimensions in a layered structure is called a quantum well. If the potential step up in the conduction band, as one passes the interface is accompanied by a corresponding step down in the valence band, then holes will also be confined in the quantum well layer (e.g. in the GaAs region for an AlGaAs-GaAs heterostructure). In such a quantum well, both electrons and holes are free to move in two dimensions but are confined in the third dimension by the barrier regions on either side of the quantum well layer.

It is possible to introduce quantum confinement in three dimensions, resulting in a QD, by applying an electric field using patterned electrical gates on the surface of a semiconductor heterostructure containing a quantum well. These gates create an additional lateral potential that traps the electrons. This type of QD is called a lateral QD. Colloidal QDs are solution processed nanocrystals, where the potential barriers are created by the interface between the semiconductor and the outside environment (air or solution). QDs can also be grown directly using epitaxial growth techniques. There are two types of epitaxially grown QDs: interface-fluctuation QDs and self-assembled QDs. Interface fluctuation QDs are formed by depositing a partial monolayer of one type of semiconductor on a monolayer flat surface of another type of semiconductor. The partial monolayer is then capped with more substrate material. This type of growth creates monolayer high islands and the difference in band gaps between the two constituent semiconductors results in a potential well that confines electrons and holes. Typically interface-fluctuation QDs are formed using GaAs and AlGaAs.

The QDs used in this work are self-assembled QDs. This type of QD is deposited using the Stranski-Krastanov (SK) growth mode. The SK process exploits strain induced by the difference in the lattice constants of dissimilar semiconductors. In the SK growth mode, one semiconductor material is deposited onto a monolayer flat surface of a different semiconductor. Once a critical layer thickness is reached, strain causes the spontaneous reorganization of the strained layer into islands. The QDs used in this work are made by depositing InAs onto a GaAs layer. Self-assembled QDs are also commonly made from InAs on alloys of InP. Once they are deposited, the InAs QDs are covered by more of the substrate material. The InAs QDs typically have a lateral dimension of about 10-30 nm and a height of 1-10 nm.

The difference in bandgap results in three dimensionally confined electronic states for electrons and holes inside the InAs QD where GaAs represents a potential barrier. As the capping layer is deposited some indium atoms are incorporated into the barrier with an amount that decreases as more monolayers are deposited. This is called the wetting layer. Since the bandgap of this 2D layer of mixed composition is lower than the barrier layer, it represents a quantum well inside of which the QDs are embedded. For the case of InAs/GaAs QDs, a schematic representation of the structure of a QD is shown in cross section in Fig 1.3(a). A scanning tunneling microscopy image of a real InAs QD is shown in Fig 1.3(b). The electronic energy structure of a QD is shown in Fig 1.3(c). The difference in band gap between InAs and GaAs results in a 3D potential well that has a depth of 100-300 meV for electrons and 30-100 meV for holes [38].

The three dimensional confinement in the QD leads to discrete atom-like energy levels and for that reason QDs are called artificial atoms. Following the atomic physics convention, the confined energy levels in a QD are labelled s, p, d and so on. The ground state optical transition corresponds to the promotion of an electron from the s-level in the valence band to the s-level in the conduction band. This ground state transition is often called the s-shell transition. The first excited state optical transition occurs between the p-valence levels and the p-conduction levels and is called the p-shell transition.

1.2.2 Optical Properties of Self Assembled QDs

An electron in a QD can be promoted from a valence level to a conduction level by the absorption of a photon, leaving a hole in the valence level. These carriers are attracted to each other via the Coulomb interaction and the bound electron-hole pair is called an exciton. The two-level system formed by the presence ($|1\rangle$) and absence ($|0\rangle$) of an exciton can be used to define a qubit. The radiative recombination of the exciton results in the emission of a photon. Hence when the exciton is excited by a laser pulse, it can act as a triggered single photon source.

The composite electron and hole making up the exciton each have a spin orientation. The conduction band in III-V semiconductors has s-symmetry with a total angular momentum of $j = 1/2$ with two spin projections $m_j = \pm 1/2$. Due to the

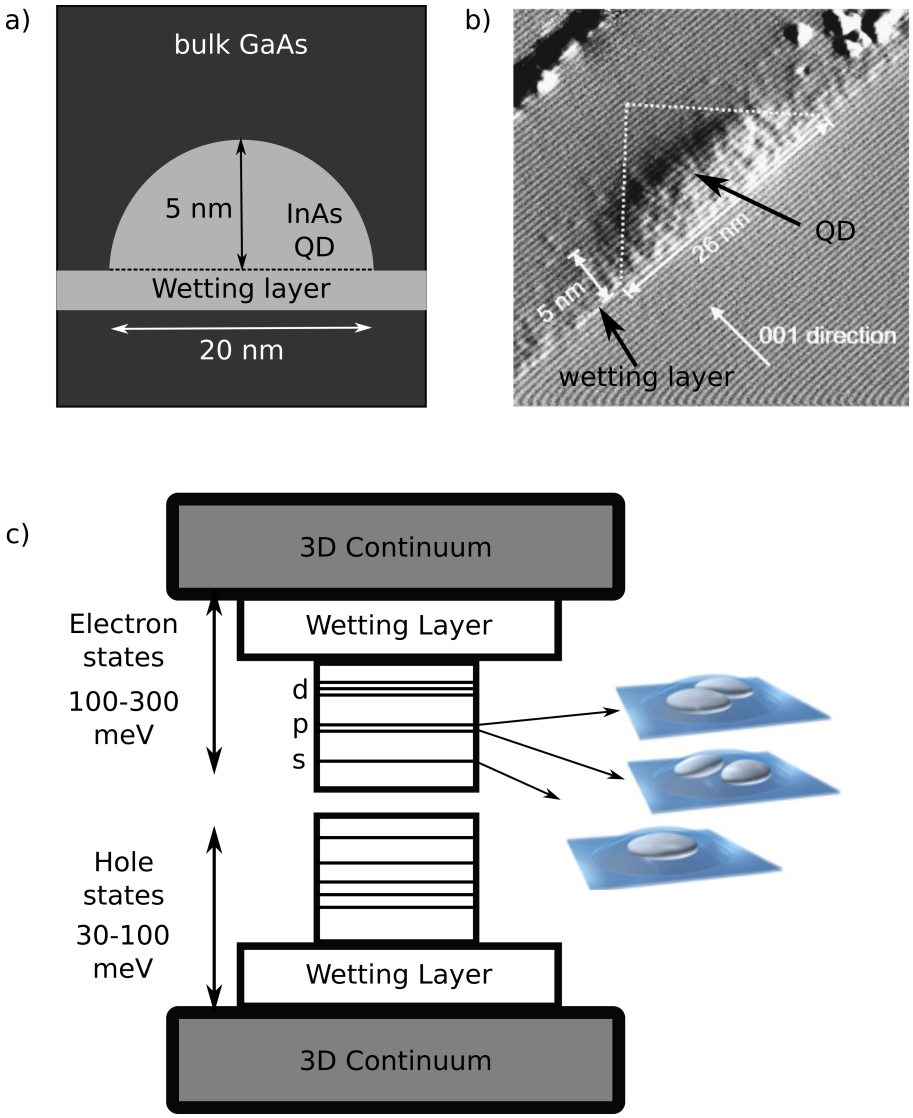

Figure 1.3: (a) Schematic of an InAs QD embedded in a GaAs matrix. Typical dimensions in the growth and lateral dimensions are shown. The wetting layer is a two-dimensional layer with a graded composition of InGaAs. (b) X-STM current image of a cleaved InAs QD showing the wetting layer. Figure adapted with permission from [39]. (c) Schematic band structure of an InAs QD. The discrete energy levels arise from the three-dimensional confinement of carriers. The wetting layer is characterized by a continuum of states that are delocalized in the in-plane directions. The 3D continuum refers to the bulk GaAs matrix surrounding the QD.

combined influences of strain and quantum confinement, the uppermost valence level is derived from the heavy-hole valence band in the corresponding bulk semiconductor. This valence level has p-type symmetry with $j = 3/2$ and $m_j = \pm 3/2$. The composite exciton then has $j = 2$ with possible spin projections of $m_j = \pm 1, \pm 2$.

Exciton states with $m_j = \pm 2$ are not optically active and are called the dark excitons because they cannot be excited by photons, which carry only one unit of angular momentum. Excitons states with $m_j = \pm 1$ may be excited optically and are called bright excitons.

If the QD is cylindrically symmetric with a round in-plane shape, the optical transitions associated with the $j = \pm 1$ bright excitons obey circularly polarized selection rules, meaning that a left (right) circularly polarized photon will excite an exciton with spin $j = +1\,(-1)$. The optical selection rules for a cylindrically symmetric QD are shown in Fig 1.4(a). These bright excitons are denoted $|\uparrow\Downarrow\rangle$ and $|\downarrow\Uparrow\rangle$ where $\uparrow$ ($\Uparrow$) indicates the spin projection of the electron (hole) within the exciton. Using linearly polarized light, which is composed of equal parts left and right circularly polarized light, it is possible to excite both $j = \pm 1$ excitons. The Coulomb interaction between excitons leads to a bound state called a biexciton. Cascaded circularly-polarized photons with opposite circular polarization can excite a biexciton. The optical transition that excites the single exciton state to the biexciton state is slightly red shifted from the ground state to exciton transition by an amount equal to the biexciton binding energy (Δ).

If the QD does not possess cylindrical symmetry, but is instead elongated, then the optical selection rules in Fig 1.4(a) are modified. The resulting exciton eigenstates are symmetric and antisymmetric combinations of the spin polarized exciton states discussed above. These are represented by $|01\rangle$ and $|10\rangle$, respectively. The orthogonal exciton states now obey linearly polarized selection rules along the long (x) and short (y) axes of the QD. The optical transitions tied to $|01\rangle$ and $|10\rangle$ are no longer degenerate in an elongated QD, but are separated by an exchange splitting (δ) which is typically 30 μeV - 100 μeV [38]. The full energy level diagram describing the optical transitions in an elongated QD is shown in Fig 1.4(b).

When using polarized light (either circularly polarized for symmetric QDs or linearly polarized along x or y for elongated QDs) the cascaded optical transitions in Fig 1.4(a) and 1.4(b) can be neglected and we are left with a simple two-level system representing the absence or presence of the exciton in the QD. This two-level system is shown in Fig 1.4(c). The QDs studied in this thesis work are elongated, so $|0\rangle \equiv |00\rangle$ and $|1\rangle \equiv |10\rangle$ for optical excitation with light polarized along the Π_x

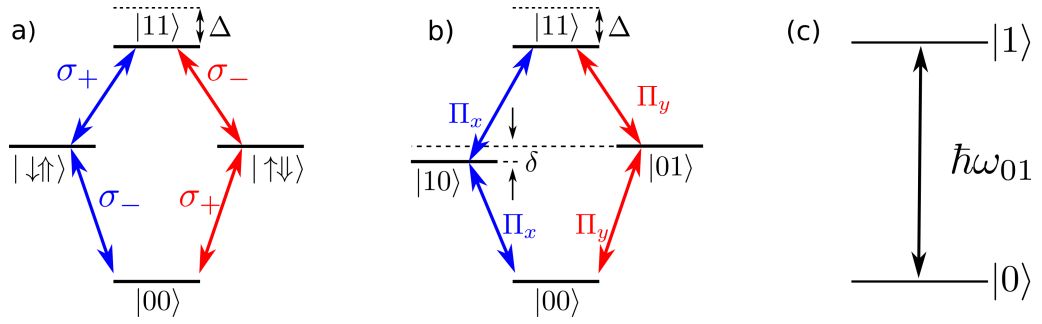

Figure 1.4: Energy level diagrams and optical selection rules for excitons in (a) cylindrically symmetric QDs and (b) elongated QDs. For symmetric QDs, exciton transitions are coupled by circularly polarized light ($\sigma_{\pm}$) and the exciton states $|\uparrow\Downarrow\rangle$ and $|\downarrow\Uparrow\rangle$ are degenerate. For elongated QDs the exciton states are symmetric and antisymmetric superpositions of $|\uparrow\Downarrow\rangle$ and $|\downarrow\Uparrow\rangle$ and are coupled by linearly polarized light ($\Pi_{x/y}$). (c) Simplified energy level diagram of an exciton qubit system.

direction.

The above description is appropriate for neutral QDs. It is possible to charge a QD with a single excess electron or hole prior to optical excitation using back gating or doping. The optical excitation would then correspond to a charged exciton, called a trion. It is possible to realize a qubit using the spin projection of only the single electron or hole and these carrier spin quantum states could be controlled using light via the trion transition. Proposals for QIP with QDs have been made using optical control including both exciton qubits [40, 41, 42], spin qubits [43, 20, 44, 45, 46] and hybrid approaches where exciton qubits are used for computation and spin qubits are used for information storage [47]. In this thesis work, our focus will exclusively be on the optical control of the quantum state of excitons.

1.3 Optical Quantum State Preparation Schemes

1.3.1 A Two-Level System Driven by Light

Optical state preparation schemes in QDs utilize the interaction with a light field to transfer the QD from one quantum state to another, where each state corresponds in the most general case to a superposition of the levels in Fig 1.4(b). The focus of this thesis work is the interaction of a pulsed laser field with the optical transition between the ground state $|00\rangle$ and one of the exciton states ($|01\rangle$ or $|10\rangle$).

As discussed above, assuming the laser pulse is linearly polarized along one of the symmetry axes of the QD, we can simplify the notation and refer to these states as $|0\rangle$ and $|1\rangle$.

Following the approach taken in [48], the Hamiltonian of a two-level atom driven by a classical electromagnetic field with ground state $|0\rangle$ and excited state $|1\rangle$ can be written as

$$H = H_s + H_i + H_{env} + H_{env-c} \tag{1.1}$$

where

$$H_s = \hbar\omega_0 |1\rangle \langle 1| \tag{1.2}$$

is the Hamiltonian describing the two confined levels of the QD representing the absence and presence of the exciton and $\hbar\omega_0$ is the transition energy of the exciton. Here the ground state is taken to have zero energy. In matrix form, Eqn (1.2) can be written as

$$H_s = \hbar \begin{bmatrix} 0 & 0 \\ 0 & \omega_0 \end{bmatrix}. \tag{1.3}$$

H_i is the atom-field interaction Hamiltonian for an electric dipole transition and is given by

$$H_i = -\vec{\mu} \cdot \vec{E}(t) \tag{1.4}$$

where $\vec{\mu} = -e\vec{r}$ is the dipole moment operator and $\vec{E}(t)$ is the time-dependent electric field of the control laser pulse. $\vec{E}(t)$ can be written as

$$\vec{E}(t) = \frac{1}{2}\{\hat{\epsilon} E_0(t) e^{-i(\omega_l t + \phi(t))} + c.c\} \tag{1.5}$$

where $E_0(t)$ is the electric field envelope, ω_l is the center frequency of the laser pulse, $\hat{\epsilon}$ is the polarization vector and $\phi(t)$ is the phase. Here the spatial variation of the electric field strength across the QD is neglected by adopting the electric dipole approximation. Invoking the rotating wave approximation, Eqn (1.4) in matrix form is given by

$$H_i = \hbar \begin{bmatrix} 0 & \frac{\Omega}{2} \\ \frac{\Omega^*}{2} & 0 \end{bmatrix} \tag{1.6}$$

where $\Omega(t) = \frac{\vec{\mu} \cdot \vec{E}(t)}{\hbar}$ is the Rabi frequency, in which $\vec{E}(t) = \hat{\epsilon} E_0(t) e^{-i(\phi(t))}$. Finally the

terms H_{env} and H_{env-c} in Eqn (1.1) account for the environment and its interaction with the system, respectively.

As discussed in section 1.1, the wavefunction for an arbitrary superposition of states $|0\rangle$ and $|1\rangle$ in a two-level system is given by

$$|\psi(t)\rangle = C_0 |0\rangle + C_1 |1\rangle \tag{1.7}$$

where C_0 and C_1 are normalization coefficients such that $|C_0|^2 + |C_1|^2 = 1$. Ignoring the environmental effects for now, the total Hamiltonian contains only the system Hamiltonian and the atom-field interaction Hamiltonian. The latter may be written in the form

$$H_i = \hbar \begin{bmatrix} 0 & \frac{\Omega}{2} \\ \frac{\Omega^*}{2} & -\Delta(t) \end{bmatrix} \tag{1.8}$$

where $\Delta(t)$ is the detuning between the laser pulse and the transition frequency of the exciton. The energy eigenvalues of the total Hamiltonian are given by

$$E_{\pm} = -\frac{\hbar\Delta}{2} \pm \frac{\hbar\tilde{\Omega}}{2} \tag{1.9}$$

where $\tilde{\Omega} = \sqrt{\Omega^2 + \Delta^2}$. The corresponding eigenvectors are

$$\begin{aligned} |\Psi_+\rangle &= \sin(\Theta/2) |0\rangle + \cos(\Theta/2) |1\rangle \\ |\Psi_-\rangle &= \cos(\Theta/2) |0\rangle - \sin(\Theta/2) |1\rangle \end{aligned} \tag{1.10}$$

where

$$\begin{aligned} \cos(\Theta) &= \frac{\Delta(t)}{\tilde{\Omega}} \\ \sin(\Theta) &= \frac{|\Omega(t)|}{\tilde{\Omega}} \end{aligned} \tag{1.11}$$

The states $|\Psi_+\rangle$ and $|\Psi_-\rangle$ in Eqn (1.10) are called the *dressed states* of the system representing the QD in the presence of the light field. These states correspond to a dynamic admixture of the bare exciton states $|0\rangle$ and $|1\rangle$ of the QD. At a given time t, the energy splitting between the dressed states and the admixture of composite bare exciton states constituting each of the dressed states are determined by the instantaneous values of the detuning $\Delta(t)$ and the Rabi frequency $\Omega(t)$ associated

with the transition. The Rabi frequency is determined by the electric field of the pulse and the dipole moment of the optical transition, which is the matrix element of the electric dipole operator between the initial and final states in the transition. The instantaneous dressed states are thus controlled by the properties of the laser pulse.

As an alternative to the dressed states picture presented above, as discussed in Sec 1.1 the evolution of a two-level system under the influence of a laser pulse can also be visualized using a Bloch sphere representation. On a Bloch sphere, the state of a two-level system is represented by a unit vector called the Bloch vector, which lies on the surface of a sphere as shown in Fig 1.1(b). The longitudinal lines on the Bloch sphere represent lines of constant phase between the bare exciton states, while the latitudinal lines represent the lines of constant relative amplitudes for the coefficients C_0 and C_1 (see Eqn (1.7)) of the bare exciton states. The north pole represents state $|1\rangle$ (for which $C_0 = 0$) and the south pole $|0\rangle$ (where $C_1 = 0$). The components of the Bloch vector are given by

$$\begin{aligned} U_x &= 2Re\{C_0 C_1^*\} \\ U_y &= -2Im\{C_0 C_1^*\} \\ U_z &= |C_1|^2 - |C_0|^2 \end{aligned} \tag{1.12}$$

The dynamics of the Bloch vector in the presence of the laser field is described by the vector equation

$$\dot{\vec{U}} = \vec{U} \times \vec{\Lambda} \tag{1.13}$$

where $\vec{\Lambda}$ is an effective torque vector whose magnitude and direction at any instant are determined by the characteristics of the laser field. According to Eqn (1.13), this optical torque vector causes the precession of the Bloch vector $\vec{U}$ around the torque vector $\vec{\Lambda}$. If $\phi(t)$ in Eqn (1.5) is zero, the torque vector is given by $\vec{\Lambda} = (-\Omega, 0, \Delta)$ such that the x-component is determined by the instantaneous value of the Rabi frequency and the z-component is determined by the instantaneous value of the

detuning. Eqn (1.13) can then be expanded to express the components of $\dot{U}$ as

$$\begin{aligned} \dot{U}_x &= -\Delta U_y \\ \dot{U}_y &= -\Delta U_x + \Omega U_z \\ \dot{U}_z &= -\Omega U_y. \end{aligned} \tag{1.14}$$

These coupled differential equations that describe the dynamics of a two-level system driven by a laser pulse are called the optical Bloch equations (OBE).

1.3.2 Pulse Shaping

The light-matter interaction Hamiltonian in Eqn (1.4) can be tailored by optical pulse shaping techniques, enabling the quantum state dynamics caused by the laser pulse to be tailored as well. In particular, both $E_0(t)$ and $\phi(t)$ in Eqn (1.5) may be separately controlled. This generalizes the torque vector in Eqn (1.13) to $\vec{\Lambda} = (-Re[\Omega], -Im[\Omega], \Delta)$. With the ability to control both $E_0(t)$ and $\phi(t)$, one can control both magnitude and direction of the torque vector $\vec{\Lambda(t)}$ at each instant. This provides the most flexible approach to manipulating the Bloch vector $\vec{U}$ and thus the quantum state of the system.

Femtosecond laser pulses are one of the fastest controllable events in a laboratory. As a result there are no electronic or mechanical components fast enough to manipulate the electric field of a laser pulse in the time domain. However the short time duration of an optical pulse corresponds to a wide frequency bandwidth. Hence we can make use of the wide spectral bandwidth of the pulse to shape the pulse in the time domain. This can be achieved using a $4f$ pulse shaper, shown schematically in Fig 1.5. In a typical $4f$ pulse shaper, the input laser pulse is separated into its constituent frequency components using a dispersive element such as a diffraction grating. The dispersed frequency components are then focused onto a spatial light modulator (SLM). An SLM is an optical element that contains two linear arrays of pixels. In each pixel, a voltage is applied that changes the index of refraction of that pixel. The SLM modulates the amplitude and/or phase of each individual frequency component of the laser pulse to impose the desired temporal

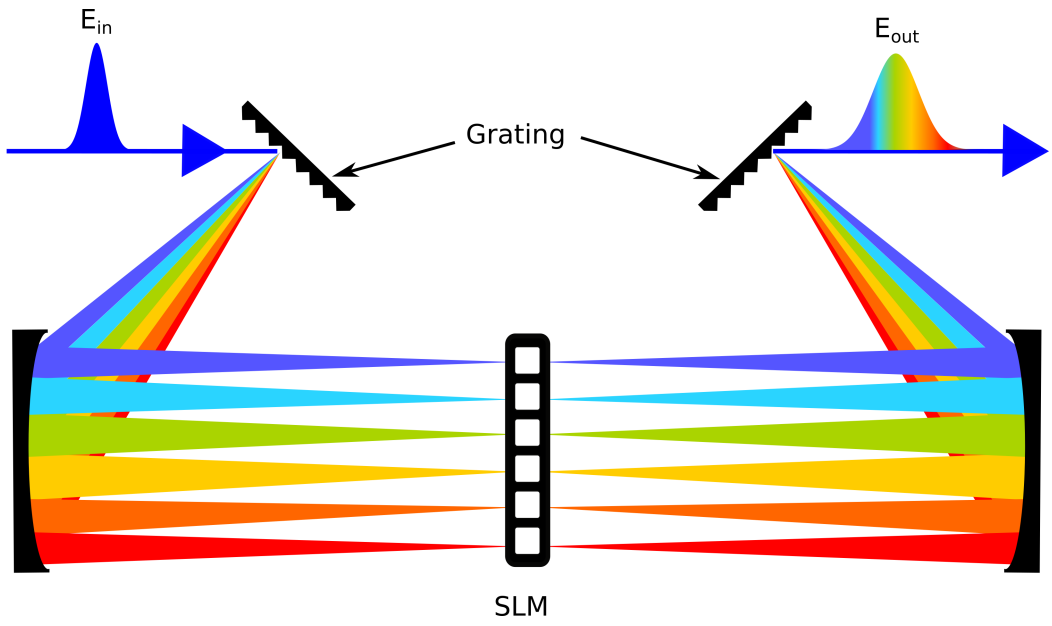

Figure 1.5: (a) Schematic of a $4f$ pulse shaper. Incoming light is spectrally dispersed using a diffraction grating. The dispersed spectral frequencies are then focused onto a dual mask SLM by a curved mirror. After passing through the SLM the modified frequency components are collimated and recombined to form the output pulse by using a curved mirror and a grating. In practice the second set of curved mirror and grating are replaced by plane mirror with a slight vertical tilt.

shape on the laser pulse. The separated frequency components are then recombined after the SLM to generate the output pulse. The action of the SLM on the electric field can be described by a mask function $M(\omega)$. In the frequency domain, the relationship between the input ($\tilde{E}_{in}(\omega)$) and the output ($\tilde{E}_{out}(\omega)$) pulses can be written as

$$\tilde{E}_{out}(\omega) = \tilde{E}_{in}(\omega)M(\omega) \tag{1.15}$$

where

$$M(\omega) = A_M(\omega)\exp(i\Phi_M(\omega)). \tag{1.16}$$

Here $A_M(\omega)$ is the amplitude mask and $\Phi_M(\omega)$ is the phase mask. Hence if the shape of the input pulse is known, an output pulse of arbitrary shape can be generated using an appropriate mask function. A more detailed description of the SLM used in this work is given in chapter 3.

In addition to arbitrarily shaping the laser pulse, a $4f$ pulse shaper can be used to compensate for unintended phase distortions suffered by the laser pulse as it

traverses through various optical elements in a setup. Consider a laser pulse with a Gaussian amplitude envelope given by

$$E(t) = E_0 e^{-at^2} e^{-i(\omega_l t - bt^2)}. \tag{1.17}$$

where a and b are the real and imaginary parts of the Gaussian pulse parameter Γ ($\Gamma = a - ib$). Here a determines the pulse duration

$$\tau = \sqrt{\frac{2ln2}{a}} \tag{1.18}$$

where τ is the full-width at half maximum (FWHM) of the pulse and b determines the instantaneous phase of the pulse through the relation $\phi(t) = -\omega_l t + bt^2$. If $b \neq 0$, the laser pulse is said to be chirped. The Fourier transform of Eqn (1.17) yields the pulse spectral amplitude

$$\tilde{E}(\omega) = \tilde{E}_0 e^{-1/4\left(\frac{a+ib}{a^2+b^2}\right)(\omega-\omega_l)}. \tag{1.19}$$

The frequency bandwidth of the pulse is given by $\Delta\omega = \sqrt{a8ln2(1+(b/a))^2}$. As a consequence of the Fourier transform relationship between Eqn (1.17) and Eqn (1.19), the pulse duration τ and the frequency bandwidth Δf, are connected through the relation

$$\Delta f \tau = (\Delta\omega/2\pi)\tau \geqslant 0.44 \tag{1.20}$$

and the product $\Delta f \tau$ is known as the time-bandwidth product. The time-bandwidth product is determined by both a (*i.e.* the duration) and b, the chirp. For the laser pulse in Eqn (1.17), the time-bandwidth product is $(2\ln 2/\pi)\sqrt{1+(b/a)^2}$. Hence for a given frequency bandwidth, the pulse duration is the shortest when the value of $\Delta f \tau$ is a minimum. This happens when the value of b in Eqn (1.17) is zero. Such a laser pulse is said to be transform limited (TL).

The dispersion suffered by the pulse as it traverses through various optical elements of the experimental setup leads to a non-zero value for the chirp parameter b. In order to compensate for dispersion, the pulse shaper applies a chirp of equal magnitude but opposite in sign to the input laser pulse.

1.3.3 Rabi Oscillations

Consider a two-level quantum system interacting with a resonant TL laser pulse, *i.e.* a pulse with $\phi(t)$ equal to a constant, such that $b = 0$. By resonant, we refer to a pulse with the detuning $\Delta = 0$ at all times. According to Eqn (1.11) for this type of control pulse, $\cos(\Theta) = 0$ and $\sin(\Theta) = 1$ which implies that $\Theta/2 = \pi/4$. In this case Eqn (1.10) becomes:

$$|\Psi_{\pm}\rangle = \frac{1}{\sqrt{2}}(|0\rangle \pm |1\rangle). \tag{1.21}$$

The dressed states are even and odd superpositions of the bare exciton states. We can also write:

$$\begin{aligned} |0\rangle &= \frac{1}{\sqrt{2}}(|\Psi_{+}\rangle + |\Psi_{-}\rangle) \\ |1\rangle &= \frac{1}{\sqrt{2}}(|\Psi_{+}\rangle - |\Psi_{-}\rangle). \end{aligned} \tag{1.22}$$

As time progress, the components $|0\rangle$ and $|1\rangle$ in the dressed states develop a relative phase that oscillates at a rate determined by the Rabi frequency Ω. This manifests as oscillations of population between the bare exciton states called Rabi oscillations. It may be shown that the final population of the excited state $|1\rangle$ at the end of the laser pulse is given by

$$P_1(\theta) = \frac{\Omega^2}{\tilde{\Omega}^2}\sin^2(\theta/2). \tag{1.23}$$

In general

$$\tilde{\Omega} = \sqrt{\Omega^2 + \Delta^2} \tag{1.24}$$

where in this case $\Delta = 0$ and

$$\theta = \int_{-\infty}^{\infty} \tilde{\Omega}(t)dt. \tag{1.25}$$

θ is called the pulse area because it is proportional to the area under the laser pulse $E(t)$. The population of an initially unexcited system can be transferred to the excited state using a laser pulse of pulse area π, while a $\pi/2$ pulse results in an equal superposition of states $|0\rangle$ and $|1\rangle$.

Now for a detuned TL control pulse, $|\Delta| > 0$. A non-zero (but constant) value of $\Delta = \Delta_0$ implies that the dressed states are no longer equal superpositions of the bare exciton states. The resulting population oscillation between states $|0\rangle$ and $|1\rangle$

does not result in a complete transfer of population. These oscillations versus pulse area now occur at a larger frequency $\tilde{\Omega}$, instead of Ω. Fig 1.6 shows the energy $E_{\pm}$ of the dressed states for the case of Rabi oscillations driven by a resonant control pulse and a control pulse detuned by an amount Δ_0.

In the Bloch sphere representation, for a resonant, transform-limited pulse (with $\phi(t) = 0$ and $\Delta = 0$), the optical torque vector $\vec{\Lambda}$ points along the $\hat{x}$ direction. According to Eqn (1.13), the Bloch vector U precesses around $\vec{\Lambda}$ in the $\hat{y} - \hat{z}$ plane. The angle swept by the Bloch vector is the pulse area, as illustrated in Fig 1.6(d). If $\Delta = \Delta_0$, *i.e.* if the pulse is TL but detuned, then the torque vector has a non-zero z component. In this case, if the system is initially in $|0\rangle$, precession occurs about a torque vector that is tilted downward from the $x - y$ plane. In the presence of this torque vector $\vec{U}$, never reaches the top of the Bloch sphere.

Using Rabi oscillations for state preparation requires precise knowledge of the transition dipole moment and the pulse needs to be exactly resonant with the transition. Otherwise, the state $|1\rangle$ is not accessible. For this reason optical control using transform-limited pulses is sensitive to fluctuations of the control laser pulse (both frequency and amplitude) as well as to uncertainties in the characteristics of the QD (dipole moment and transition energy).

1.3.4 Adiabtic Rapid Passage

Adiabatic rapid passage represents a robust method for exciting the quantum system from $|0\rangle$ to $|1\rangle$ or vice versa, corresponding to inversion of the two-level system [49]. In this control process, the frequency of the light field is swept through the resonance associated with the two-level system. This is achieved using a linearly chirped laser pulse whose electric field is given by

$$E(t) = \frac{1}{2}\{\hat{\epsilon}E_0(t)e^{-i(\omega t+\alpha t^2)} + c.c\} \tag{1.26}$$

where α is called the temporal chirp. For such a pulse, the instantaneous frequency $\omega_{inst} = \omega + 2\alpha t$ is time-dependent and the detuning Δ is a function of time, given by:

$$\Delta(t) = -2\alpha t \tag{1.27}$$

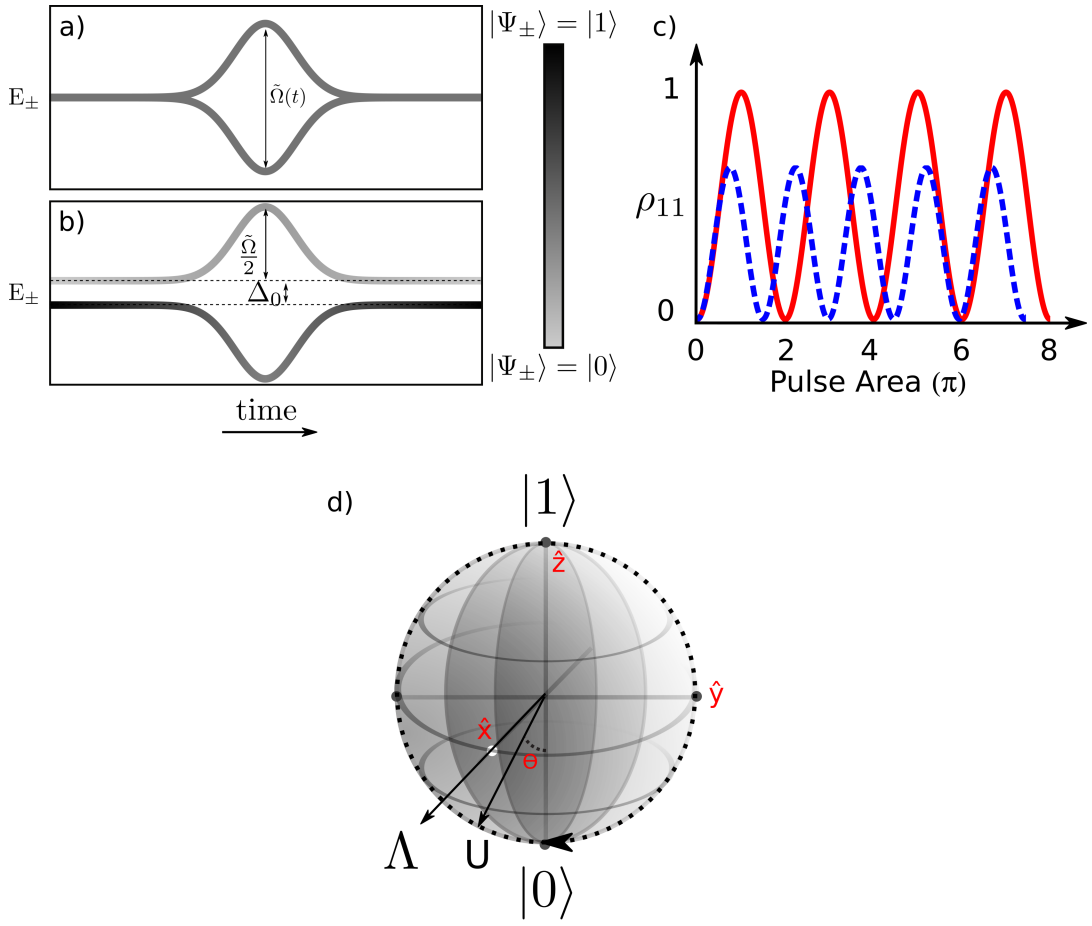

Figure 1.6: Energies $E_\pm$ of dressed states $|\Psi_\pm\rangle$ for a two-level system interacting with a) a resonant TL pulse and b) a TL pulse detuned by an amount $-\Delta_0$. Dressed states $|\Psi_\pm\rangle$ are equal superpositions of the bare exciton states $|0\rangle$ and $|1\rangle$ when $\Delta = 0$. This results in an oscillation of population between states $|0\rangle$ and $|1\rangle$ (red solid curve in (d)). When $\Delta \neq 0$ states $|\Psi_\pm\rangle$ are no longer equal superpositions of $|0\rangle$ and $|1\rangle$ and hence the resulting population oscillations do not lead to complete population transfer. (d) Dynamics of $\vec{U}$ and $\vec{\Lambda}$ on a Bloch sphere for resonant Rabi rotations: The Bloch vector rotates around the $\vec{\Lambda}$ vector in the $\hat{y} - \hat{z}$ plane sweeping an angle determined by the pulse area θ, of the control pulse.

Experimentally it is possible to realize both positively ($\alpha > 0$) and negatively ($\alpha < 0$) chirped pulses. The key feature of ARP is that the parameters governing the optical field change slowly enough that the system remains in one or the other of the two dressed states (Eqn (1.10)) throughout the control process, and the quantum state of the system evolves because the dynamic admixture of the two basis states $|0\rangle$ and $|1\rangle$ evolves due to the time-dependence of the laser pulse used to drive the system.

We can derive an expression for the adiabaticity condition by temporarily recasting the basis states as the dressed states instead of the bare exciton states. In the dressed state basis, the state vector $|\Psi(t)\rangle$ of the system can be written as

$$|\Psi(t)\rangle = A_+(t)\,|\Psi_+(t)\rangle + A_-(t)\,|\Psi_-(t)\rangle \tag{1.28}$$

where the state vector $|\Psi(t)\rangle$ is a solution to the time-dependent Schrödinger equation,

$$\hbar\frac{\partial}{\partial t}\,|\Psi(t)\rangle = -iH_i(t)\,|\Psi(t)\rangle\,. \tag{1.29}$$

The action of $iH_i(t)$ on $|\Psi(t)\rangle$ can be written as,

$$iH_i(t)\,|\Psi(t)\rangle = iE_+(t)A_+(t)\,|\Psi_+(t)\rangle + iE_-(t)A_-(t)\,|\Psi_-(t)\rangle\,. \tag{1.30}$$

where $E_\pm$ are the eigenvalues associated with $|\Psi_\pm\rangle$. The time derivatives of the dressed states $|\Psi_\pm(t)\rangle$ is given by

$$\frac{d}{dt}\,|\Psi_-(t)\rangle = -[\sin(\Theta/2)\,|0\rangle + \cos(\Theta/2)\,|1\rangle]\frac{1}{2}\frac{d\Theta}{dt} = -\frac{1}{2}\frac{d\Theta}{dt}\,|\Psi_+(t)\rangle \tag{1.31}$$

and

$$\frac{d}{dt}\,|\Psi_+(t)\rangle = \frac{1}{2}\frac{d\Theta}{dt}\,|\Psi_-(t)\rangle\,. \tag{1.32}$$

Using Eqn (1.31) and Eqn (1.32), we can obtain the time derivative of $|\Psi(t)\rangle$ as

$$\begin{aligned}\hbar\frac{d}{dt}\,|\Psi(t)\rangle = \hbar[\dot{A}_+(t) - \frac{1}{2}A_-(t)\dot{\Theta}]\,|\Psi_+(t)\rangle + \\ \hbar[\dot{A}_-(t) + \frac{1}{2}A_+(t)\dot{\Theta}]\,|\Psi_-(t)\rangle\end{aligned} \tag{1.33}$$

Using Eqns (1.29), (1.30), (1.33), and the orthogonality of $|\Psi_\pm\rangle$, we get the following coupled differential equations for the coefficients $A_\pm$,

$$\begin{aligned}\hbar\dot{A}_+(t) &= iE_+(t)A_+(t) - \frac{\hbar}{2}A_-(t)\dot{\Theta} \\ \hbar\dot{A}_-(t) &= \frac{\hbar}{2}A_+(t)\dot{\Theta} + iE_-(t)A_-(t).\end{aligned} \tag{1.34}$$

We can obtain uncoupled differential equations for the coefficients $A_\pm$ if the

term $\dot{\Theta} \ll |E_+ - E_-|$, which amounts to the adiabatic approximation. The time derivative of Θ is given by

$$\frac{d}{dt}\Theta = \frac{d}{dt}\tan^{-1}\left(\frac{\Omega(t)}{\Delta}\right) = \frac{\Delta\dot{\Omega} - \Omega\dot{\Delta}}{\tilde{\Omega}^2} \tag{1.35}$$

The adiabaticity condition then requires

$$\Delta\dot{\Omega} - \Omega\dot{\Delta} \ll [\Omega^2 + \Delta^2]^{3/2} \tag{1.36}$$

This condition will hold for intense laser fields (large $\tilde{\Omega}$) and for large values of $\dot{\Delta}$ ($\dot{\Delta} = \alpha$).

We can gain insight into the system evolution by considering the state of the system for very early and very late times, corresponding to the initial and final states. Focusing first on the case where $\alpha > 0$ for t=$-\infty$, from Eqn (1.27) the detuning Δ is positive for large early times and $|\Delta| \gg |\Omega|$. In this case, from Eqn (1.11) the value of $\cos\theta$ equals 1 and $\sin\theta$ equals 0 such that $\theta = 0$. From Eqn (1.10) the dressed states for large negative times are:

$$\begin{aligned} |\Psi_-(-\infty)\rangle &= |0\rangle \\ |\Psi_+(-\infty)\rangle &= |1\rangle \end{aligned} \tag{1.37}$$

Because the control process is adiabatic, the system that starts off in $|\Psi_-\rangle$ will remain in this state throughout the control process. But $|\Psi_-\rangle$ represents a dynamic admixture of the bare QD states and this admixture evolves as time progresses according to Eqn (1.10) and Eqn (1.11). At t=∞, long after the pulse is over, $\Delta < 0$ and $|\Delta| \gg |\Omega|$. In this case $\cos\theta = -1$ and $\theta = \pi$. Eqn (1.10) then gives :

$$\begin{aligned} |\Psi_-(\infty)\rangle &= -|1\rangle \\ |\Psi_+(\infty)\rangle &= |0\rangle \end{aligned} \tag{1.38}$$

An initially unexcited system (*i.e* a system in state $|0\rangle$) therefore starts in the lower energy dressed state $|\Psi_-\rangle$ entirely and ends up in $|1\rangle$ after the laser pulse is over, thereby exciting the system. The full dynamic evolution of the dressed states for ARP are shown in Fig 1.7(a) which shows the energies $E_\pm$ of the dressed states

versus time for the case of a chirped control pulse driving a two-level system.

For a negatively chirped pulse, the initial and the final compositions of states $\Psi_{\pm}$ are reversed from that of Eqn (1.37) and Eqn (1.38). At t=$-\infty$

$$\begin{aligned} |\Psi_{-}(-\infty)\rangle &= |1\rangle \\ |\Psi_{+}(-\infty)\rangle &= |0\rangle \end{aligned} \tag{1.39}$$

and at t=$+\infty$

$$\begin{aligned} |\Psi_{-}(\infty)\rangle &= |0\rangle \\ |\Psi_{+}(\infty)\rangle &= |1\rangle \end{aligned} \tag{1.40}$$

The cases of positive and negative pulse chirp may be represented on the same dressed states diagram by reading the time axis either from left to right or from right to left. Hence the system evolves along the $|\Psi_{+}\rangle$ state throughout the control process. For the case of a positively chirped pulse in Fig 1.7(a), the direction of time is from the left to the right while for the case of a negatively chirped pulse, time progress from right to left.

If in addition to the chirp, the control pulse has a constant detuning Δ_0, then as per Eqn (1.9) and Eqn (1.10), the energy splitting between the dressed states $|\Psi_{\pm}\rangle$ increases by Δ_0 and the extrema near $t = 0$ in the dressed state energies are no longer when the pulse intensity is maximum, but is displaced on either side of $t = 0$ for these two states. The evolution of the dressed state energies as a function of time when driven by a control pulse with a constant detuning Δ_0 is shown in Fig 1.7(b). In this case, the value of Ω required to satisfy the adiabaticity criteria given in Eqn (1.36) is larger. Consequently, the threshold pulse area required for complete population transfer is higher. However in contrast to Rabi rotations, complete population transfer to state $|1\rangle$ is still possible once the threshold pulse area is crossed.

Within the Bloch sphere picture, for ARP the detuning Δ that determines the z-component of the optical torque vector, is a function of time and the value of Δ goes from a negative value to a positive value during the pulse. Thus the optical torque vector $\vec{\Lambda}$ moves from the south pole to the north pole. The torque equation in Eqn (1.13) predicts that the Bloch vector $\vec{U}$ precesses around $\vec{\Lambda}$, however both $\vec{\Lambda}$ and $\vec{U}$ initially point to the south pole, so this precession begins once $\vec{\Lambda}$ deviates

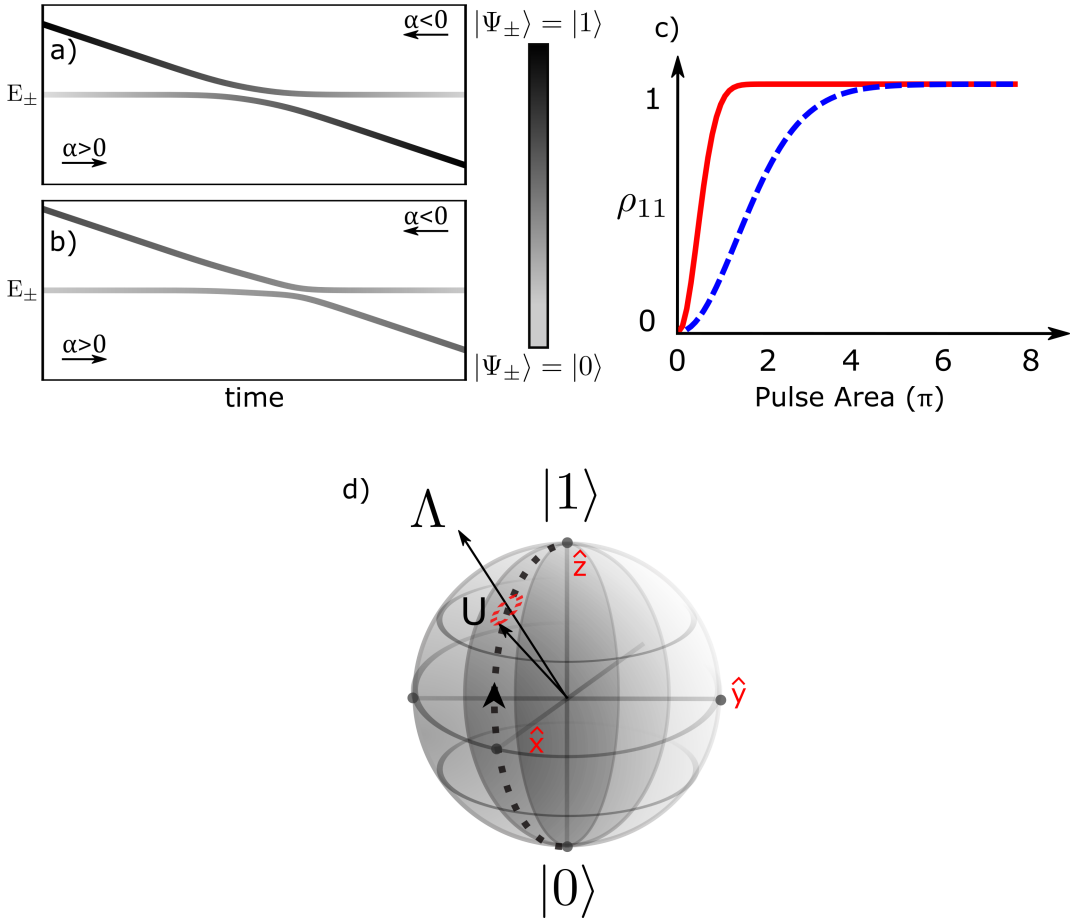

Figure 1.7: a) Energies $E_\pm$ of dressed states $|\Psi_\pm\rangle$ for a two-level system interacting with a chirped control pulse a) without and b) with a constant detuning. During ARP, the system stays in one of dressed states $|\Psi_\pm\rangle$ throughout, while the admixture of the constituent bare exciton states evolves as the pulse progresses to leave the system in the excited state. The sign of the chirp determines which dressed state the system remain in. For a positively chirped control pulse, the system would remain in $|\Psi_-\rangle$ and for negatively chirped control pulse $|\Psi_+\rangle$. c) The final population of the excited state $|1\rangle$ as a function of pulse area (Θ) for a chirped control pulse without (red solid curve) and with a constant detuning (blue dashed line). (d) Dynamics of $\vec{U}$ and $\vec{\Lambda}$ on a Bloch sphere for ARP: As the pulse frequency sweeps, the $\vec{\Lambda}$ vector goes from the south pole to the north pole dragging the Bloch vector along with it.

slightly from the south pole. If the adiabaticity criteria (Eqn (1.36)) is maintained, the Bloch vector $\vec{U}$ will precess tightly around the torque vector $\vec{\Lambda}$ as it moves to the north pole such that at the end of the laser pulse, the final state of the system is $|1\rangle$, achieving a population inversion. The state evolution during ARP in a Bloch sphere picture is depicted in Fig 1.7(d).

1.4 The Role of Phonons

Dephasing processes limit the number of operations that can be performed on a qubit because the time for loss of coherence represents the temporal window inside of which individual gates must be carried out. The exciton dephasing time in QDs at low temperatures is primarily limited by the radiative lifetime of the exciton, with reported values between 400 - 1000 ps depending on the size of the QD [50, 51]. The quality of optical control can be improved by performing qubit operations using ultrafast pulses with pulse durations much shorter than the dephasing time.

While the process of radiative recombination represents a fundamental limitation to the quality of optical control, since the gate time using a short laser pulse can be very fast relative to the recombination time (e.g with a subpicosecond gate time, the ratio of gate time to dephasing time can be as large as 10^3 to 10^4) the performance of QDs in quantum technology is not impeded substantially by this process. However, there is another source of dephasing related to the driving pulse itself. This is called *excitation induced dephasing* and is caused by the interaction of the exciton with phonons in the host lattice. Phonons are quantized modes of vibration occurring in a crystal lattice. A lattice vibrational mode of angular frequency ω_k and momentum $\hbar k$, where k is the wavevector of the vibrational mode, has an energy of $\hbar\omega_k$. Vibrational modes where neighboring atoms in the unit cell of a lattice move out of their equilibrium positions in phase are called acoustic phonons whereas vibrational modes resulting in out-of-phase movement of atoms are called optical phonons. These vibrational modes are then further divided into longitudinal and transverse modes depending on the direction of movement of the atoms with respect to the wave vector of the phonon. In III-V semiconductors like GaAs and InAs, there are two atoms per basis leading to 6 possible phonon modes: one longitudinal acoustic (LA) mode, two transverse acoustic (TA) modes, one longitudinal optical (LO) mode and two transverse optical (TO) modes.

The equilibrium lattice positions of atoms in a crystal are determined in part by the electrostatic potential due to all charge carriers. Hence the electronic state of the QD is affected by the presence of lattice vibrations. For self-assembled QDs, due to the relatively small lattice mismatch and similar elastic properties of the QD and

surrounding material, it is a good approximation to treat only the coupling of confined carriers in the QD to bulk phonon modes in the barrier material [52, 53, 54]. The homogeneous compression or expansion caused by acoustic phonons induces a local change in the lattice constant, resulting in shifts in the energy of the charge carriers. This type of electron-phonon interaction is called the deformation potential interaction. In III-V semiconductors, which are polar due to the inequivalent sharing of electrons between the group III and the group V constituents, there are two other mechanisms of coupling tied to the interaction of the electron with the electric field generated by the phonon. These include piezoelectric coupling to all acoustic modes and the Fröhlich interaction with LO phonon modes. It has been shown that the deformation potential coupling to LA phonons has the largest impact on optical control schemes involving excitons [54]. We will therefore limit the discussion below to this mechanism [52, 53, 54].

The Hamiltonian describing the bulk LA phonon modes is given by

$$H_{ph} = \sum_q \hbar\omega_q \hat{b}_q^\dagger \hat{b}_q \tag{1.41}$$

where $\hat{b}_q$ ($\hat{b}_q^\dagger$) are annihilation (creation) operators for LA phonons with wavevector q. The deformation potential coupling to an exciton in the QD is described by the Hamiltonian

$$H_{ph-int} = \sum_q \hbar(g_q \hat{b}_q^\dagger + g_q^* \hat{b}_q) \left|1\right\rangle \left\langle 1\right| \tag{1.42}$$

where g_q is the exciton-phonon coupling coefficient for a phonon of wavevector q. The influence of the phonons on the exciton dynamics is characterized by the phonon spectral density function $J(\omega)$, defined as

$$J(\omega) = \sum_q |g_q|^2 \delta(\omega - \omega_q). \tag{1.43}$$

In Eqn (1.43), g_q determines the electron-phonon coupling strength. The coupling strength differs for electrons and holes due to their differing wavefunctions and can be written as

$$g_q^{e(h)}(q) = F^{e(h)}(q) \frac{|q| D_{e(h)}}{\sqrt{2V\rho\hbar\omega_q}} \tag{1.44}$$

where V and ρ are the volume of the unit cell and the density of the crystal respectively, $D_{e(h)}$ is the deformation potential constant for electrons (holes) and $F^{e(h)}(q)$ is the electron (hole) form factor. The electron (hole) form factor is defined as

$$F^{e(h)}(q) = \int_V |\psi_{e(h)}(r)|^2 e^{iqr} d^3r. \tag{1.45}$$

Here $\psi_{e(h)}$ is the wavefunction of the confined electron (hole), so that the form factor is the spatial Fourier transform of the probability distribution for the confined carriers.

Analytical expressions for $J(\omega)$ can be obtained by assuming that the QD is spherical in shape and that the confinement potential is harmonic in nature. Under this assumption, taking equal confinement lengths for electrons and holes, the wavefunction for the carriers will have the form

$$\psi_{e(h)}(r) = \frac{1}{\pi^{3/4}} \left(\frac{1}{d^2}\right)^{3/4} e^{(-r^2/2d^2)} \tag{1.46}$$

where d characterizes the confined volume of the charge carrier dictated by the size of the QD. In this case, the form factor for the ground state exciton can be written as

$$F^{e(h)}(q) = e^{(-q^2d^2/4)}. \tag{1.47}$$

$J(\omega)$ for this case can then be calculated by inserting Eqn (1.44) and Eqn (1.47) in Eqn (1.43). Converting the summation in Eqn (1.43) into an integral using $\sum_q \rightarrow V/(2\pi)^3 \int d^3q$ and using the dispersion relation of LA phonons $\omega_q = c_s|q|$, where c_s is the speed of sound in the material, we get,

$$J(\omega) = \alpha\omega^3 e^{-(\omega/\omega_c)^2} \tag{1.48}$$

where

$$\alpha = (D_e - D_h)^2/(4\pi^2\rho c_s^5) \tag{1.49}$$

and $\omega_c = \sqrt{2}c/d$ is a cut-off frequency that depends on the size of the QD. Fig 1.8(a) shows the form of $J(\omega)$ from Eqn (1.48) as a function of phonon energy for QDs of two different sizes. The width of $J(\omega)$ is determined by the spatial extent

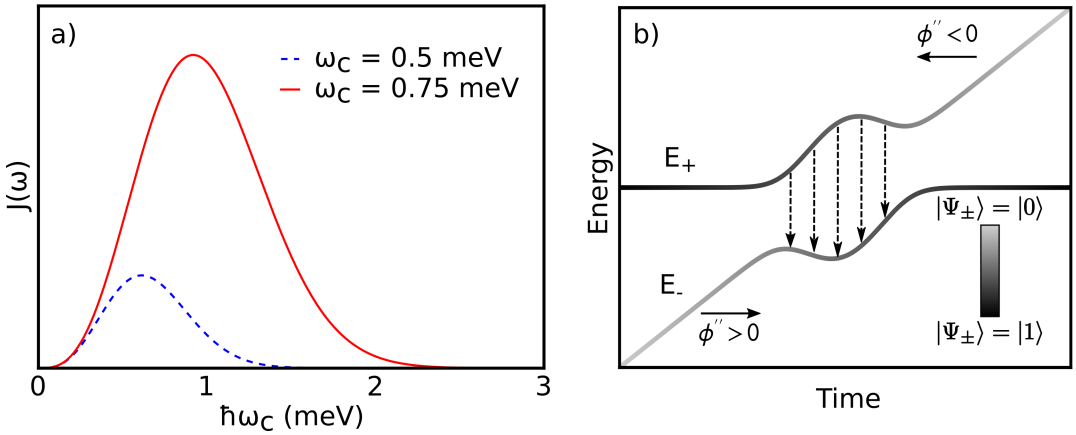

Figure 1.8: a) Phonon spectral density $J(\omega)$ as a function of phonon energy for a cut-off frequency $\hbar\omega_c = 0.5$ meV (blue dashed curve) corresponding to a QD size of 19 nm and $\hbar\omega_c = 0.75$ meV (solid red curve) corresponding to a QD size of 12.7 nm (b) Phonon assisted transitions between dressed states in ARP. Arrows indicate phonon emissions from state $|\Psi_+\rangle$ to $|\Psi_-\rangle$ which results in a loss of coherence during population transfer through ARP.

of the wavefunction of the exciton through the electron (hole) form factor (see Eqn (1.45)). For larger QDs, a large value of d leads to a form factor of narrower width in k-space and consequently a narrower $J(\omega)$. Physically, the exciton-phonon coupling is stronger when the wavelength of phonons matches the spatial extent of the exciton wavefunction (*i.e.* the size of the QD). When the wavelength of the phonon is much larger than the size of the QD, corresponding to low phonon energies, this amounts to a translation of the whole QD in space. The effect of such a translation is negligible on the state of the exciton. When the wavelength of the phonon is much smaller than the QD, corresponding to high phonon energies, the instantaneous change in the QD dimensions caused by the phonon is very small because the fast oscillations in the atomic displacement average over the volume of the QD. As a result, the influence of LA phonons on the state of the exciton is again negligible in this limit. Hence $J(\omega)$ exhibits a maximum at a finite frequency and the cut-off frequency is larger for smaller QDs. At low frequencies $J(\omega) \sim \omega^3$ and in the high frequency limit $J(\omega)$ acts as a Gaussian function.

The OBEs in Eqn (1.14) are modified in the presence of electron-LA phonon coupling. This modified set of equations can be derived by adding the phonon bath and its interaction to Eqn (1.1). Here the phonon bath is treated as a large system

whose state is unaffected by the exciton-phonon interaction and the modified OBEs can be written as,

$$\begin{aligned}
\dot{U}_x &= -\Delta U_y - \left(\frac{\Delta\Omega}{\tilde{\Omega}^2}\right) Re[K(\tilde{\Omega})]U_z - \frac{\pi\Omega J(\tilde{\Omega})}{2\tilde{\Omega}} - \left(\frac{\Omega}{\tilde{\Omega}}\right)^2 Re[K(\tilde{\Omega})]U_x \\
\dot{U}_y &= -\Delta U_x + \Omega\left(1 + \frac{Im[K(\tilde{\Omega})]}{\tilde{\Omega}}\right)U_z - \left(\frac{\Omega}{\tilde{\Omega}}\right)^2 Re[K(\tilde{\Omega})]U_y \\
\dot{U}_z &= -\Omega U_y
\end{aligned} \tag{1.50}$$

The additional terms include dephasing caused by phonons and are described by the phonon bath correlation function, given by

$$\begin{aligned}
K(t) &= \int_0^\infty d\omega J(\omega) coth\left(\frac{\hbar\omega}{2k_bT}\right) cos(\omega t) \\
K(\Omega) &= \int_0^\infty dt K(t) e^{i\Omega t}
\end{aligned} \tag{1.51}$$

These extra terms cause the exciton to suffer from an intensity dependent dephasing arising from the real part of $K(\omega)$ and a renormalization of the Rabi frequency from the imaginary part of $K(\omega)$ [55]. In the dressed states picture, these dephasing processes are caused by transitions between the dressed states $|\Psi_\pm\rangle$. These transitions can occur via phonon absorption or phonon emission events. Phonon emission induced transitions are depicted in Fig 1.8(b) by the dashed arrows. *The phonon interaction is the strongest such that the rate of phonon induced transitions between the dressed states is largest when the energy splitting between the dressed states matches the peak of the phonon spectral density function*. This reflects the fact that $J(\omega)$ limits the bandwidth of phonons that are coupled to the QD. The characteristics of the optical pulse also determine the rate of these phonon-induced transitions because the size of the splitting between the dressed states is determined by Ω.

These resonant, phonon-induced transitions between the dressed states have a strong impact on the optical control process because they partially destroy the coherent exciton state as it is being driven by the light field. This loss of coherence limits the fidelity of quantum state manipulation. It also affects the quality of photons emitted by the QD. For the two optical control processes relevant for this

thesis work (Rabi rotations and ARP), these dephasing processes have a strong impact. For Rabi rotations, the phonon transitions cause a damping of the oscillations in the occupation of $|1\rangle$ versus the pulse area [38, 54]. An example of this effect is shown in Fig 1.9 from Ref [38]. In the experiments in Ref [38], photocurrent was used to read-out the occupation of the exciton at the end of the laser pulse. This occupation oscillates as a function of pulse area Θ from Eqn (1.23) and Eqn (1.25). The square root of the average power in the pulsed laser beam, which is proportional to pulse area, is shown on the x-axis in Fig 1.9.

For ARP, the impact of the phonon-induced transitions depends on temperature, pulse area, and the sign of the pulse chirp. The sign of α dictates whether the system undergoes evolution along the higher or lower energy dressed state. At low temperatures, phonon absorption processes are highly unlikely. Hence the evolution along the lower energy-dressed state ($|\Psi_-\rangle$), which corresponds to a positively chirped driving pulse, is unaffected by phonons and suffers no dephasing. For a negatively chirped pulse, where the system traverses the higher energy dressed state ($|\Psi_+\rangle$), phonon emission leads to a transition to the lower energy dressed state and hence causes dephasing [38, 54, 56]. This asymmetry disappears at higher temperatures as both phonon absorption and emission processes become equally likely [57]. For negatively chirped pulses, where dephasing can occur, the strength of electron-phonon coupling depends also on pulse area because the dressed state splitting must still match the peak of $J(\omega)$ for strong coupling to occur. Fig 1.10(a) shows the calculated exciton occupation for a negatively chirped pulse, a TL pulse and a positively chirped control pulse from Ref [58] and Fig 1.10(b) shows an experimental measurement of the chirp sign dependence of ARP from Ref [56].

Since the damping process is strongest when the peak frequency of $J(\omega)$ matches the energy separation between the dressed states, the non-monotonic dependence of $J(\omega)$ leads to a non-monotonic dependence of the damping rate on the Rabi frequency of the laser pulse. It has therefore been predicted that for large pulse areas when the Rabi energy gets higher than the cut-off frequency for $J(\omega)$, *i.e.* for the electron-phonon interaction, Rabi rotations should reappear [59]. This is often referred to as the *reappearance regime*. This regime has not been observed experimentally yet for Rabi rotations because experimental demonstration using

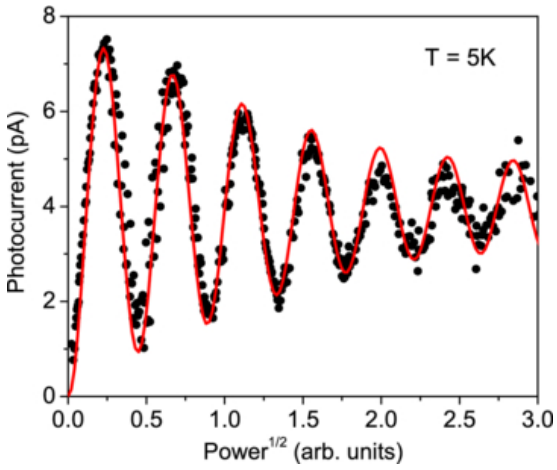

Figure 1.9: (a) Experimental demonstration of Rabi rotations. The exciton occupation at the end of the laser pulse is detected by the photocurrent created by ionizing the exciton. Photocurrent is shown as a function of square-root of excitation power, which is proportional to the pulse area. Red solid curves are a fit to a model including excitation induced dephasing due to interaction with LA phonons. Figure adapted with permission from [38]

Gaussian laser pulses requires extremely high pulse areas. This is because, for a continuously varying pulse shape such as a Gaussian pulse, the resulting energy splitting between the dressed states would always coincide with the peak of $J(\omega)$ at some point during the pulse [54]. This problem can be mitigated by using pulses shapes characterized by abrupt starts and ends, for example rectangular pulses, but it can never be eliminated completely [60].

For ARP, in contrast, it is possible to access the reappearance regime because the separation between the dressed states is non-zero throughout the entire control process. As a result, a full decoupling of the exciton from LA phonons is experimentally accessible with a large enough Rabi energy [61, 54].

In addition to excitation induced dephasing, at higher temperatures the exciton-LA phonon interaction can lead to a pure dephasing of the exciton coherence. At high temperatures, when there is a larger occupation of thermal modes, phonons can interact with the exciton and cause virtual transitions to higher excited states [62]. Such scattering processes do not result in a population transfer but dephase the exciton, leading to a broadening of the zero phonon line decreasing the indistinguishability of the emitted photons [63]. This phonon induced pure dephasing can be suppressed by working at a temperature lower than 10 K [64]. It can also be

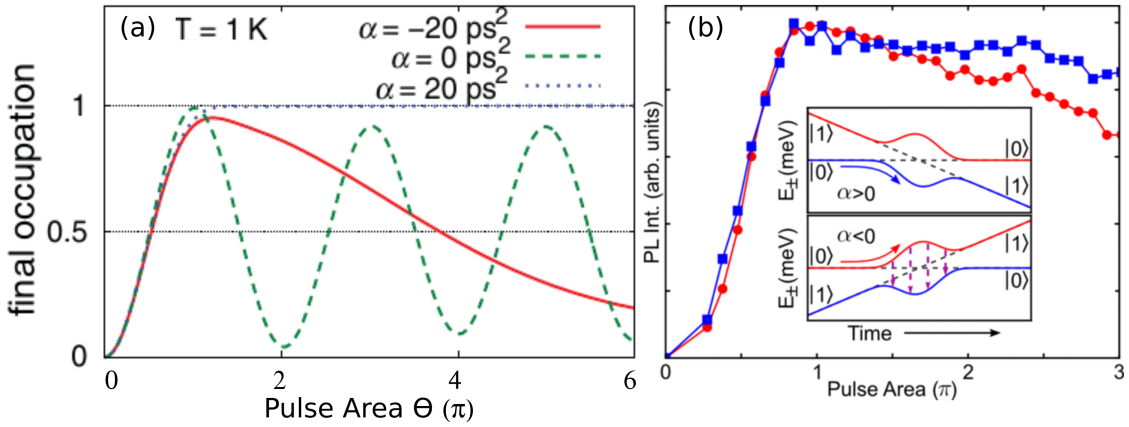

Figure 1.10: (a) Calculated final occupation of the exciton state for negatively chirped (red solid curve), TL (green dashed curve) and positively chirped (blue dotted curve) control pulses. Figure adapted with permission from [58]. (b) Experimental measurement of the chirp sign dependence of ARP. The plot shows PL intensity as a function of pulse area for negatively (red dots) and positively (blue squares) chirped control pulses. Figure adapted with permission from [56].

made negligible by working with QDs possessing strong quantum confinement such that the energy spacing between the QD levels is much larger than the occupied phonon energies, a condition that is satisfied by the QDs used in this work.

1.5 Past Research Progress in the Optical Control of Excitons in Quantum Dots

1.5.1 Quantum Dots as Non-classical Light Sources

High quality sources of single and entangled photons are essential for the development of applications such as quantum cryptography and quantum computation [21, 65, 66]. Single photons are one of the leading qubit candidates due to their largely decoherence free nature, many encoding degrees of freedom such as polarization, time bin or path and the ease of applying one-qubit logic gates [21]. The vulnerability of current encryption methods such as RSA to the potential realization of quantum computation systems has motivated the development of new encryption protocols [67]. Their implementation requires high quality sources of single or entangled photons [68, 69].

The properties that determine the quality of a single photon source are single

photon purity, indistinguishability and brightness. The single photon purity is the probability that each wavepacket has only one photon. An ideal single photon source will emit only one photon when triggered. The single photon purity of a source is normally characterized by the second-order intensity correlation function $g^{(2)}(\tau)$ measured using a Hanbury Brown and Twiss interferometer. In Hanbury Brown and Twiss interferometry, a beam of light is sent to a beamsplitter and one detector is kept at both outputs of the beamsplitter and the distance of each detector from the beamsplitter can be varied, introducing a time delay τ. The detector outputs are then connected to correlation electronics measuring coincident detection events between the two detectors. An ideal single photon source has a $g^{(2)}(0) = 0$ indicating no coincidence counts between the detectors, whereas a laser field gives a $g^{(2)}(0)$ value of 1. The indistinguishability of a source refers to the similarity between the emitted photons in a single photon train. For two photons to be indistinguishable they should have identical spectral bandwidth, pulse width, polarization, carrier frequency and mode profile. The indistinguishability of emitted photons is affected by the nature of excitation and various dephasing processes present in the source. The brightness of the single photon source determines the probability that the emitted photon, once triggered, is detected by the detection apparatus. For perfect brightness every single photon emitted by the source should be detected by the detector. Less than perfect brightness will result in missing photons in a single photon stream, increasing the necessary complexity of cryptographic and computation schemes. Brightness is a composite quantity including intrinsic quantum efficiency, collection efficiency (for example into an optical fiber) and all inefficiencies in the detection apparatus.

In QDs, the recombination of a confined electron-hole pair or exciton will result in the emission of a single photon. Thus, when excited by a laser pulse shorter than the lifetime of an exciton, a QD can act as a triggered single photon source. Since the ground state optical transition in the QD may only be occupied by a single exciton at a time, unlike attenuated lasers or spontaneous down-conversion based sources, the brightness of single emitter sources like QDs is intrinsically decoupled from their single photon purity. QDs also offer the advantage that their optical transitions may be controlled by varying the QD size. This implies that QDs can be

tailored to work in convenient bandwidths such as one of the telecommunication bands or that of efficient silicon detectors [70, 71, 72].

Photons emitted from a single QD were isolated for the first time in 1994 [73, 74]. Later in 2000 Michler *et al.* demonstrated the first QD single photon source through $g^{(2)}(0)$ measurements [75]. In this work by Michler, the photon emission was triggered using a laser tuned to the bulk GaAs barriers surrounding the QD. Yuan *et al.* demonstrated a QD based electrically triggered single photon source in 2002 [76]. The non-resonant excitation of QDs, corresponding to excitation in either the bulk barriers surrounding the QD or the quantum well levels tied to the wetting layer, normally results in low single photon purity since the probability for multiple carriers successively relaxing into the energy levels of the QD is high. The single photon purity can therefore be improved by directly exciting carriers into the confined energy levels within the QD. High single photon purity ($g^{(2)}(0) < 0.05\%$) has been reported in the literature for both p-shell excitation and strictly resonant excitation in QDs [77, 78].

The indistinguishability of photons is determined by the ratio of pure dephasing to the spontaneous emission rate. It is limited by various dephasing processes arising from the interactions of the exciton with the solid-state environment such as charges in the QD vicinity through the quantum confined Stark effect [64], phonon assisted virtual transitions to higher excited states [62, 64, 79], the emission of photons into the acoustic phonon sideband [80, 81] and timing jitter induced by the excitation process [82]. Pure dephasing arising due to the interaction of the exciton with the charges around the QD and virtual phonon transitions can both be minimized by increasing the spontaneous emission rate by embedding the QD in a resonant cavity [83, 84]. Embedding QDs in a resonant cavity also helps in the suppression of photon emission into the acoustic phonon sideband by favouring the emission along the cavity resonance [85, 84]. Virtual phonon transitions can also be suppressed by working at cryogenic temperatures [64, 79] or through engineering the QD dimensions to increase the spacing between the energy levels [86]. Timing jitter associated with the excitation process can be minimized by exciting carriers directly into the QD energy levels [65]. Experiments that used ARP as the excitation process have yielded photons with an indistinguishability of $99.5 \pm 0.7\%$ [87]. The

highest reported value of indistinguishablity from a QD source was 99.56% from resonantly excited QDs embedded in a micropillar cavity [88].

The high refractive index of the GaAs matrix (n $\approx$ 3.5) surrounding the QD would cause most of the light emitted by the QD in a planar semiconductor wafer to undergo total internal reflection. Without strategies to mitigate this effect, the probability that a photon emitted by the QD escapes the wafer and is available for collection is about 1%. This value can be improved through the use of engineered structures to improve light extraction such as microcavities [89, 90], waveguides [91, 92] and microlenses [93]. For instance, QDs embedded in micropillar cavities have demonstrated extraction efficiencies as high as 80% [89, 90].

At present, QDs are one of the highest performing single photon emitter platforms due to the deterministic nature of their emission and the ease of coupling to guided optical modes. A comparison of various single photon emitter platforms is given in Table 1.1. Among all competing technologies, QD based sources have reported the highest single photon emission purity and indistinguishability [94]. The high standards of performance required by photonic QIP systems, call for highly efficient state preparation protocols to improve the source brightness [95]. The cryogenic temperatures required for the operation of QD based single photon sources make their large scale deployment challenging. Experiments that constitute this thesis work address some of these challenges by advancing the applicability of ARP as an efficient state preparation protocol and by developing the ARP control process to potentially allow high temperature operation of QD based single photon sources.

The radiative relaxation of the biexciton in QDs is known as the biexciton cascade and can serve as a source of polarization-entangled photons. The biexciton state with a total angular momentum $J = 0$ is composed of two electrons and two holes with $S = \pm 1/2$ and $J = \pm 3/2$ and can be written as $|\uparrow\downarrow\Uparrow\Downarrow\rangle$. Fig 1.4(a) shows the energy level diagram and selection rules for an exciton-biexciton four-level system in a symmetric QD. The radiative decay of the biexciton proceeds by the emission of a photon, leaving a single exciton, which then also undergoes radiative decay and emits a photon. The polarization state of the emitted photon pair

Emitter	SPDC	Atoms and Ions	QDs	NV centers	FWM
Wavelength (nm)	600-1700	discrete values	900-1550	600-800	600-1550
P/D	P	D	D	D	P
Indistinguishability	99% [96]	93% [97]	99.56% [88]	66% [98]	97% [96]
$g^{(2)}(0)$	0.004 [99]	0.0003 [100]	7.5×10^{-5} [78]	0.07 [101]	0.007 [99]
Efficiency	0.84 [102]	0.88 [103]	0.97 [104]	0.35 [105]	0.26 [106]
Max Brightness	2.01 Mhz [107]	55 kHz [108]	28.3 Mhz [109]	850 kHz [105]	855 kHz [110]
Entanglement Fidelity	0.9959 [111]	0.93 [112]	0.978 [113]	-	0.997 [114]

Table 1.1: Comparison of single photon emitter technologies. P (D) refers to probabilistic (deterministic) sources. Table adapted with permission from Ref [94].

can be written as

$$\left|\Psi^{+}\right\rangle = \frac{1}{\sqrt{2}}(\left|L_{xx}\right\rangle\left|R_{x}\right\rangle + \left|R_{xx}\right\rangle\left|L_{x}\right\rangle) \tag{1.52}$$

which corresponds to a maximally entangled Bell state where L_{xx} indicates a left circularly polarized biexciton photon, R_x indicate a right circularly polarized exciton photon and so on. Entangled photons are an essential component of many quantum information proposals such as quantum repeaters [115], quantum key distribution [69], measurement based quantum computing [116], sensitive interferometry [27] and microscopy [117]. Ever since Benson et al [118] published the concept of entangled photon generation from quantum dots, there have been numerous research groups working on QD-based entangled photon sources [119, 120, 121, 122, 123, 66, 124]. Recent research has enabled high fidelity preparation of the biexciton state through various excitation schemes including two-photon Rabi rotations, ARP and phonon assisted excitation [125, 126, 127]. Polarization entangled photons created via the biexciton cascade have shown high entanglement fidelity and have made QDs one of the most robust sources of entangled photons [66, 122, 128].

Even though the study of state preparation schemes (Rabi rotations and ARP) and dephasing mechanisms in this thesis work is mostly carried out within the context of excitons in QDs, these considerations are also applicable for the preparation of biexciton states in QDs as ARP has been used for exciting biexcitons in QDs [126]. Electron-LA phonon interactions have also been shown to affect the state preparation efficiency of biexcitons [53, 126, 54]. The insights provided by the experiments

and numerical calculations that constitute this thesis work will also therefore aid in improving the performance of QD based entangled photon sources.

1.5.2 Single Qubit Gates

Within the Bloch vector representation of an exciton qubit introduced in Sec 1.3.1, Rabi rotations carried out using a resonant TL laser pulse are characterized by a rotation of the Bloch vector about the $\hat{x}$-axis sweeping an angle θ, which is equal to the pulse area. This rotation modifies the coefficients $|C_0|$ and $|C_1|$ as well as their relative phase. Rabi rotations therefore represent a simple example of a single qubit gate. The possible quantum states on the Bloch sphere that are accessible is however limited since the motion of the Bloch vector during Rabi rotations is restricted to the $\hat{y}$-$\hat{z}$ plane.

Complete control over a qubit requires the ability to induce rotations of the Bloch vector about multiple axes. This is normally achieved using a pair of pulses with a time delay τ between them [38]. The first pulse creates a superposition of ground and excited states, thereby rotating the Bloch vector about the $\hat{x}$-axis. If the second pulse has a phase difference of $\phi = \omega_l \tau$ with respect to the first pulse it will induce a rotation about the $\cos(\phi)\hat{x} + \sin(\phi)\hat{y}$ direction. Experimentally these phase locked pulse pairs are created using a path-stabilized Michelson or Mach–Zehnder interferometer that maintains a fixed path difference between the pulses [129, 130]. These experiments, which makes use of quantum interference between qubit wavefunctions, are commonly referred to as Ramsey interference experiments [38].

Ramsey interference has been experimentally demonstrated in QDs by several groups [131, 132, 133, 134, 135]. Fig 1.11 shows Ramsey interference measurements for a negative trion transition measured using the resonance fluorescence technique by Lee *et al* [135]. The occupation of the trion oscillates as a function of the delay between the pulses. The difference between the maximum and minimum occupation at a given delay is defined as the interference visibility. The reduction in interference visibility as the delay increases is a consequence of the dephasing of the qubit. The authors in Ref [135] determined a dephasing time of 510 ± 10 ps by fitting the data to an exponential decay.

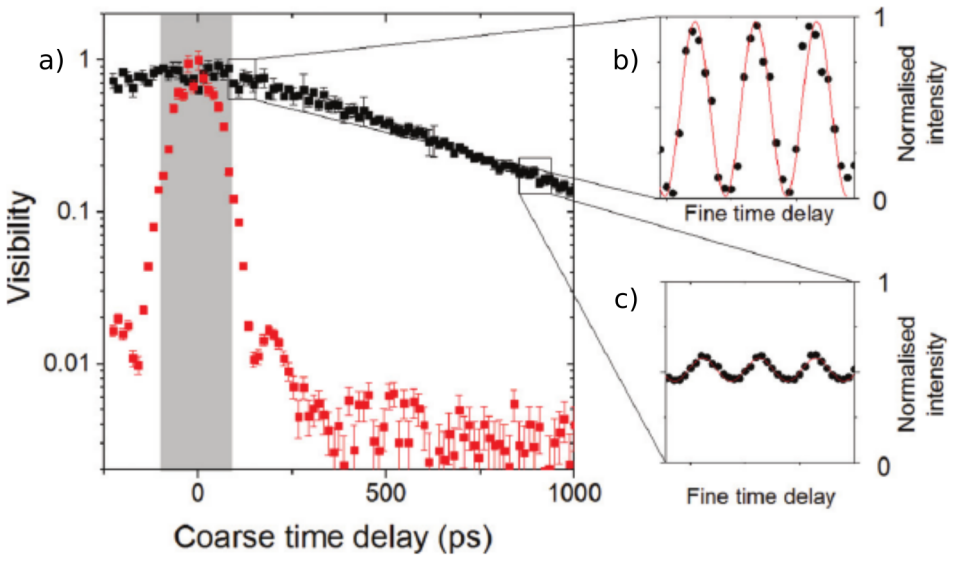

Figure 1.11: Ramsey Interference. a) Interference visibility of input laser pulses (red squares). Interference visibility of Ramsey interference of the negative trion transition (black squares). A pair of laser pulses with a programmable time delay between them is used to excite a negative trion transition in an InAs QD. For every pulse separation, the time delay between the pulse pairs is finely varied causing constructive and destructive quantum interference of the trion wavefunctions. The interference visibility is the difference of the resonance fluorescence signal between points of constructive and destructive quantum interference. (b) Resonance fluorescence intensity at short pulse separation (50 ps) as a function of fine time delay. (c) Resonance fluorescence intensity at long pulse separation (1000 ps) as a function of fine time delay. The decrease in the amplitude of the oscillations between long and short pulse separations is a consequence of the dephasing of the exciton. Figure adapted with permission from [135].

Rotation along the equatorial plane of the Bloch sphere needed for arbitrary single qubit rotations can also be achieved through the optical Stark effect [136]. Here a resonant pulse is used to excite the exciton and then a second non-resonant laser pulse is used to manipulate its quantum state. Because this second pulse is non-resonant, $\Delta \gg \Omega$ so that the optical torque vector is primarily aligned with the $\hat{z}$-axis. The detuning of the second pulse should be large to avoid significant changes in occupation. By using both resonant and non-resonant pulses in succession, one can induce rotations about $\hat{x}$ and $\hat{z}$ and thereby access points on the entire Bloch sphere.

1.5.3 Two-Qubit Gates

Any scalable circuit model quantum computing platform would require the ability to perform two-qubit gates in addition to single qubit operations. One such operation involving two qubits is a controlled-rotation (C-ROT) gate. The C-ROT gate operation on a two-qubit system is as follows: an rotation gate is applied to a qubit if and only if the second qubit, called the control qubit, is in state $|1\rangle$. A C-ROT gate was demonstrated in QD systems using the 4-level scheme involving both excitons and the biexciton (See Fig 1.4(b)). In this scheme, the two qubits were encoded in excitons excited by $\hat{x}$ and $\hat{y}$ polarized light. The non-zero biexciton binding energy implies that the transition energy of the single exciton to biexciton transition is lower than the energy of the ground state to single exciton transition. One can exploit the polarization-dependent selection rules together with the spectral selectivity of the two transitions to realize a C-ROT gate. A C-ROT gate was demonstrated in interface-fluctuation QDs by Li *et al* [137] and later in self-assembled QDs by Boyle *et al* [138]. The logic operation of the C-ROT gate and experimental results from Ref [138] are shown in Fig 1.12.

1.5.4 Optimal Quantum Control

Optimal quantum control through pulse shaping provides a versatile method for complete control of the Bloch vector. This approach is less cumbersome than the approach described above because only a single pulse is required. Here, a pulse shaper is used to shape the electric field of the laser pulse, thereby tailoring the light-matter interaction. This approach can be used to drive the Bloch vector to any arbitrary point on the Bloch sphere. Optimal quantum control could be used to implement a complex instruction set quantum computer where multiple gate operations are applied using a single shaped laser pulse. In addition to exploiting the relative ease of pulse shaping, this method can potentially reduce the time required to carry out operations [8].

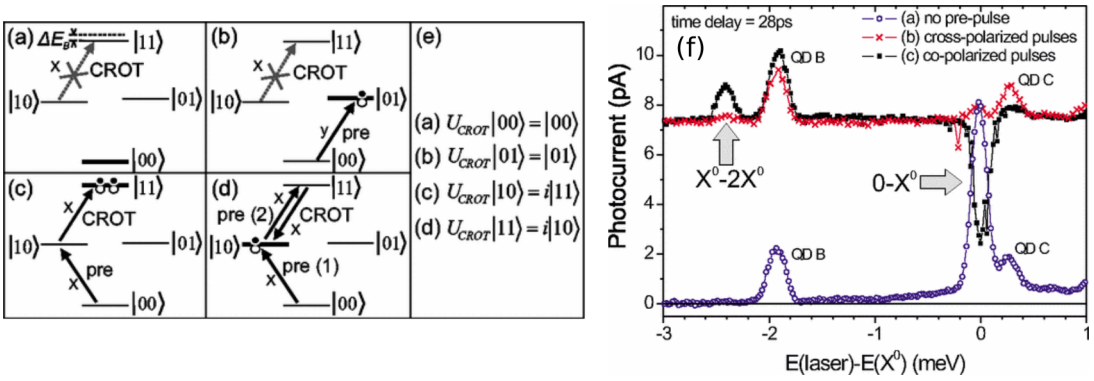

Figure 1.12: Principle of operation of a two qubit C-ROT gate in the four-level exciton-biexciton system. The occupation of each type of exciton (induced with x polarized or y polarized light) are the two bits on which the CROT gate is acting. The CROT pulse shown, which is x polarized, flips the state of the y-polarized exciton if and only if the x polarized exciton is present. This gate uses both the polarization selection rules and the difference in energy between the ground-state-to-exciton and the exciton-to-biexciton transitions. (a)-(d) show the relevant transitions corresponding to the truth table in part (e). (f) Experimental demonstration of C-ROT gate. Photocurrent signal from the QDs as a function of laser detuning for no pre-pulse (blue dots), cross-polarized pre-pulse (red crosses) and co-polarized pre-pulse (black squares). A photocurrent can be measured when the laser is tuned to the $X^0 - 2X^0$ transition only if the X^0 state is populated by the pre-pulse. X^0 is populated only if the pre-pulse is co-polarized with the C-ROT pulse. (QD B and QD C are adjacent QDs not used in the experiment). Figure adapted with permission from [138].

The application of optimal quantum control to semiconductor QDs has only recently been pursued experimentally [139, 140, 141, 142]. Recent theoretical studies by Mathew *et al* explored the feasibility of this approach to simultaneously controlling three individual quantum dots using a single laser pulse [142]. Mathew's work showed that the Bloch vectors of multiple QDs may be simultaneously, independently controlled, enabling access to an arbitrary point on the Bloch sphere for each QD. This highlights the feasibility of developing a small quantum simulator where 10-30 QDs could be manipulated, limited only by the resolution of the pulse shaping system. Experimental investigations in this direction have demonstrated simultaneous deterministic control over two distinct QD excitons by employing a 2π rotation in one QD and a π rotation in the other QD using a single shaped laser pulse [141].

1.5.5 Qubit-Qubit Interactions

Any quantum computer platform requires the ability to control multiple qubits and the means of introducing coupling between them. Existing experimental demonstrations of optical control of coupled QDs have all involved QD molecular structures [143, 144, 145, 146]. In such structures, two layers of self-assembled QDs are grown in succession with a very thin GaAs barrier in between. In this case, the presence of a QD in the first layer creates a strain field that induces the formation of the second QD above it. Since the tunnel barrier is very thin, the QDs exhibit direct tunnel-coupling. Thus tunnel coupling has been used to realize two qubit operations in QD systems [143, 144]. There are several proposals aimed towards achieving multi-qubit operations involving spatially uncoupled qubits in QDs. Conditional operations between spatially separated QDs can be achieved via dipole-dipole interactions in the presence of a static electric field [147], through Coulomb interactions [148] or via coupling through an optical microcavity [20, 149]. The entanglement of spins in distant quantum dots is also possible using optical interconnects, which enable teleportation based gates. [150, 151]

1.5.6 Optical Quantum State Preparation

As discussed in Sec 1.3.3, Rabi rotations are a versatile method of state preparation that allows for the creation of excitons or biexcitons and represents the earliest demonstrations of coherent optical control in QDs [152, 153, 154, 155, 156, 157, 158]. An example of an experimental demonstration of Rabi rotations is shown in Fig 1.9. The red curve shows a fit to theory that incorporates dephasing tied to LA phonons. Rabi rotations are routinely used for state preparation applications such as single photon generation [159, 160]. Rabi rotations may also be carried out using two-photon transitions leading to initialization of the biexciton [125] for generating polarization-entangled photon pairs [120, 121]. Fig 1.13(a) and Fig 1.13(b) shows a comparison of Rabi oscillations of the single exciton state and two-photon Rabi oscillations of the biexciton state from Ref [125].

Quantum state preparation using ARP was first demonstrated in atomic systems

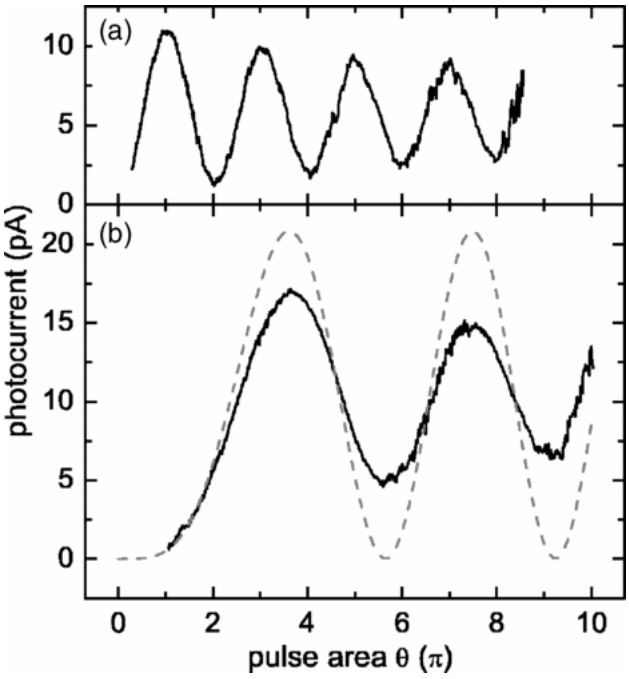

Figure 1.13: (a) Photocurrent measurement of Rabi oscillations of the single exciton state. (b) Photocurrent measurement of two-photon Rabi oscillations of the biexciton state (solid line). The dashed curve is a fit to a theoretical model. Figure adapted with permission from [125].

[48, 161]. The first demonstration of ARP in QDs was done in 2011 by two different groups using control pulses with a duration of 5 ps [162] and 40 ps [163]. These are long gate times for ARP. This was followed by in 2014 by our group, which demonstrated the first ARP gate in QDs using subpicosecond control pulses, representing a 20 fold reduction in gate time [56]. These experiments were also the first to isolate the electron-LA phonon coupling in QDs via chirp sign dependent measurements, representing a crucial advance as discussed in the next section.

State preparation using ARP has also been used to trigger single photon sources [87] and to create biexcitons in QD systems [126]. Outside of quantum information, chirped pulses have also been used to turn fluorescent emitters on and off in a STED based fluorescence microscopy scheme for high resolution imaging [164].

1.5.7 Progress in the Understanding of Electron-Phonon Coupling in QDs

A considerable research effort over the past decade has focused on understanding electron-phonon interactions in QDs as well as understanding the impact of these

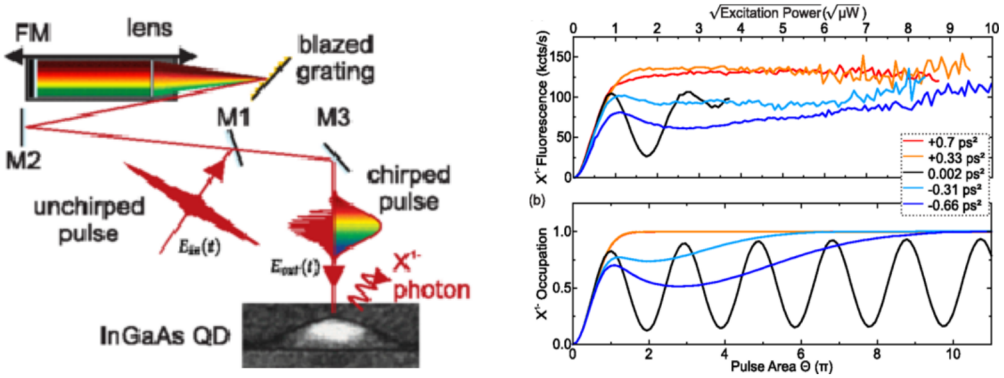

(a) (b)

Figure 1.14: Experimental demonstration of the reappearence regime for ARP, corresponding to suppression of electron-phonon dephasing. (a) Schematic diagram of the experimental apparatus used. A 4-f pulse shaper is used to control the chirp applied to the excitation laser pulse. The chirped pulse is then focused onto a QD sample using a microscope. A transmission electron microscope image of the QD is also shown. (b) The top panel shows resonance fluorescence measurement of exciton occupation as a function of the square root of the excitation power for different values of chirp and the bottom panel shows the calculated occupation of the exciton. Figure adapted with permission from [61].

processes on the performance of QDs in technologies such as qubits and single and entangled photon sources [54]. A number of theoretical methods have been used to study exciton-phonon interaction in QDs including correlation expansion [165, 166], perturbative methods [167], path-integral methods [168, 60] and master equation approaches [169, 170] and experiments have focused on characterizing the phonon sideband [80, 171] as well as the exciton-induced dephasing tied to coupling with LA phonons [158, 157, 56, 87, 61].

As discussed in Sec 1.4, an intensity dependent damping of Rabi rotations has been observed in numerous experiments (e.g. see Fig 1.9) [158, 157]. The impact of phonons on the exciton inversion efficiency in the ARP scheme was first predicted theoretically (Fig 1.10(a)) [58] and was first observed experimentally by Mathew *et al.* (Fig 1.10(b)) [56]. Shortly after the report of Mathew *et al.*, positively chirped pulses were used in a single photon source application demonstrating a $g^2(0) = 0.003(2)$ and an indistinguishability of 99.5±0.7% [87]. In addition to being a robust state preparation mechanism, the chirp sign dependence of ARP makes it a unique tool to study exciton-phonon interactions in QD systems [172]. Although

models of Rabi rotations including LA phonon coupling provided strong evidence that LA phonon coupling is the dominant dephasing process, ambiguity remained because a competing mechanism based on the coupling of the exciton with carriers in the wetting layer was also being considered [173]. The chirp-sign dependence of ARP enabled the first unambiguous proof of the dominance of LA phonon coupling [56].

The so-called "reappearance regime" discussed in Sec 1.4, for which the splitting between the dressed states is made to be higher than the available phonon energies through strong driving, was first theoretically predicted for Rabi oscillations [59]. Since this regime requires extremely large driving intensities, there have been no experimental demonstrations of this effect for Rabi rotations. This reappearance regime has been very recently observed in an ARP [61] experiment exploiting the non-zero splitting that exists between the dressed states throughout the control process. In the experiments in Ref [61] the suppression of phonon induced dephasing was manifest by the difference between positively and negatively chirped driving pulses vanishing at high pulse areas [61]. This work is shown in Fig 1.14. Because large pulse areas exceeding 8π were required to reach the reappearance regime, further work is needed to make this a practical approach to improving control fidelity. Nevertheless, the ability to completely suppress electron-phonon coupling would have dramatic implications for applications of QDs in QIP systems because high performance optical control protocols at elevated temperatures may become possible.

Exciton-LA phonon interactions have also been exploited for the preparation of exciton and biexciton states [127, 174, 175, 176]. In this approach, proposed by Glässl *et al*, a blue detuned excitation pulse is used to drive the QD, resulting in the preparation of an exciton state along with the emission of a phonon [177]. State preparation is most efficient at high pulse areas, long pulse durations and when the detuning of the control pulses matches the peak of the phonon spectral density function. Fig 1.15(a) shows photocurrent measurements of phonon assisted excitation of the exciton state and the biexciton state from Ref [175]. The blue solid line is a numerical calculation of the exciton occupation. Fig 1.15(b) shows the detuning dependence for phonon assisted excitation of the exciton. The ARP approach

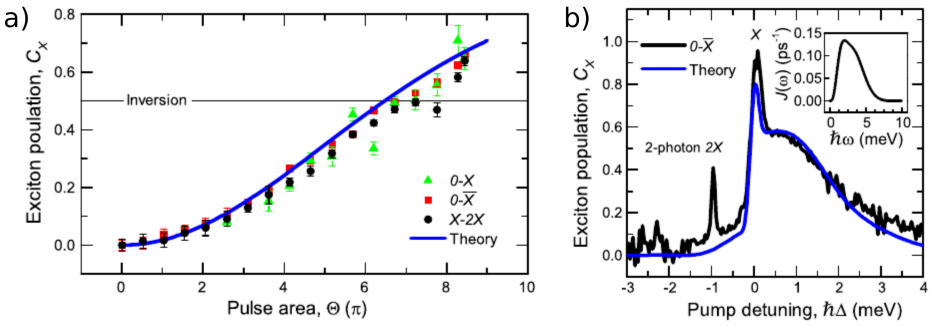

Figure 1.15: (a) Experimental demonstration of phonon assisted excitation of the exciton and the biexciton transition in a QD. Photocurrent measurement of occupation for both excitons (green triangles and red squares) and the biexciton state (black circles) using a blue detuned pulse ($\hbar\Delta = 0.83$ meV). (b) Detuning dependence of phonon assisted excitation (black solid line). The blue solid line in both panels are calculated exciton occupation. Inset: Calculated phonon spectral density function $J(\omega)$. For maximum efficiency the detuning of the excitation pulse should match the peak of $J(\omega)$. Figure adapted with permission from [175].

used in this thesis work offers better tolerance to variations in QD properties, lower laser resources and faster operation times than the phonon assisted approach.

1.6 Thesis in the Context of Existing Work

A robust preparation of excitons is an essential step in any QIP system using exciton qubits and for quantum state initialization in single photon sources. Similar optical state preparation schemes are also used for inverting biexcitons for entangled photon sources, and for manipulating the spin states of individual carriers using trion transitions. By advancing state preparation schemes using ARP, this thesis work is contributing to advancing QIP applications of QDs. High fidelity optical state preparation in QD based systems requires the state preparation protocol to be tolerant to the fluctuations in experimental conditions and dephasing processes inherent to the solid state system. Recent experimental and theoretical studies have underscored the utility of ARP as a robust state preparation protocol [172, 56, 87, 61]. This thesis work probes the limitations to the applicability of this protocol by studying the dependence of inversion efficiency on the detuning of the laser pulse from the optical transition. This work also investigates the feasibility of ARP as a method of state

preparation for an ensemble of QDs and uses it as a tool to study the dominant dephasing mechanism - phonon mediated dephasing - in QDs [38, 54]. Understanding and mitigating this dephasing channel is essential for the progress of a QD based photonic qubit system. ARP, with its chirp sign dependent coupling to the phonon bath is a unique tool to study this process [172, 56, 56, 87, 61].

1.6.1 Telecom-Compatible Quantum Control

Most early demonstrations of coherent control in QDs used interface-fluctuation QDs [178, 137, 136, 179, 180] due to their large optical dipole moments (∼100 Debye) and near infrared transition energies that are compatible with efficient silicon optical detectors and Ti-sapphire lasers. However, the random nature of their growth process results in large variability in the spatial and size distribution of the QDs, hindering the development of a scalable QIP infrastructure based on interface-fluctuation QDs. Self-assembled QDs, even though they possess lower optical dipole moments (∼25 Debye), offer a greater degree of control over the ground state transition energies and much lower growth inhomogeneities [181]. Furthermore laser annealing can be used to fine tune their optical properties [182, 183] and advances in site-controlled growth techniques allow for site-selected growth of QDs [184]. Hence the community has largely shifted towards self-assembled QDs as the choice for coherent control experiments [154, 185, 158, 162, 163, 141, 56, 87, 175, 61, 126].

The vast majority of such experiments have focused on QDs that were grown under conditions that favor the formation of small QDs with ground state optical transition energies in the range of 920 - 950 nm [154, 185, 158, 162, 163, 87, 175, 61]. *The pursuit of quantum control on telecom compatible QDs is needed to facilitate the integration of the QIP hardware based on the these QDs with classical computational systems*. However working with QDs emitting in the telecom band is challenging due to low efficiencies and high dark currents associated with InGaAs detectors. As a result, very few quantum control experiments have been carried out in this spectral window. Our research group made essential inroads in this area as the first to report quantum control experiments on both single [56] and pairs of uncoupled QDs [141] with emission compatible with telecom O band (1260 - 1360

nm) which corresponds to the low dispersion window in optical fibers. The work by Mathew *et al* demonstrating ARP for the first time in telecom compatible QDs laid the foundation for quantum light sources using semiconductor QDs [56]. Since then there have been other efforts to generate telecom compatible emitters. The majority of these experimental efforts relied on incoherent excitation of QD excitons for single photon generation [186, 187]. The single photon purity achieved in these experiments were limited by the probability of multiphoton emissions inherent to incoherent excitation. Coherent excitation using TL pulses reduced multiphoton emission probability and reported high single photon purity in telecom compatible sources in experiments conducted by Miyazawa *et al* [77]. As discussed earlier, state preparation using TL pulses is highly susceptible to fluctuations in the experimental conditions and the optical properties of the QD. *By further developing the ARP control protocol to enable the parallel initialization of multiple distinct single photon sources, the work described in this thesis work will further the development of telecom compatible quantum light sources.*

1.6.2 The Need for Optical Control Schemes Tolerant to QD Variations and Laser Pulse Fluctuations

There are a variety of applications for quantum light sources in quantum technology that would benefit from parallel triggering of a number of photon sources in parallel using the same laser pulse. For applications such as linear optical quantum computing, indistinguishability of photons is important but for other applications such as quantum cryptography, synchronous operation of sources of high single photon purity is sufficient without the need for indistinguishability. The stochastic nature of the self-assembly process results in a distribution of QD size, composition and concomitant optoelectronic properties. The development of scalable quantum networks requires synchronous operation of multiple quantum emitters that can be triggered in parallel using a single pulsed laser source [19]. For instance, the interference between photons emitted by distant sources is a key experiment in the development of photonic qubit systems and all-optical quantum repeater protocols [188]. In recent experimental demonstrations of two-photon interference involving remote QD sources, the QDs have either been excited in the wetting layer surrounding the QDs

[189, 190], or individual QDs with near-identical size and shape have been hand-picked out of the larger ensemble enabling the simultaneous resonant pumping of an excited state transition within both QDs [190, 191, 70]. The former approach compromised the performance of the system due to multiple carrier capture events, while the latter is an impractical approach for a scalable network due to the low yield of useful emitters. *It is therefore essential to develop optical control strategies that are immune to variations in QD properties.* ARP is a robust state preparation protocol that promises tolerances to moderate variations in experimental conditions and the optical properties of the QD [192, 87]. Even though there have been several demonstrations of ARP in individual QDs [162, 163, 56, 87, 61], they have all been performed using resonant control pulses. The robustness of this protocol, especially the tolerance to detuning, has never been quantified. *The experiments performed in this thesis work quantifies the detuning tolerance of ARP, supporting the application of this approach to triggering multiple inequivalent quantum light sources in parallel.*

1.6.3 Simultaneous Inversion Gates for Parallel Quantum State Initialization

The majority of quantum control experiments in QDs were done using TL control pulses [178, 137, 136, 154, 185, 158, 175]. The first experimental demonstration of quantum control using pulse shaping was the demonstration of adiabatic rapid passage using chirped pulses in 2011 [162, 163]. These experiments were done using linearly chirped pulses with a duration larger than 15 picoseconds. ARP was then demonstrated in the femtosecond domain in experiments conducted by our group [56]. We have also extensively explored the simultaneous arbitrary control of multiple quantum dots using pulse shape engineering [141, 56]. These studies included the experimental demonstration of parallel control of two uncoupled QDs [141]. In Ref [141], a single shaped laser pulse was used to implement π and 2π rotations simultaneously on two uncoupled QDs. This demonstration was followed by theoretical investigations of using pulse shaping to drive multiple QDs to an arbitrary point on the Bloch sphere [142]. These advances have laid the groundwork for parallel quantum state initialization in quantum technology applications such as optical memories and nodes in a distributed quantum network. These advances have also enabled the first exploration of the feasibility of complex instruction set

quantum computing with solid-state qubits, building upon earlier demonstrations in molecular systems [10]. Since ARP is a robust inversion gate, it would also find application for parallel quantum state initialization in these schemes as well as in circuit model implementations using QDs as qubits. *However there have been no experimental demonstrations of simultaneous ARP in multiple QDs.* This thesis work builds upon this recent experimental and theoretical research to extend optical control towards an ensemble of QDs. *Experiments performed in this thesis work demonstrated the use of ARP for parallel quantum state inversion in two different QDs with different transition energies and dipole moments for the first time.* The parallel initialization of the quantum states of multiple QDs using ARP should serve to advance the scalability of a QD based QIP system by greatly simplifying the excitation process.

1.6.4 The Suppression of Phonon-mediated Dephasing

While considerable progress has been made in understanding the impact of phonons on the optical control of excitons in QDs, only one experiment has reported the complete suppression of exciton-phonon coupling. This was observed at a pulse area over 8π [61] (see Fig 1.14). Efforts to reduce the pulse area required for quantum control would aid the development of practical QIP systems. Theoretical calculations have suggested that modifying the shape and size of the QD may enable the electron-phonon coupling strength to be engineered [60, 193]. *However no experiments exploring this potential have been reported.*

The integration of a photonic QIP system with the current telecommunications infrastructure would be simplified by the development of efficient single photon sources in the telecom band. *This thesis work studies phonon mediated dephasing in self-assembled QDs emitting in the telecom band using ARP. Our experiments demonstrated complete suppression of phonon mediated dephasing during state preparation using ARP.* We achieved a four-fold reduction in the threshold pulse area required to reach the decoherence suppression regime compared to previous experiments [61] owing to the relatively large size of the QDs studied in this work. Our calculations provide insight into the dependence of exciton-phonon coupling on the physical dimensions of the QD. Our calculations also, for the first time, probe the dependence

of electron-phonon coupling on the optical transitions (s-shell and p-shell) used for quantum control. Our work indicates that an even lower threshold for decoherence suppression should be possible by employing resonant excitation of the QD.

1.7 Structure of the Thesis

The structure of this thesis is as follows: Chapter 2 contains a detailed description of the spectral density function describing the electron-LA phonon coupling in QDs, including the methods used to calculate this function. Chapter 3 describes the experimental apparatus and techniques used in this thesis work. Chapter 4 contains the results of experimental demonstrations of suppression of phonon-mediated dephasing for the first time at low pulse areas and in telecom-compatible QDs. Chapter 5 presents the experimental measurements of the detuning tolerance of ARP in QDs, showing high exciton state preparation efficiency over a 20 meV laser tuning bandwidth using ARP. Chapter 6 presents the experimental demonstration of simultaneous ARP in multiple QDs. Conclusions are presented in Chapter 7 along with a discussion of useful directions for future work.

Chapter 2

Phonon Spectral Density Function

This thesis work contains a study of the dependence of the impact of electron-phonon coupling on the optical transitions used to drive the exciton (i.e. the s-shell or p-shell transition) as well as on the size and shape of the QD. In this chapter, a detailed description of the phonon spectral density function $J(\omega)$ is given and expressions for $J(\omega)$ for these two transitions are derived.

2.1 Dependence on Exciton Wavefunction

As discussed in chapter 1, $J(\omega)$ describes exciton phonon coupling to LA phonons and determines the influence of the phonon degrees of freedom on the dynamics of the exciton where

$$J(\omega) = \sum_q |g_q|^2 \delta(\omega - \omega_q). \tag{2.1}$$

and

$$g_q^{e(h)}(q) = F^{e(h)}(q) \frac{|q| D_{e(h)}}{\sqrt{2V\rho\hbar\omega_q}}. \tag{2.2}$$

The influence of the exciton wavefunction character on $J(\omega)$ comes through the form factor,

$$F^{e(h)}(q) = \int_V |\psi_{e(h)}(r)|^2 e^{iqr} d^3r. \tag{2.3}$$

where $\psi_{e(h)}$ is the wavefunction of the confined electron (hole). Since $F^{e(h)}(q)$ is the spatial Fourier transform of the probability density, the symmetry of the confined carrier wavefunctions in real space will dictate the symmetry of the form factor in k-space. This symmetry will then determine the frequency dependence of $J(\omega)$ via the $\delta(\omega - \omega_q)$ function in Eqn (2.1) that connects the wavevector to the frequency via the dispersion relation of the LA phonons $\omega_q = c_s|q|$, where c_s is the speed of sound in the material. As discussed in chapter 1, this frequency dependence of

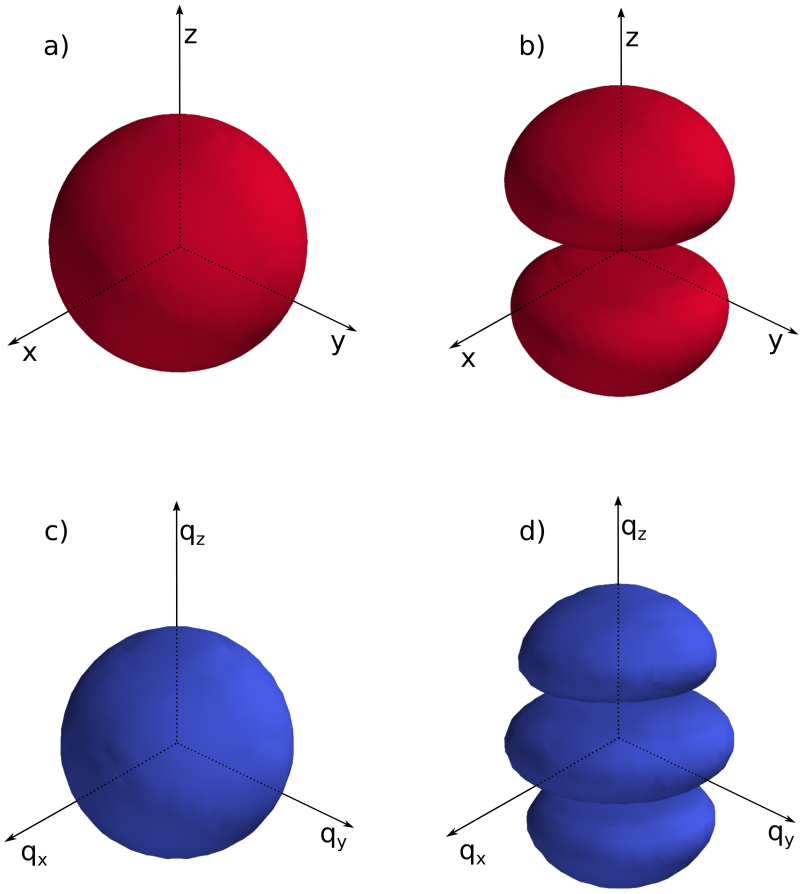

Figure 2.1: (a) Wavefunction of an electron (or a hole) for an s-shell exciton. (b) Wavefunction of an electron (or a hole) for a p-shell exciton. (c) Electron (hole) form factor for an s-shell exciton. (d) Electron (hole) form factor for a p-shell exciton.

$J(\omega)$ will depend on the size of the QD because the form factor limits the range of frequencies in $J(\omega)$. As we will show below, this frequency dependence is also determined by the shape of the QD. In this chapter, the case of spherical QDs will be considered first contrasting s and p-shell optical transitions. This will be followed by a discussion of more realistic QD shapes for self-assembled QDs, being smaller in height than in lateral extent.

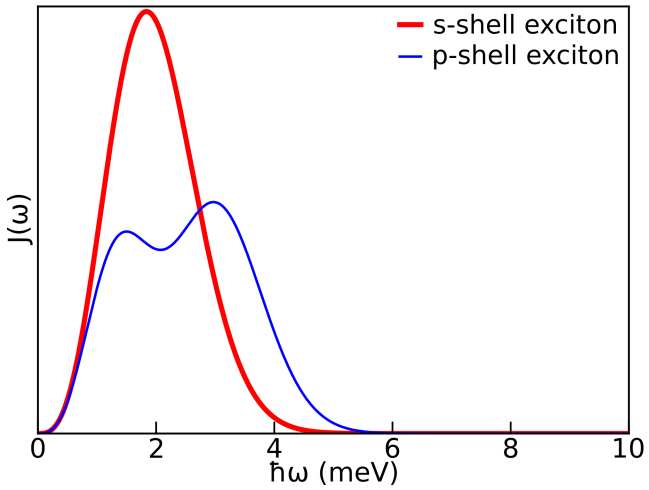

Figure 2.2: Phonon spectral density $J(\omega)$ as a function of phonon energy for an s-shell exciton (thick red curve) and p-shell exciton (thin blue curve) for a spherical QD of diameter 6.3 nm.

2.1.1 s-shell vs p-shell Excitons in Spherical QDs

As discussed in chapter 1, for the s-shell optical transition in the QD, the carrier wavefunction is given by

$$\psi_s = \frac{1}{\pi^{3/4}} \left(\frac{1}{d^2} \right)^{3/4} e^{-r^2/2d^2}. \tag{2.4}$$

in which the confinement length is taken to be the same for electron and hole wavefunctions, so we will drop the subscript $e(h)$ from here on. The resulting form factor given by

$$F_s(q) = e^{(-q^2 d^2/4)}. \tag{2.5}$$

The probability density for an electron in the s-shell shown in Fig 2.1(a) and the corresponding form factor in Fig 2.1(c). The resulting spectral density function is

$$J(\omega) = \alpha \omega^3 e^{-(\omega/\omega_c)^2} \tag{2.6}$$

where α is given by Eqn (1.49).

For the purposes of this thesis, the wavefunction of the p-shell exciton can be approximated to be that of the the first excited state of a harmonic oscillator. For a spherical QD with equal confinement lengths for electrons and holes, the exciton

wavefunction for the p-shell can be written as

$$\psi_p = \frac{\sqrt{2}}{\pi^{3/4}}\left(\frac{1}{d^2}\right)^{5/4} exp(-r^2/2d^2)\cdot z \tag{2.7}$$

in Cartesian co-ordinates, where $r = \sqrt{x^2+y^2+z^2}$ and d is the FWHM spatial width of the exciton wavefunction. Here the growth direction is taken to be along the z-axis. The probability density is then given by

$$|\psi_p|^2 = \frac{2}{\pi^{3/2}}\left(\frac{1}{d^2}\right)^{5/2} exp(-r^2/d^2)\cdot z^2 \tag{2.8}$$

This p-shell probability density is shown in Fig 2.1(b). The form factor $F_p(q)$ can then be calculated using Eqn (2.3) to be

$$F_p(q) = \frac{1}{2}(2-d^2q_z^2)\, exp(-d^2q^2/4) \tag{2.9}$$

where $F_p(q)$ is a function in q space with $q = \sqrt{q_x^2+q_y^2+q_z^2}$. Switching to spherical polar co-ordinates, Eqn (2.9) can be written as

$$F_p(q) = \frac{1}{2}(2-d^2q^2\cos^2\theta)\, exp(-d^2q^2/4) \tag{2.10}$$

This p-shell form factor is shown in Fig 2.1(d). Inserting Eqn (2.10) for each of the electron and hole wavefunctions into Eqn (2.2), the exciton-phonon coupling is given by

$$g_q^2 = \left(\frac{|q^2|}{2V\rho\omega_q}\right)\left(\frac{D_e-D_h}{2}\right)^2 (2-d^2q^2\cos^2\theta)^2\, exp(-d^2q^2/2). \tag{2.11}$$

Using Eqn (2.11) and converting the sum in Eqn (2.1) to an integral using $\sum_q \rightarrow V/(2\pi)^3\int d^3q$, we get

$$J(\omega) = \frac{V}{(2\pi)^3}\int_V \left(\frac{|q^2|}{2V\rho\omega_q}\right)\left(\frac{D_e-D_h}{2}\right)^2 (2-d^2q^2\cos^2\theta)^2 e^{(-d^2q^2/2)}\delta(\omega-\omega_q)dV \tag{2.12}$$

An analytical expression for $J(\omega)$ can be obtained by solving this integral. Using the

dispersion relation for LA phonons $\omega_q = c_s|q|$, $J(\omega)$ for this case is given by

$$J(\omega) = \alpha\omega^3 e^{-(\omega/\omega_c)^2}\left[\left(\frac{1}{5}\right)\left(\frac{\omega}{\omega_c}\right)^4 - \left(\frac{2}{3}\right)\left(\frac{\omega}{\omega_c}\right)^2 + 1\right] \tag{2.13}$$

where $\alpha = (D_e - D_h)^2/(4\pi^2\rho c_s^5)$ and $\omega_c = \sqrt{2}c/d$.

Fig 2.2 shows $J(\omega)$ as a function of frequency (or phonon energy) for an s-shell exciton and a p-shell exciton in a spherical QD of diameter 6.3 nm. For the s-shell exciton, at low frequencies $J(\omega)\sim\omega^3$ and in the high frequency limit $J(\omega)$ acts as a Gaussian function. $J(\omega)$ for the p-shell exhibits a double peak structure and a larger cut-off frequency. These differences can be traced back to the symmetries of corresponding form factors in Fig 2.1(c) and Fig 2.1(d). The larger cut-off frequency is a result of the relatively larger extent of the p-shell form factor in k-space while the double lobe feature is a result of the zeros in the $\hat{q}_z$ direction for $F^{e(h)}(q)$.

2.1.2 Implications of the Different s-shell and p-shell Wavefunction Symmetries for Optical State Preparation

As discussed in chapter 1, LA phonons interact with an exciton in the QD through the deformation potential and the impact of this interaction depends on the size of the QD. The deformation potential represents a local change in bandgap of the semiconductor due to applied stress. For example, for a Rabi rotation experiment, the control pulse drives the charge configuration of the QD at the Rabi frequency Ω. This variation in the charge configuration modulates the crystal lattice via the deformation potential at a frequency Ω. Hence the charge carriers interact with phonons that have an energy given by $\hbar\Omega$ [38]. If the wavelength of the phonon is much larger than the size of the QD, this vibrational mode essentially results in a translation of the whole QD. The effect of such a translation is negligible on the exciton dynamics. If the wavelength of the phonon is much smaller than the QD, the instantaneous change in the dimensions of the QD due to such a vibrational mode is very small because the fast oscillations in the atomic displacement average over the volume of the QD. Consequently the influence of the phonon on the state of the exciton is again negligible. Hence the interaction strength of a given vibrational mode is closely tied to the dimensions of the QD.

As discussed earlier in Sec 1.4, the interaction of the exciton with LA phonons leads to transitions between the dressed states $|\Psi_{\pm}\rangle$. The energy splitting between the dressed states is determined by the properties of the control laser pulse. According to Eqn (1.9), at any instant this separation is given by $\hbar\sqrt{\Omega^2 + \Delta^2}$. Exciton-phonon interactions are the strongest when the system is driven at Rabi energies that matches the peak of $J(\omega)$. Hence the exciton-phonon interaction strength can be minimized by driving the system at Rabi energies much higher or lower than the peak of $J(\omega)$. When a Rabi rotation experiment is performed using control pulses with a continuously varying pulse shape such as a Gaussian, the instantaneous Rabi energy due to such a pulse will always span across a region where $J(\omega)$ is non zero. As a result, the reduction of dephasing caused by exciton-phonon interactions during a Rabi rotation experiment using Gaussian pulses require extremely high pulse areas and a complete suppression is impossible.

In the case of state preparation using ARP, the energy splitting between the dressed states is always non-zero. For a positively chirped control pulse the system evolves along the lower energy dressed state. In this case a phonon absorption needs to happen for a transition to the higher energy dressed state. In contrast, for negatively chirped control pulses, as the system evolution is along the higher energy dressed state, a transition to the lower energy dressed state requires phonon emission. At cryogenic temperatures, since there are no phonons to absorb, phonon absorption is unlikely but phonon emissions are still possible. When the system is driven by a control pulse of large enough pulse area that the energy separation between the dressed states is much higher than the peak of $J(\omega)$, the exciton-phonon interaction may be suppressed completely and consequently there are no phonon transitions between the dressed states. In this case the difference between excitation using a negatively chirped pulse and a positively chirped pulse disappears.

For a large QD, the peak of $J(\omega)$ happens at low phonon energies. Hence the pulse area required to reach the suppression regime will get lower as the size of the QD gets larger. The dependence of $J(\omega)$ on the symmetry of the exciton wavefunction implies that the cut-off pulse area for the suppression of exciton-phonon coupling also depends on the exciton wavefunction. The larger extent of the form factor in k-space for the p-shell exciton relative to the s-shell exciton results in a

larger cut-off frequency for the p-shell exciton. This implies that for a given QD dimension, the threshold pulse area required for the suppression of the exciton phonon interaction is larger for the p-shell exciton compared to the s-shell exciton.

2.1.3 Excitons in Lens Shaped QDs

The case of a spherically symmetric QD is analytically solvable and so is a useful starting point, however real self-assembled QDs are typically lens-shaped, with a smaller height in comparison to their lateral extent. Atomic force microscopy measurements on a QD sample grown under similar conditions as the sample used in this work indicate that the QDs studied have an average lateral size of 17 nm and height of 5 nm. This asymmetry in the dimensions of the QD would affect the exciton-phonon interaction since the cut-off frequency is larger for smaller QDs. Hence the shortest length scale -in this case height- will determine the cut-off frequency and by extension the threshold pulse area above which the exciton-phonon interaction is suppressed.

The confining potential for such QDs can be approximated by a three dimensional harmonic potential with the same confinement length in the x and y directions and a lower confinement length in the z direction. The exciton wavefunction for the s-shell exciton for this case can be written as

$$\psi_s(x,y,z) = \frac{1}{\pi^{3/4}}\left(\frac{1}{dl_z^{1/2}}\right)e^{(-a^2/2d^2)}e^{(-z^2/2l_z^2)} \tag{2.14}$$

where $a = \sqrt{x^2+y^2}$, d is the width of the wavefunction in the lateral direction and l_z is the width of the wavefunction in the z direction. The corresponding form factor $F(q)$ can be written as

$$F_s(q) = e^{(-d^2(q_x^2+q_y^2)/4)}e^{(-l_z^2q_z^2/4)} \tag{2.15}$$

For p-shell excitons, the exciton wavefunction is given by

$$\psi_p(x,y,z) = \frac{\sqrt{2}}{\pi^{3/4}}\left(\frac{1}{dl_z^{3/2}}\right)ze^{(-a^2/2d^2)}e^{(-z^2/2l_z^2)} \tag{2.16}$$

and the corresponding form factor is given by

$$F_p(q) = \frac{1}{2}(2 - l_z^2 q_z^2) e^{(-d^2(q_x^2+q_y^2)/4)} e^{(-l_z^2 q_z^2/4)} \tag{2.17}$$

Inserting Eqn (2.15) and Eqn (2.17) into Eqn (2.2) and following the same procedure as the previous section, $J(\omega)$ for an s-shell exciton in a lens shaped QD can be written as

$$J(\omega) = A \int_V \frac{|q|^2}{\omega_q} e^{(-d^2(q_x^2+q_y^2)/2)} e^{(-l_z^2(q_z^2)/2)} \delta(\omega - \omega_q) dV \tag{2.18}$$

and for the p-shell exciton

$$J(\omega) = \frac{A}{4} \int_V \frac{|q|^2}{\omega_q} (2 - l_z^2 q_z^2)^2 e^{(-d^2(q_x^2+q_y^2)/2)} e^{(-l_z^2(q_z^2)/2)} \delta(\omega - \omega_q) dV \tag{2.19}$$

where the term $A = \frac{(D_e - D_h)^2}{(2\pi)^3 8\rho}$. In the calculations of the exciton inversion using ARP including exciton-phonon interactions in chapter 4, the integrals in Eqn (2.18) and Eqn (2.19) were solved numerically. Fig 2.3 shows $J(\omega)$ as a function of phonon energy for s-shell and p-shell excitons in a lens shaped QD of of height 6.3 nm and lateral size 12.9 nm. For comparison $J(\omega)$ for a spherical QD (originally plotted in Fig 2.2) is also shown in Fig 2.3. For this spherical QD the diameter is equal to the height of the lens shaped QD. The higher degree of confinement for the spherical QD results in a slightly larger cut-off frequency compared to the corresponding lens shaped QD. Because of the overall ω^3 factor in Eqn (2.6), in addition to the larger cut-off frequency, the magnitude of $J(\omega)$ is also larger. It can be seen that the smallest dimension of the QD plays the dominant role in determining the cut-off frequency. These results indicate that the exciton-phonon interaction can be tailored by engineering the shape of the QD.

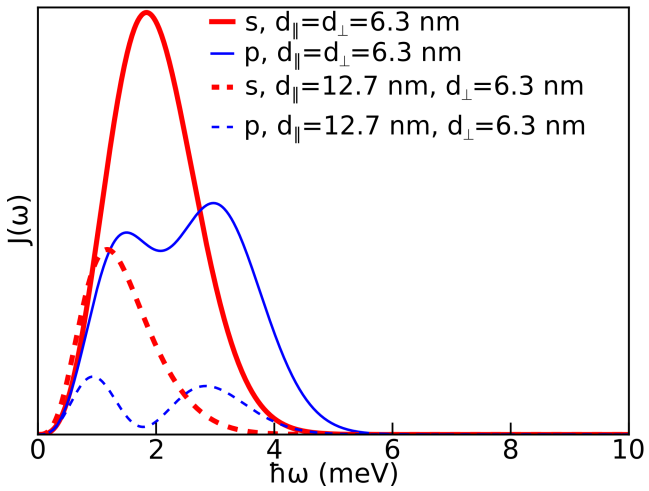

Figure 2.3: Phonon spectral density $J(\omega)$ as a function of phonon energy for s-shell (red curves) excitons and p-shell excitons (blue curves) in a spherical QD of diameter 6.3 nm and a lens shaped QD of height 6.3 nm and lateral size 12.9 nm.

Chapter 3

Experimental Methods

This chapter describes the experimental techniques used in this thesis work to carry out the quantum control of excitons in self-assembled semiconductor QDs. Section 3.1 describes the structure of the QD sample used in this work followed by a discussion of the photoluminescence spectrum of the sample and the techniques used to isolate single QD emission lines from the ensemble. Section 3.3 describes continuous wave photoluminescence (CWPL) spectroscopy and photoluminescence excitation (PLE) spectroscopy used to characterize the QD electronic structure. Section 3.4 describes the experimental setup used for quantum control experiments. Section 3.5 contains a description of the pulse shaping apparatus used for both dispersion compensation to create chirped pulses to do ARP on single QDs. Finally section 3.6 delves into techniques used to spatially and temporally characterize the control laser pulse.

3.1 InAs/GaAs Quantum Dot Sample

The QD sample used in this work (UFC-628, piece #7) was grown using molecular beam epitaxy by Dennis Deppe's group at the University of Central Florida. The typical emission wavelengths of InAs/GaAs QDs at room temperature are 1.3 μm or shorter. One of the objectives of this thesis work is to advance QDs with telecom compatible emission wavelengths for applications in quantum technology. Since photoluminescence is used for quantum state read-out in this work, the optical control experiments must be carried out at cryogenic temperatures. This required modifying the traditional growth conditions used to achieve a ground state transition wavelength at 1.3 μm at cryogenic temperatures. Thus unusually large InAs QDs on GaAs were needed. In addition, a relatively low areal density of QDs was desired to enable the spatial and spectral isolation of the s-shell emission lines from individual QDs. A schematic diagram of the sample structure is shown in Fig 3.1(a).

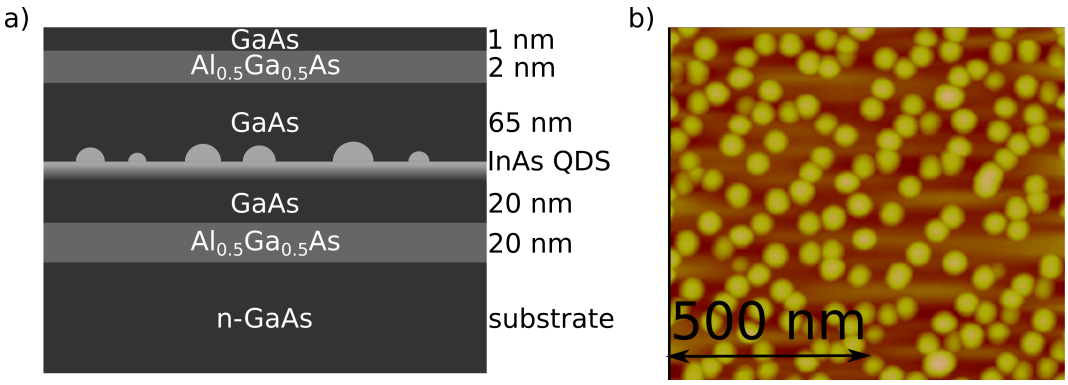

Figure 3.1: (a) Schematic diagram of the layer structure of QD sample UFC-628. (b) Atomic force microscopy image of a QD sample grown under similar conditions as the sample used in this work.

The InAs QDs are embedded in a GaAs matrix. The sample is grown on an n-doped GaAs substrate with AlGaAs layers on either side of the QD layer to prevent the diffusion of optically excited electron-hole pairs, when pumped into the GaAs barriers surrounding the QDs, away from the QD layer. Fig 3.1(b) shows an AFM image of QDs on a sample grown under similar conditions as the sample used in this thesis work. The QDs have an average height of 5 nm and the lateral dimensions lie between 15 nm and 20 nm. To achieve large, low density InAs QDs, the growth was conducted at a lower substrate temperature than usual to decrease the intermixing of gallium and indium to create an indium rich core. The confinement energy of the QDs is then further shifted to lower values by covering the dots with $In_{0.2}Ga_{0.8}As$ prior to depositing GaAs.

Fig 3.2(a) shows the ensemble PL spectrum from the QD sample at 10 K. Four peaks were observed. Using PLE spectroscopy to be discussed below, we determined that these four peaks represent emission from the s-shell and p-shell transitions in two distinct QD sub-ensembles with different average sizes. These emission peaks are indicated by dashed lines in Fig 3.2(a). The high energy subset marked with red dashed lines have a p-shell emission peak at 1152 nm and an s-shell emission peak at 1220 nm with an s-p separation of about 60 meV. The low energy subset marked with blue dashed lines have a p-shell emission peak at 1190 nm and an s-shell emission peak at 1294 nm with an s-p separation of 80 meV.

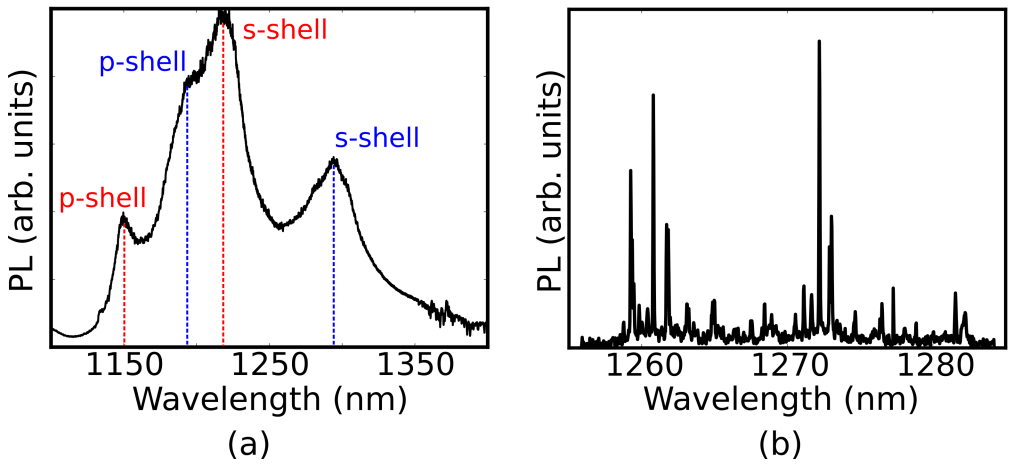

Figure 3.2: (a) Spectrally resolved ensemble PL from sample UFC-628. Red and blue dotted lines indicate PL emissions from two different subsets of QDs with different average sizes. (b) Spatially resolved micro-PL collected from the aperture M21S18.

3.2 Non-degenerate Photoluminescence Technique for Quantum State Read-out

In the experiments performed in this work, laser pulses are used to create a p-shell exciton population. The p-shell exciton then non-radiatively relaxes into the s-shell [38] which then undergoes radiative relaxation resulting in the emission of a photon that can be detected experimentally. The PL intensity from the relaxation of the s-shell exciton gives a measure of the final quantum state of the p-shell at the end of the control pulse. Fig 3.3 depicts this quantum state read-out scheme. The simplicity of this method makes it one of the earliest and the most widely used techniques for exciton state readout in QD systems [131, 154, 185, 194]. The primary advantage of this technique is that the large energy difference between the p-shell and the s-shell optical transitions facilitates the rejection of scattered pump light when detecting the weak PL emission from the single QD. The energy splitting between the s-shell and the p-shell in the samples used in this work is about 85 meV, which allows for filtering out the excitation laser with dichroic mirrors as well as a monochromator.

Other commonly used methods for quantum state read-out include photocurrent detection [195, 158, 157] and resonant fluorescence [196, 61, 197, 88, 79].

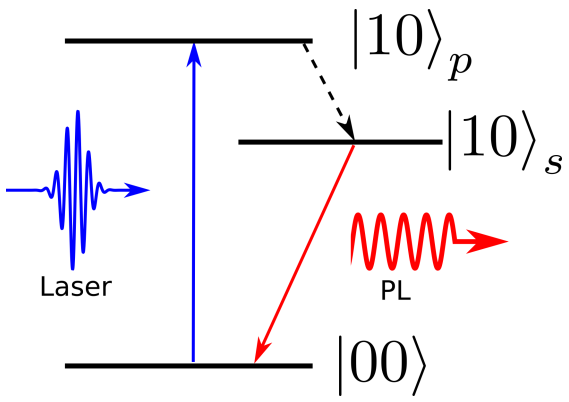

Figure 3.3: Quantum state control and readout scheme. Laser pulses couples the crystal ground state ($|00\rangle$) to p-shell exciton ($|10\rangle_p$) transition. The P-shell exciton then undergoes non-radiative relaxation into an s-shell exciton ($|10\rangle_s$). PL from radiative relaxation of the s-shell exciton gives a measure of the laser excited population.

Photocurrent measurements require QDs to be embedded in a photodiode structure and a bias voltage is then applied across the QD layer. This bias voltage induces ionization of the exciton and tunneling of carriers trapped in the QD towards opposite electrodes, giving rise to a current. One disadvantage of the photocurrent technique is that the ionization of the exciton represents a source of dephasing. In addition, it is not possible to distinguish between the excitation of unintended quantum states besides the s-shell excitation, since any excited electron-hole pair results in a current. The advantage of this technique is the convenience of electrical measurement. In resonance fluorescence measurements, optical pulses are used to excite an s-shell exciton and the intensity of the fluorescence from the radiative decay of the exciton is measured. The experimental challenge is to separate the signal photon from the much stronger scattered light from the excitation laser beam. Early experiments used orthogonal polarizations for excitation and detection along with spatial filtering where the excitation laser beam makes a large incident angle at the sample [198]. Resonance fluorescence measurements usually use samples where QDs are embedded in microcavities, planar waveguides or microlenses which enhance the coupling of emitted photons to the detection channel, which is then orthogonally polarized to the excitation beam.

The experiments involved in this work were done on QDs with p-shell transitions between 1160 nm and 1175 nm. The lower energy subset of QDs was chosen

because of their low areal density (~10 μm^{-2}). Even then a laser beam with a diffraction limited spot size (~2 μm) would illuminate about 30 QDs. With high-resolution spectral detection, this number of QDs is already low enough to enable the isolation of individual QD emission peaks. However for PL experiments for which carriers are injected into the GaAs barriers, carriers can diffuse laterally outside the excitation spot prior to being trapped by QDs and undergoing recombination. Hence additional spatial filtering is necessary to limit the spatial area of the sample for which the PL emission is detected so that isolation of individual QD emission peaks will be possible. This is done by depositing a gold mask, with sub-micron apertures, onto the surface of the sample. The mask was deposited onto the sample by CMC Microsystems using electron-beam lithography. Fig 3.4(a) shows a schematic diagram of the gold mask and a single sub mask is shown in Fig 3.4(b). Each of the sub-masks, labeled 1-25, have apertures with different diameters. The apertures are labeled by the sub-mask number and an alphanumeric index that specifies its position on a given sub-mask. Fig 3.2(b) shows the spectrally resolved PL from a 0.6 μm aperture (S18) on sub-mask 21. Discrete emission lines from individual QDs are clearly visible.

3.3 Continuous-Wave Photoluminescence Spectroscopy and Photoluminescence Excitation Spectroscopy

Continuous-wave PL and PLE spectroscopy are techniques used to characterize the electronic structure of the QDs. In continuous-wave PL, a continuous wave laser beam is used to excite carriers above the GaAs bandgap. These carriers then relax via phonon emission and carrier-carrier scattering. Some of these carriers will end up in the discrete energy levels of the QD and undergo radiative recombination. The electronic structure of the quantum dot can then be inferred by spectrally resolving the emitted light or PL.

In PLE spectroscopy, a tunable pulsed laser beam is used to directly excite carriers into the QD excited states. The carriers then non-radiatively relax to the QD ground state and undergo radiative recombination. The energy of the excited state can then be identified by scanning the wavelength of the excitation laser while measuring the PL intensity from the s-shell ground state optical transition. In this work,

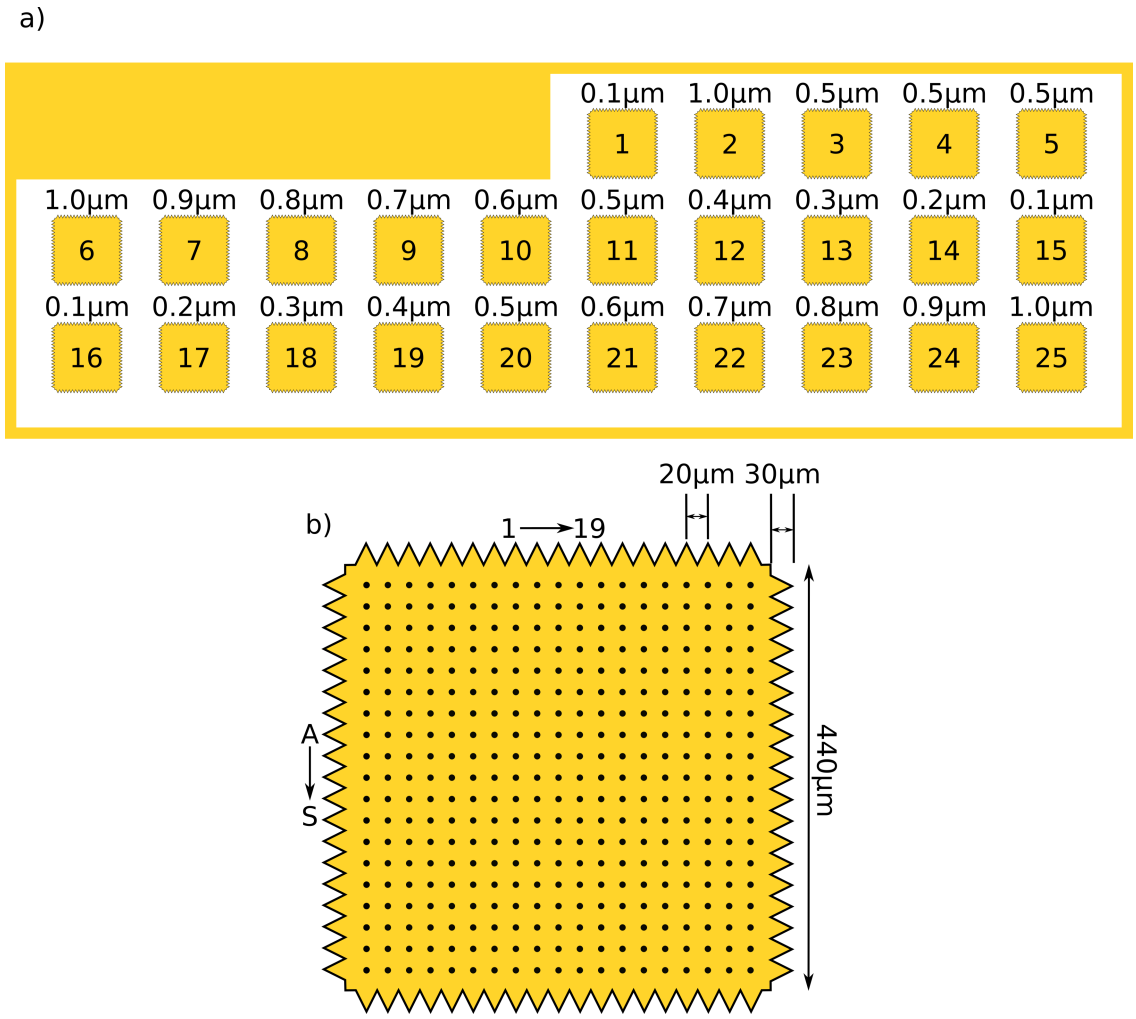

Figure 3.4: (a) Schematic diagram of the gold mask that was deposited onto the surface of the QD sample to enhance the spatial resolution of individual QD emission peaks. The gold mask is made up of 25 sub-masks each with an array of apertures of a fixed diameter indicated near the sub-mask indices. (b) Detailed schematic diagram of the sub-mask structure that makes up the gold mask on the QD sample. The apertures in the sub-mask are indexed with an alphanumeric scheme indicating the row and column they are positioned in.

the transition energy of the p-shell exciton was measured using PLE spectroscopy, by measuring PL from the s-shell exciton. PLE was used to distinguish between the two subsets of QD sizes shown by the dashed lines in Fig 3.2(a).

Since a tunable laser is required for PLE, and the only tunable laser available was a pulsed optical parametric oscillator (OPO), further effort is required to ensure sufficient spectral resolution of the PLE signal. The pulsed output from the OPO was dispersed into component frequencies using a diffraction grating in a setup similar

to the pulse shaper in Fig 3.5. A slit of width 0.1 mm was used to replace the SLM. The slit would isolate all but a single frequency component of width 1 ± 0.25 nm which is then used to excite the QD. The excitation wavelength was tuned by changing the position of the slit to let a different frequency component through.

3.4 Quantum Control Experimental Apparatus

The experimental apparatus used to do quantum control experiments in single QDs is illustrated in Fig 3.5. The laser pulses used in the experiments are generated using an infrared OPO (MIRA OPO from Coherent Inc.). The OPO produces pulses with a transform-limited duration of 120 fs at a repetition rate of 76 MHz. The OPO has a tunable wavelength between 1100 nm and 1600 nm. The laser pulses are tuned to match the p-shell transition in the QD of interest. The pulses from the OPO then pass through a $4f$ pulse shaper, which uses a 128 pixel LCD SLM in the Fourier plane (MIIPS Box 128 from Biophotonic Solutions) (See Sec 3.5 for more details about the pulse shaper). The pulse shaper is used for both dispersion compensation and to apply a chirp to the pulses. The shaped pulses are then focused onto a diffraction limited spot on the sample, which is held at 10 K in a continuous flow cryostat (ST-500 from Janis Research Company). A recirculating cryocooler (from Janis Research Company) maintains the flow of liquid helium to the ST-500 to maintain the sample temperature at 10 K throughout the experiments. A high numerical aperture microscope objective (100$\times$ Plan Apo, long working distance, NIR, infinity-corrected objective with 0.7 numerical aperture from Mitutoyo) is used to focus the laser beam onto the sample. The sample is mounted on a 3D nano-positioner (ANP101 stages with ANC300 controller from Attocube Systems AG). The nano-positioner allows the aperture of interest for a given experiment to be brought into the laser focus. The p-shell exciton excited by the laser pulse undergoes non-radiative relaxation to the s-shell exciton and the PL emitted by the s-shell exciton is then collected using the same microscope objective used for excitation. A dichroic mirror is used to separate the PL from the excitation laser light. The PL is frequency resolved using a 0.75 m focal length spectrometer (SP 2750 from Princeton Instruments) and detected using a 1024 pixel liquid nitrogen cooled InGaAs charge-coupled device (CCD) array detector (Symphony II IGA from Horiba Jobin

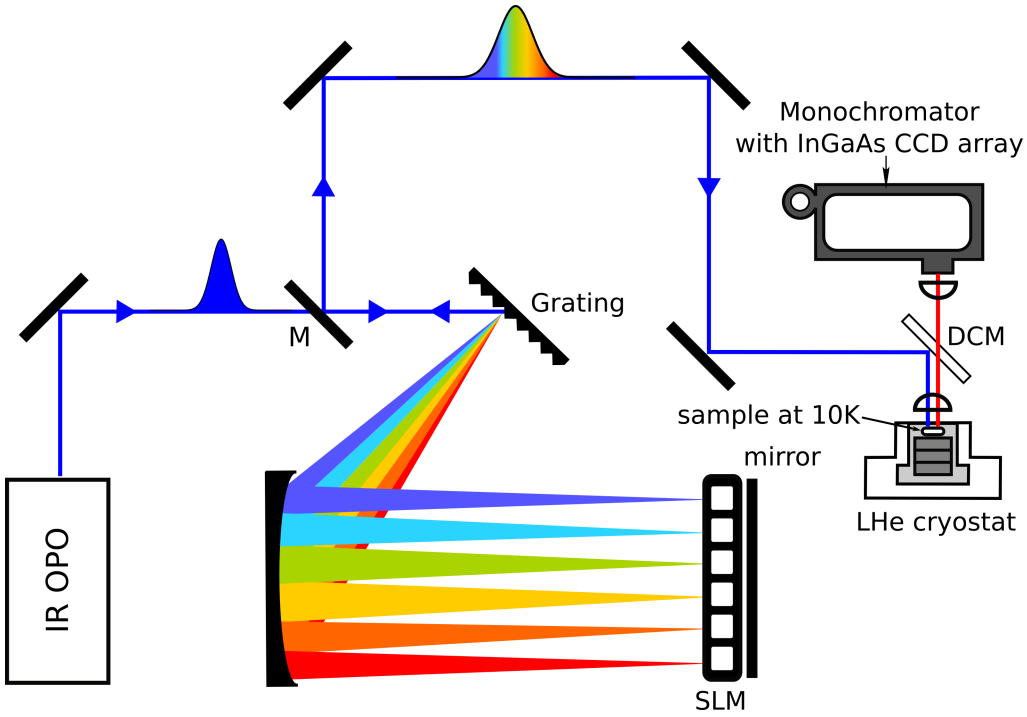

Figure 3.5: Experimental setup for quantum control experiments. Laser pulses from the OPO go through a $4f$ pulse shaper with a dual mask SLM. The shaped pulses are then reflected by a dichroic mirror and focused on to the QD sample, held at 10K, using a microscope objective. PL from the sample is filtered to remove scattered pump laser light by the dichroic mirror and then spectrally resolved and detected using a monochromator and an InGaAs charge-coupled device detector.

Yvon).

The experiments described in chapters 4, 5 and 6 report measurements of the PL intensity as a function of the average pulse power to perform Rabi rotations and ARP. A variable neutral density filter is used to control the amount of laser power incident on the sample.

3.5 Femtosecond Pulse Shaping

In the optical control schemes used in this work, the QD exciton is driven to an arbitrary quantum state by manipulating the light-matter interaction Hamiltonian. The interaction Hamiltonian may be tailored in the general case by controlling the amplitude $E_0(t)$ and/or the phase $\phi(t)$ of the control pulse. The amplitude and phase of the optical pulse are controlled using a $4f$ pulse shaper operating in a reflection

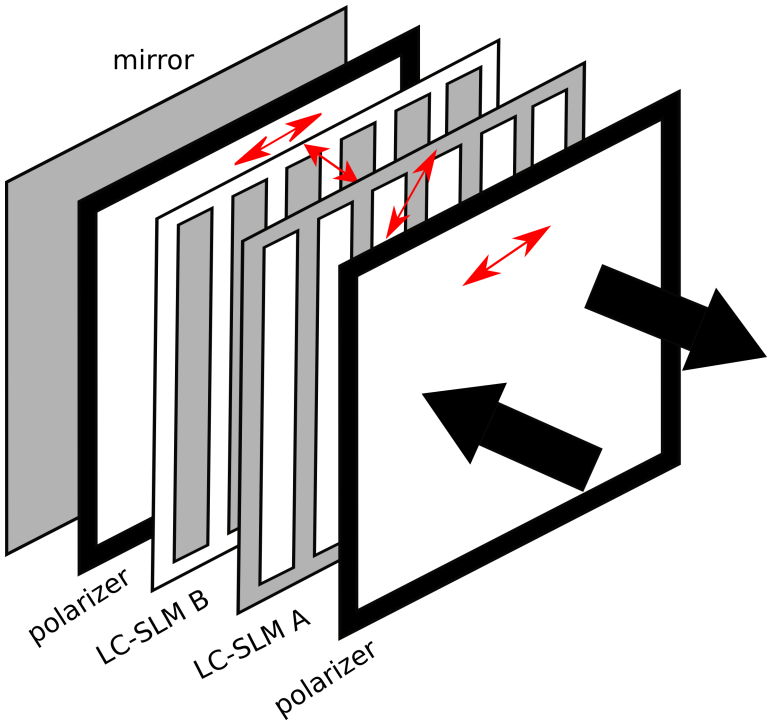

Figure 3.6: Schematic diagram of the dual mask SLM. Each mask is made up of a 128-pixel liquid-crystal array with a pixel pitch of 100 μm and a gap of 2 μm between the pixels. The optical axes of the liquid crystal arrays are oriented $\pm 45^{\circ}$ from the horizontal and they are sandwiched between a set of crossed polarizers. Red arrows indicate the optical axis orientation of each element.

configuration, as shown in Fig 3.5. The constituent frequency components of the incoming laser pulse are dispersed using a grating and then focused onto the SLM using a curved mirror. The separated frequency components are then recombined after passing through the SLM a second time. This second pass is achieved using a planar mirror to reflect the beam backwards through the same optics but with a slight vertical tilt. This tilt allows the shaped beam to be selected from the incoming (unshaped) beam at mirror M in Fig 3.5.

A schematic diagram of the SLM is depicted in Fig 3.6. The SLM consists of two 128-pixel liquid crystal retarders sandwiched between two horizontal polarizers. The optic axes of the liquid crystal retarders are aligned at 45° and -45° with respect to the polarizers. Applying a voltage across the liquid crystal elements gives rise to a birefringence. This voltage induced birefringence at a single pixel is given by

$$\phi(\omega, V) = \frac{\omega \Delta n(\omega, V) l}{c} \tag{3.1}$$

where Δn is the change in refractive index for a frequency ω on applying a voltage V, l is the thickness of the crystal and c is the speed of light. The action of the SLM on the input laser pulse can be described by a mask function

$$M(\omega) = A_M(\omega)\exp(i\Phi_M(\omega)) \tag{3.2}$$

where $A_M(\omega)$ is the amplitude mask and $\Phi_M(\omega)$ is the phase mask given by

$$\begin{aligned} A_M(\omega) &= \cos\left[\frac{\phi_1(\omega)-\phi_2(\omega)}{2}\right] \\ \Phi_M(\omega) &= \exp\left[i\frac{\phi_1(\omega)+\phi_2(\omega)}{2}\right]. \end{aligned} \tag{3.3}$$

The transmitted power depends on the difference between the birefringence induced by two retarders, while the phase is a function of the average of the two birefringences. By choosing the values of ϕ_1 and ϕ_2, both the amplitude and phase of the electric field can be independently controlled. The shaped output pulse in the frequency domain is then given by

$$\tilde{E}_{out}(\omega) = \tilde{E}_{in}(\omega)M(\omega) \tag{3.4}$$

where $\tilde{E}_{in}(\omega)$ is the Fourier transform of the input pulse. After the SLM, the frequency components are spatially recombined and the resulting control pulse $E_{out}(t)$ is the Fourier transform of $\tilde{E}_{out}(\omega)$.

The adiabatic rapid passage experiments involved in this thesis work use the pulse shaper to apply a linear chirp to the control pulses using the following phase-only mask

$$M(\omega) = \exp\left[i\frac{(\phi''(\omega-\omega_0)^2}{2}\right] \tag{3.5}$$

where ϕ'' is the spectral chirp applied and ω_0 is the center frequency of the pulse. The resulting linearly-chirped Gaussian pulse with center frequency ω_0 can be written as

$$E(t) = E_0\exp\left[\frac{-t^2}{\tau^2} - i\omega_0 t - i\alpha t^2\right] \tag{3.6}$$

where the frequency sweep rate α is given by

$$\alpha = \frac{2\phi''}{(\tau_T L^2/2\,ln2)^2 + (2\phi'')^2} \tag{3.7}$$

where τ_{TL} is the TL pulse width.

While a 4-f pulse shaper can impart arbitrary pulse shapes onto a laser pulse, the upper and lower bounds of the temporal features that can be implemented are determined by the resolution of the optical elements and the finite transform-limited duration of the input pulse. The latter is characterized by the time-bandwidth product of the input laser pulse, which for a Gaussian pulse is given by

$$\delta t \Delta f \geqslant 0.44 \tag{3.8}$$

where δt is the pulse duration and Δf is the frequency bandwidth of the pulse. A finite lower limit for the time-bandwidth product is a consequence of the Fourier transform relationship between time and frequency. The upper bound determining the longest possible temporal feature of the pulse is set by the finite spot-size of the laser beam and the resolution of the diffraction grating. This spatiotemporal coupling can be understood by writing the spectral amplitude of the electric field immediately after the SLM.

$$E_{out}(x,\omega) = E_{in}(\omega) e^{-(x-a\omega)^2/w_0^2} M(x). \tag{3.9}$$

Here $M(x)$ is the physical masking function, $a = x/\omega$ is the spatial dispersion and w_0 is the spot-size of a single frequency component given by

$$\begin{aligned} a &= \frac{\lambda^2 f}{2\pi c d \cos(\theta_d)} \\ w_0 &= \frac{\cos(\theta_{in})}{\cos(\theta_d)} \left(\frac{f\lambda}{\pi w_{in}} \right) \end{aligned} \tag{3.10}$$

where w_{in} is the input beam spot-size, c is the speed of light, d is the grating period, λ is the wavelength, f is the focal length of the curved mirror and θ_{in} (θ_d) is the input (diffracted) angle. $E_{out}(x,\omega)$ in eq 3.9 is in general a non-separable function of space and frequency. The wavelength dependence of a results in varying amounts

of diffraction for the different frequency components of the incoming pulse and this results in non-zero amplitudes for higher order Hermite-Gaussian modes. When the higher order Hermite-Gaussian modes are filtered out, the spectral mask function can be written as

$$M(\omega) = \left(\frac{2}{\pi w_0^2}\right)^2 \int dx M(x) e^{-2(x-a\omega)^2/w_0^2}. \tag{3.11}$$

Equation 3.11 shows the spectral mask $M(\omega)$ as a convolution of the physical masking function and the Gaussian intensity profile of the spectral components. This determines the spectral resolution $\delta\omega$ of the pulse shaper, given by

$$\delta\omega = (ln2)^{1/2} w_0/a \tag{3.12}$$

which in turn determines the maximum temporal window T specified by

$$T = \frac{4ln2}{\delta\omega} = \frac{2(ln2)^{1/2} w_0 \lambda_0}{cd\cos(\theta_i)}. \tag{3.13}$$

The pulse shaper as depicted in Fig 3.5 makes use of a plane ruled reflectance grating of blaze wavelength 1.2 μm, blaze angle 22° and a groove period of $1/600$ mm in Littrow configuration with $\theta_{in} = \theta_d = 22^\circ$. For an input beam diameter of 3.5 mm, centered at 1160 nm with a bandwidth of 18 nm, the maximum temporal window T is 12.5 ps and the minimum temporal window δt is about 100 fs.

3.6 Pulse Characterization

Optical quantum control schemes rely on the precise characterization of the laser pulse parameters such as spectral intensity, phase, duration and the focused spot size at the sample. This section describes the techniques employed in this work to characterize the control laser pulse.

3.6.1 Dispersion Compensation

As it traverses through various optical elements in the setup, the laser pulse suffers dispersion, meaning that ϕ becomes dependent on time in an unintended manner. It is critical that these phase distortions are corrected prior to applying the intended phase mask for a given quantum control experiment. In our setup, dispersion compensation is achieved using a phase retrieval technique called multiphoton intrapulse interference phase scan (MIIPS). MIIPS is a single beam technique that uses the phase dependence of the spectrum of second-harmonic generation (SHG) to calculate the spectral phase $\phi(\omega)$ accrued due to dispersion. Once $\phi(\omega)$ is known, a mask function may be applied to compensate for it. In practice, this mask function is added to the intended phase mask used for quantum control.

Fig 3.7 shows the MIIPS setup. The MIIPS algorithm is applied to the laser pulse at an equivalent focus to the sample created by inserting a flat mirror prior to the cryostat. The laser beam after passing through a 4-f pulse shaper is focused onto a β barium borate (BBO) crystal. The SHG light generated by the BBO is focused into an optical fiber which is connected to a spectrometer (USB4000 from Ocean Optics). The 4-f pulse shaper applies a reference phase $f(\omega)$ to the pulse, which is varied until the spectral phase ϕ is compensated. The SHG spectrum is used as feedback for this iterative compensation process, where the maximum SHG light at each ω indicates optimal dispersion compensation.

The spectral dependence of the SHG intensity is given by

$$I(2\omega) \propto \left| \int |E(\omega+\Omega)||E(\omega-\Omega)| exp\left\{i[\phi(\omega+\Omega)+\phi(\omega-\Omega)]\right\} d\Omega \right|^2 \tag{3.14}$$

The SHG intensity will be maximum when the phase factor $\phi(\omega+\Omega)+\phi(\omega-\Omega)$ in Eqn 3.14 is zero, which is the case for a transform-limited pulse. The phase distortions can be compensated if the reference spectral phase applied by the pulse shaper $f(\omega) = -\phi$. The reference phase applied by the pulse shaper is of the form:

$$f(\omega) = \alpha \sin(\gamma\omega - \delta) \tag{3.15}$$

In order to find the compensation phase for the spectral phase ϕ, the phase factor

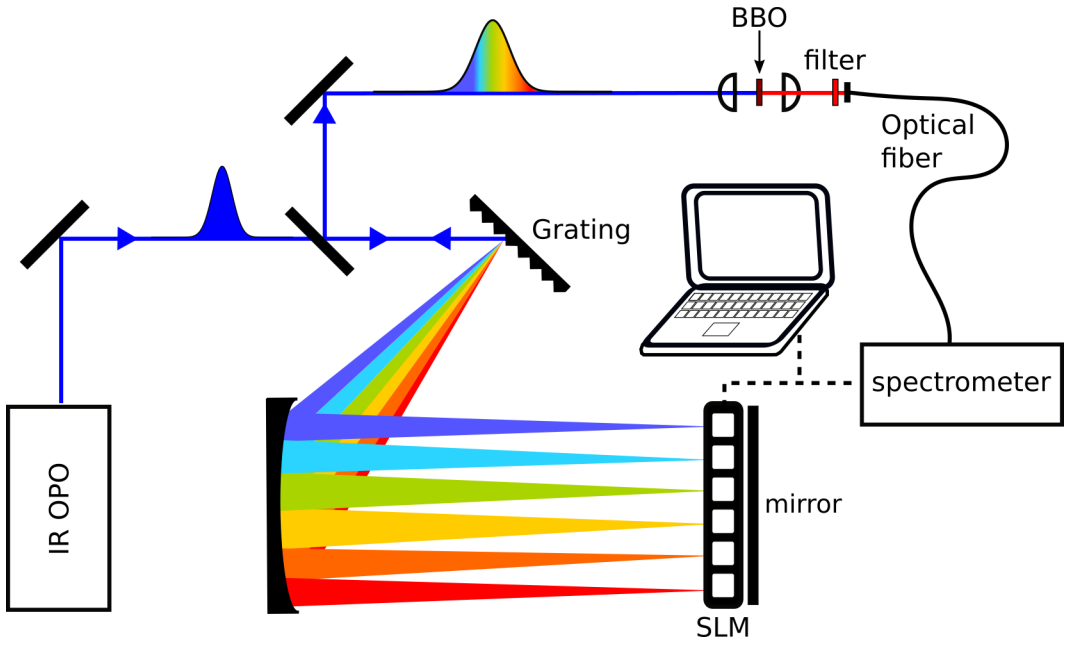

Figure 3.7: Experimental setup for dispersion compensation using MIIPS. Laser pulses from the OPO after passing through a $4f$ pulse shaper are focused into a BBO crystal. The SHG light generated by the BBO is then coupled to a spectrometer through an optical fiber. The MIIPS algorithm uses the light measured by the spectrometer as feedback where the maximum SHG light at each ω determines the optimal phase mask for dispersion compensation.

δ in Eqn 3.15 is varied between 0 and 4π. Typical values for α and γ are 1.5π and 100 fs, respectively. Once the optimum compensation phase mask is found, the MIIPS routine outputs a value of the ratio τ/τ_{TL}, where τ is the actual pulse duration and τ_{TL} is the transform-limited pulse duration determined from the measured pulse spectrum. After the iterative compensation process, the pulse duration is typically within 2% of the shortest possible pulse duration for a given bandwidth, *i.e.*, $\tau/\tau_{TL} \leq 1.02$.

3.6.2 Laser Spot Size Measurement

The effective intensity of the control laser pulse seen by the QD depends on the spot size of the laser on the sample. For example, the average laser power P_{avg} required for a Rabi rotation of Θ radians is given by [199],

$$P_{avg} = \left(\frac{1.76}{\tau_{TL}}\right)\left(\frac{\hbar\Theta}{\mu\pi}\right)^2(\pi w^2)(c\epsilon_0 n)\nu_{rep} \tag{3.16}$$

where τ_{TL} is the transform-limited pulse duration for a sech^2 pulse, μ is the transition dipole moment, w is the spot size of the laser, n is the refractive index and ν_{rep} is the repetition rate of the laser. In this work, the spot size of the laser on the sample was measured using a knife-edge technique. An edge of the gold mask on the GaAs surface of the sample was used as the knife in this case, enabled by the large difference in reflectivity of the bare GaAs surface and the surface of the gold. The reflected light was measured using an InGaAs photodiode. The sample was scanned from the mask region to the bare GaAs region using the nano-positioner, with a lateral resolution of 150 nm. Modeling the drop in reflectivity as a step function and assuming the laser beam has a Gaussian spatial mode, the intensity of the reflected light seen by the photodiode can be written as

$$I(x) = I_0 + \frac{\Delta I}{2} erfc\left[\sqrt{(2)}\left(\frac{x_0 - x}{w}\right)\right] \tag{3.17}$$

where x is the distance moved, x_0 is the position of the metal-semiconductor edge, ΔI is the difference in reflected light intensity between gold and the GaAs surface, and w is the spot size. Fitting the photodiode output to Eqn 3.17 gives a spot size of 1.7 $\pm$ 0.1 μm, where the uncertainty was obtained from the standard deviation of the fitting parameters.

Chapter 4

Low Threshold Suppression of Decoherence Tied to Exciton-Phonon Coupling in Telecom-Compatible Quantum Dots

Authors: A Ramachandran[1], G. R. Wilbur[1], S. Freisem[2], D. G. Deppe[2], and K. C. Hall[1]

[1]Department of Physics and Atmospheric Science, Dalhousie University, Halifax, Nova Scotia B3H4R2, Canada
[2]The College of Optics and Photonics, University of Central Florida, Orlando, Florida 32816-2700, USA

This chapter contains a manuscript that is being prepared for submission to Nano Letters. Ajan Ramachandran developed the techniques, performed the experiments and the data analysis. Grant Wilbur assisted with data collection and numerical calculations. Sabine Freisem and Dennis Deppe developed and grew the sample. Kimberley C. Hall and Ajan Ramachandran conceived and designed the experiments. Ajan Ramachandran and Kimberley C. Hall wrote the manuscript with input from all authors.

4.1 Abstract

We demonstrate full suppression of dephasing tied to deformation potential coupling of confined electrons to longitudinal acoustic (LA) phonons in optical control experiments on large semiconductor quantum dots (QDs) with emission compatible with the low-dispersion telecommunications band at 1.3 μm. By exploiting the sensitivity of the electron-phonon spectral density to the size and shape of the QD, we demonstrate a four-fold reduction in the threshold pulse area required to enter the decoupled regime for exciton inversion using adiabatic rapid passage (ARP). Our

calculations of the quantum state dynamics provide good agreement with our experimental results and indicate that the symmetry of the QD wave function provides an additional means to engineer the electron-phonon interaction. Our findings will support the development of solid-state quantum emitters in future distributed quantum networks using semiconductor QDs.

4.2 Manuscript

A quantum emitter is a physical system that can be used to encode a quantum state via some internal degree of freedom (e.g. exciton, electron spin, valley) and is coupled to light via a dipolar transition that enables the conversion of that quantum state into the state of a photon and vice versa. Such quantum emitters can be applied to quantum light sources for applications in quantum cryptography or quantum imaging [65, 66] and a collection of coupled quantum emitters can be used to realize a small quantum simulator or quantum memory node in a distributed quantum network [19]. Among solid-state quantum emitter systems, semiconductor QDs are particularly attractive due to their high radiative quantum efficiencies [19], their strong optical coupling [200, 178, 153], the ability to achieve inter-QD interactions via confined optical modes [20, 46] or direct tunneling [144, 146, 143], and their tunable emission in the range of standard telecommunication wavelengths essential for long-distance quantum information transfer [65, 201, 202]. The performance of QD-based single and entangled photon sources has continued to improve over the past decade[75, 203, 204, 90, 191, 88, 119, 205, 121, 206, 207, 109, 208], with the latter recently surpassing the commercial standard based on parametric down conversion [65]. Progress towards the development of functional quantum networks using QDs has also occurred at a remarkable pace, including demonstrations of fast [56] and arbitrary [209, 141, 142, 210, 139, 140] single qubit rotations, two-qubit gates [144, 146, 143, 137, 138], spin-photon entanglement [211, 212, 213], spin-spin entanglement [214, 151], and quantum state transfer [215, 214].

The performance of the above technologies using QDs is limited by dephasing caused by coupling of the quantum-confined electrons with phonons in the

solid-state environment. For optically-mediated quantum state control, the dominant decoherence channel is deformation potential coupling to longitudinal acoustic (LA) phonons, which reduces the fidelity of state manipulation through resonant phonon-induced transitions between the dressed states of the QD in the presence of the laser field [38, 54, 197]. These transitions lead to a strong damping of Rabi oscillations [158, 157] and limit the effectiveness of exciton inversion schemes using adiabatic rapid passage (ARP) at elevated temperatures [56, 87].

The finite size of the QD provides an opportunity to mitigate the impact of the electron-phonon interaction on the quality of optical control by limiting the range of phonon frequencies that can contribute to dephasing [38, 54]. This limited range of coupled phonon modes, which becomes smaller the larger the QD, may be combined with the use of short laser pulses to suppress resonant phonon transitions by increasing the energy separation between the dressed states beyond the coupled phonon frequency band [56, 157, 59, 193, 60, 61, 126] . Here we exploit this feature to demonstrate full suppression of phonon-mediated decoherence in large QDs emitting at 1.3 μm. The use of large, telecom-compatible QDs in our experiments is not only attractive for future long-distance quantum communication in distributed quantum networks [19, 65], but also dramatically reduces the strength of the laser field needed to reach the decoupling regime for the electron-LA phonon interaction. Through calculations of the quantum state dynamics incorporating LA-phonon coupling, we analyze the dependence of the threshold pulse area for decoherence suppression (Θ_T) on the size and shape of the QD and contrast Θ_T for resonant and quasi-resonant control schemes. While the latter schemes offer considerably larger brightness in single-photon source applications [65], we show that larger pulse areas are required to reach the decoupling regime due to the differing wave function symmetry between the QD ground and first excited state. The demonstration of low-threshold, high-fidelity inversion in our experiments points to the potential for practical QD-based quantum light sources that could be initialized in parallel and operated at elevated temperatures.

We demonstrate decoherence suppression using ARP, for which frequency-swept optical control pulses are used to invert the exciton transition in the QD [216, 49]. The control pulse is given by $E(t) = \frac{1}{2}E_p(t)\exp\left[-i(\omega_l t + \alpha t^2)\right]$, where $E_p(t)$ is the

pulse envelope, ω_l is the center frequency, and α is the temporal chirp. The energies of the dressed states of the QD in the presence of this control pulse ($|\Psi_\pm\rangle$) are depicted in Fig. 4.1(a). The splitting between the dressed states is given by $\sqrt{\Omega(t)^2 + \Delta(t)^2}$, where $\Omega(t) = \frac{\mu E_p(t)}{\hbar}$ and $\Delta(t) = -2\alpha t$ are the instantaneous values of the Rabi frequency and the detuning of the laser field from the exciton transition, respectively. For a sufficiently strong pulse intensity and chirp, the control process is adiabatic and the system remains in one of the two dressed states while the admixture of the bare QD states ($|0\rangle$ and $|1\rangle$) evolves, resulting in inversion of the two-level system. The sign of α determines which of the two dressed states $|\Psi_\pm\rangle$ the system traverses as it evolves from $|0\rangle$ to $|1\rangle$.

LA-phonons can cause resonant transitions between the dressed states during the optical pulse (depicted by dashed arrows in Fig. 4.1(a)), representing the dominant contribution to dephasing. These transitions can occur provided that phonons with energies equal to the dressed state splitting are coupled to the exciton [38, 54]. The exciton-LA phonon coupling strength is dictated by the phonon spectral density $J(\omega) = \sum_{\mathbf{q}} |g_{\mathbf{q}}|^2 \delta(\omega - \omega_{\mathbf{q}})$ where $\omega_{\mathbf{q}} = c_s q$ is the LA phonon frequency for bulk GaAs phonon modes, which provides an accurate treatment for electron-phonon coupling within the strained InGaAs QD due to the similar elastic properties of the QD and the barrier layers [217]. The coupling strength is given by $g_{\mathbf{q}} = \frac{q}{\sqrt{2V\rho\hbar\omega_{\mathbf{q}}}}(D_e - D_h)P[\psi(\mathbf{r})]$, where $D_{e(h)}$ is the deformation potential constant for the electron (hole), V is the volume of the unit cell, ρ is the mass density, c_s is the speed of sound, and $P[\psi(\mathbf{r})] = \int d^3\mathbf{r}|\psi(\mathbf{r})|^2 e^{i\mathbf{q}\cdot\mathbf{r}}$ is the form factor for the QD. For the simplest case of a spherical QD, $J(\omega) = A\omega^3 e^{-(\omega/\omega_c)^2}$ [Fig. 4.1(b)], where $\omega_c = 2\sqrt{2}c_s/d$ is a cutoff frequency that depends on d, the diameter of the QD. The smaller the QD, the larger $J(\omega)$ and ω_c (i.e. the stronger the coupling at a given phonon frequency and the wider the bandwidth of coupled phonon modes).

At any instant during the control pulse for which the dressed state splitting is much larger than ω_c, the electron and LA-phonons are decoupled and dephasing is suppressed. This decoupling regime has been studied theoretically for both Rabi rotations [59, 60] and ARP [193]. For ARP, the use of a frequency-swept optical pulse leads to a nonzero dressed state splitting at all times during the control process. This has the consequence that complete suppression of decoherence is possible for

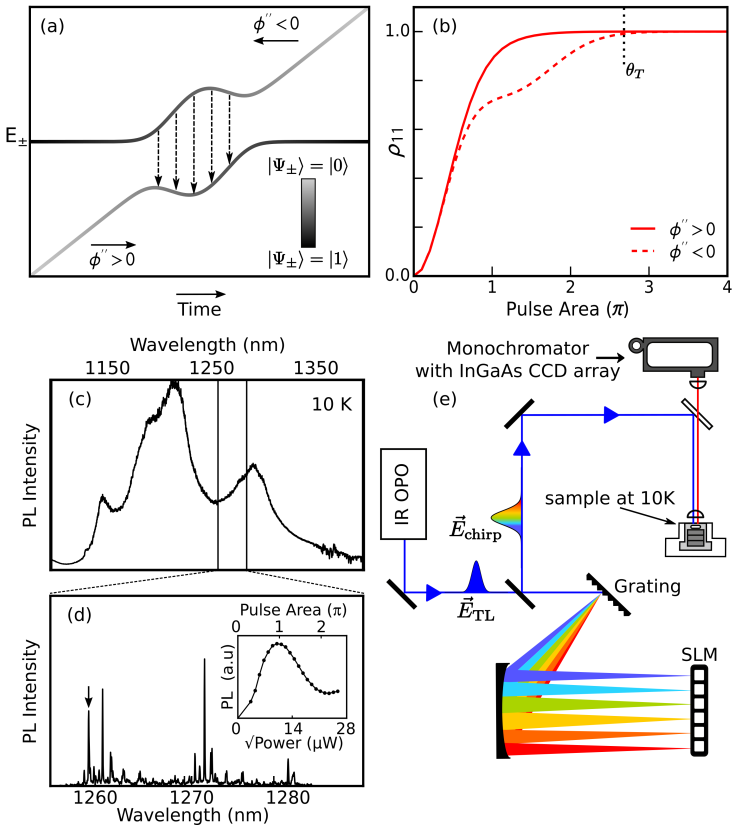

Figure 4.1: (a) The temporal evolution of dressed states energies $|\Psi_\pm\rangle$ during ARP induced by a frequency-swept optical pulse. The system evolves from $|0\rangle$ to $|1\rangle$ in the higher- (lower-) energy dressed state for negative (positive) pulse chirp. The dashed arrows indicate transitions between the dressed states caused by LA phonon emission. At elevated temperatures, upward transitions caused by phonon absorption would also occur. (b) Calculated occupation of the exciton ($|1\rangle$) as function of pulse area for positive (solid) and negative (dashed) pulse chirp. Θ_T is the threshold pulse area to reach the decoupled regime for the electron-phonon interaction, defined in the theoretical calculations as the pulse area for which the difference between the curves is 1%. (c) PL spectrum of the QD sample under continuous-wave excitation at 830 nm. (d) Micro-PL showing the GS emission from individual QDs. Inset: Rabi rotation measurement on the QD marked with the arrow. The position of the first peak with respect to laser power is used to determine the relationship between average power and pulse area for each QD (e) Schematic diagram of the quantum control apparatus. Pulses from the OPO laser source are dispersion-compensated and chirped using a 4-f pulse shaper. Chirped control pulses resonant with the ES transition are focused onto the sample using a microscope objective and the final quantum state of the exciton is read-out through detected photoluminescence on the GS transition.

large enough values of $\Omega(t)$ and $\Delta(t)$. Importantly, this suppression occurs at all temperatures, with substantial implications for the development of practical quantum emitters systems for distributed quantum networks. For such applications, a low threshold pulse intensity for decoherence suppression is desirable to lower the power requirements of the quantum network and to facilitate parallel quantum state initialization of individual quantum emitters using a single laser source [191, 121, 150, 151, 70]. Due to the dependence of the phonon spectral density on the form factor, one can engineer the rate of decoherence tied to exciton-LA phonons by varying the size and shape of the QD.

Adiabatic rapid passage was carried out on an In(Ga)As/GaAs QD structure grown using molecular beam epitaxy under conditions to generate large QDs with a ground state emission near 1.3 μm at cryogenic temperatures. The ensemble photoluminescence (PL) is shown in Fig. 4.1(c). To isolate a collection of QDs for quantum control experiments, a metallic mask containing an array of apertures was deposited onto the sample surface using e-beam lithography. The results of microPL experiments on a 0.6 μm aperture is shown in Fig.4.1(d). Quantum control was carried out under near-resonant pumping, corresponding to excitation of the first excited state (ES) optical transition in the QD, with detection of the PL emitted from the ground-state (GS) optical transition. The laser source used is an optical parametric oscillator. A 4f pulse shaper was used for both dispersion compensation and to impose spectral chirp (ϕ''). ϕ'' is related to the temporal chirp α by $\alpha = 2\phi''/[\tau_0^4/(2\ln(2))^2 + (2\phi'')^2]$, where τ_0 = 120 fs is the transform-limited pulse width. For all experiments, the sample was held at 10 K in a liquid-helium flow-through microscopy cryostat. A high numerical aperture objective was used for pumping the QDs and collecting the emitted GS PL. The PL was detected using a 0.75 m monochromator and a liquid-nitrogen cooled InGaAs array detector.

The decoupling regime for exciton-LA phonon coupling may be detected experimentally by comparing the exciton inversion for positive and negative values of pulse chirp [56]. As shown in Fig. 4.1(a), for negative (positive) chirp, the system evolves from $|0\rangle$ to $|1\rangle$ on the higher- (lower-) energy dressed state. At low temperatures, phonon emission contributes to dephasing by inducing downward transitions between the dressed states but phonon absorption is suppressed. Phonon

coupling therefore impacts the quantum control process only for state evolution on the higher-energy dressed state (i.e. for negative pulse chirp). The chirp-sign dependence of the exciton occupation calculated using a density matrix approach [139] incorporating deformation coupling to LA phonons following the model presented in Ref.[55] is shown Fig. 4.1(b). For positive pulse chirp within the adiabatic regime, the exciton occupation is insensitive to changes in pulse area reflecting the robustness of the ARP control scheme for exciton inversion. The difference between the exciton occupations for positive and negative pulse chirp varies with pulse area following the shape of $J(\omega)$: the difference is a maximum when the dressed state splitting matches the peak value of $J(\omega)$, and drops for both larger and smaller pulse areas. For pulse areas well above ω_c, the optically-driven system is decoupled from LA-phonons. To quantify the onset of the decoupled regime in the theoretical calculations, we define the threshold pulse area Θ_T as that for which the exciton occupation for negative chirp reaches 1% of that for positive chirp.

The results of ARP experiments on three different QDs are shown in Fig. 4.2(a)-(c). The convergence of the PL intensities for negative and positive pulse chirp for all QDs indicates complete suppression of decoherence tied to electron-LA phonon coupling. The threshold pulse area required to reach the decoupling regime varies between QDs due to their slight differences in size and/or shape. These differences are also reflected in the variation in the GS emission wavelength (1.259 μm to 1.273 μm for the QDs in Fig. 4.2). The calculated chirp sign dependent state dynamics for a lens-shaped QD ($d_{\parallel}$ = 7.3 nm, $d_{\perp}$ = 6 nm) are shown in Fig. 4.2(d), capturing the general trends seen in the experimental curves. The measured values of Θ_T are in the range 2.2π to 3.5π.

Decoherence suppression is observed in our experiments at much lower pulse areas than in previous quantum control experiments on QDs [56, 158, 157, 61, 126]. In experimental demonstrations of Rabi rotations, which have reached pulse areas as large as 14π [158, 157], the maximum Rabi frequencies used were large enough to detect the nonmonotonic dependence of damping on pulse area near the peak of $J(\omega)$ but were still well below the decoupling regime [158, 157]. In recent experiments involving ARP on excitons [61, 126], the decoupling regime

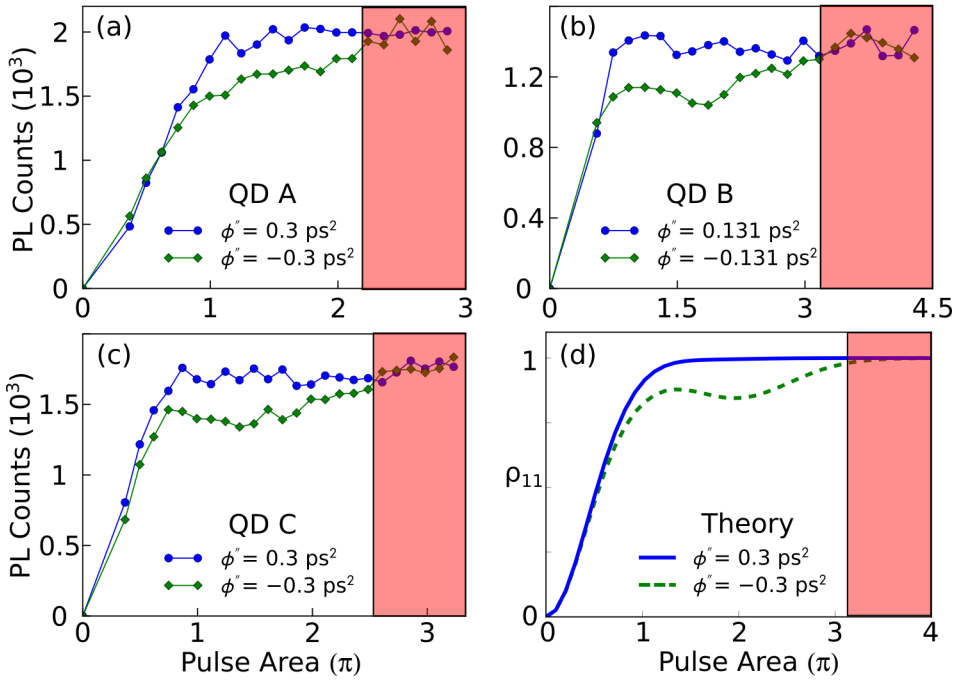

Figure 4.2: (a)-(c) PL intensity versus pulse area for positively- and negatively-chirped control pulses for three different QDs (QD A, QD B and QD C) with GS emission wavelengths at 1259 nm, 1273 nm and 1265 nm respectively. (d) Calculated exciton occupation for chirped-pulse excitation on the ES transition for a QD with $d_\perp = 6.0$ nm, $d_\parallel = 7.3$ nm. For these calculations, the 1/e point of the GS wave function of a simple-harmonic oscillator was taken as the QD dimension, and the ES is the corresponding p-orbital with in-plane cylindrical symmetry. The range of pulse areas with suppressed exciton-LA phonon coupling is indicated by the shaded box.

was reached at the end of the range of experimentally-accessible pulse areas, corresponding to a value of Θ_T exceeding 8π. The 4-fold smaller values of Θ_T in Fig. 4.2 reflect the much larger QDs used in our experiments, with GS emission wavelengths close to 1.3 μm in contrast to the 930-950 nm emitting QDs used in previous work [158, 157, 61, 126].

Our quantum control experiments were carried out under quasi-resonant pumping (i.e. the laser was tuned to the ES transition in the QD). Both resonant and quasi-resonant excitation schemes have been used in high-performance single photon sources [75, 203, 204, 90, 191, 88, 119, 205, 121, 206, 207, 109][1]. As both

[1]For ES pumping, the indistinguishability is typically lower than for GS pumping due to timing jitter [65], which is expected to be less prominent in the QDs studied here due to rapid ES to GS carrier relaxation times of a few picoseconds or less [218, 219, 220].

pumping schemes suffer from decoherence tied to LA-phonon coupling and previous theoretical models have only considered the case of GS pumping [38, 54], it is instructive to compare the two pumping schemes with regard to the coupling strength and threshold pulse area required for decoherence suppression. Fig. 4.3(a) shows the calculated spectral density for GS and ES wave functions in both spherical and lens-shaped QDs. The size dependence of $J(\omega)$ for the GS exciton is consistent with earlier studies showing stronger coupling in the spherical QD due to the larger degree of quantum confinement [193, 60]. There are two notable differences between the spectral density for optical driving of the GS and the ES: $J(\omega)$ for the ES exhibits a double peak structure and is characterized by a larger cutoff frequency. These differences may be traced back to the form factors for the GS and ES wave functions [Fig. 4.3(a), inset]. The lobed structure of the ES form factor is the origin of the dip in $J(\omega)$, and the larger frequency bandwidth is caused by the spread of the form factor to larger wave vectors for a given QD size.

The larger bandwidth of $J(\omega)$ for the ES pumping configuration leads to a larger threshold pulse area for decoherence suppression. Fig. 4.3(b) and Fig. 4.3(c) show the results of calculations of Θ_T for QDs with various QD shapes and sizes. For a given choice of QD dimensions, Θ_T is larger for ES pumping than for GS pumping. These results imply that resonant excitation schemes would offer an advantage over near resonant pumping geometries of lower power requirements for quantum network applications. Our findings also indicate that the values of Θ_T we observe are expected to be even lower if GS pumping is used.

An ideal quantum emitter will be designed to minimize Θ_T while maintaining a GS transition that is compatible with standard telecommunications wavelengths for long-distance applications. The results in Fig. 3(c) indicate that both the height and in-plane dimensions of the QD may be used to engineer Θ_T. The dimensions corresponding to the QDs used in this work, characterized by Θ_T between 2 and 3π [white box in Fig. 4.3(c)], represent a near-optimum case for the InGaAs/GaAs family of QDs emitting near 1.3 μm. Lower values of Θ_T would be expected for QDs in the InAsP/InP family [202] with weaker quantum confinement and compatibility with the low-loss communication band at 1.55μm.

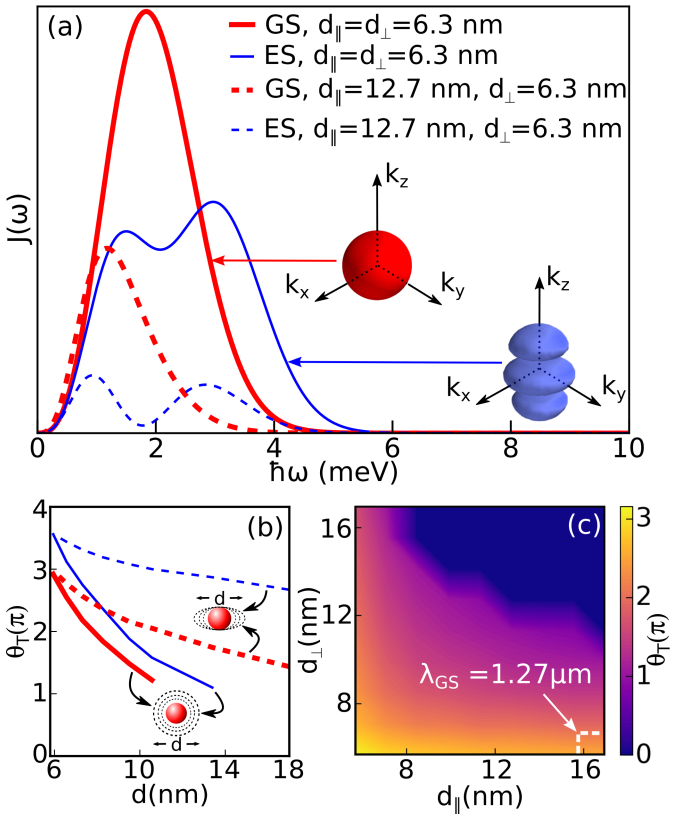

Figure 4.3: (a) Comparison of the calculated phonon spectral density $J(\omega)$ for optical driving of excitons on the GS and ES optical transitions. Thick (thin) curves show $J(\omega)$ for the GS (ES), with solid (dashed) curves corresponding to results for a spherical (lens-shaped) QD. Inset: Electron-hole form factors for GS and ES excitons in a spherical QD. (b),(c) Calculated threshold pulse area for GS and ES excitons in QDs of varying size and shape. For the dashed curves in (b), the height of the QD is taken to be 6.3 nm. In (c), $d_{\parallel}$ ($d_{\perp}$) correspond to the QD in-plane diameter (height). The dimensions and threshold pulse areas corresponding to the QDs used in our experiments are indicated by the white dashed square.

In summary, we demonstrate complete suppression of decoherence for optically-mediated exciton inversion using ARP on large QDs with telecom-compatible emission wavelengths. By exploiting the ability to engineer the strength of electron-phonon coupling by varying the size and shape of the QD, we achieve a four-fold reduction in the threshold pulse area required to reach the decoupling regime. Our observation of low-threshold decoherence suppression would facilitate parallel quantum state inversion in single and entangled photon sources with the potential for operation at elevated temperatures[191, 121, 150, 151, 70], while the telecom-compatible emission wavelengths of our QDs would support the development of

distributed quantum networks incorporating long-distance quantum state transfer [19]. Our calculations provide insight into the nature of phonon coupling for optical driving of the first excited state optical transition and indicate a new direction for engineering the strength and bandwidth of coupling via the symmetry of the QD wave function. These findings may aid efforts to exploit coherent phonon wave packet emission for coupling the quantum states of neighbouring QDs [221, 193]. Our calculations also indicate that even lower threshold pulse areas for decoherence suppression than those reported here may be expected for resonant pumping schemes. Our results will support the application of semiconductor QDs in future distributed quantum networks.

4.3 Acknowledgements

This research is supported by the Natural Sciences and Engineering Research Council of Canada.

Chapter 5

Quantification of the Robustness of Adiabatic Rapid Passage for Quantum State Inversion in Semiconductor Quantum Dots

Authors: A Ramachandran[1], J Fraser-Leach[1], S. Freisem[2], D. G. Deppe[2], and K. C. Hall[1]

[1]Department of Physics and Atmospheric Science, Dalhousie University, Halifax, Nova Scotia B3H4R2, Canada
[2]The College of Optics and Photonics, University of Central Florida, Orlando, Florida 32816-2700, USA

This chapter contains a manuscript that is being prepared for submission to Applied Physics Letters. Ajan Ramachandran developed the techniques, performed the experiments and the data analysis. James Fraser-Leach assisted with data collection. Sabine Freisem and Dennis Deppe developed and grew the sample. Kimberley C. Hall and Ajan Ramachandran conceived and designed the experiments. Ajan Ramachandran and Kimberley C. Hall wrote the manuscript with input from all authors.

5.1 Abstract

Adiabatic rapid passage (ARP) is demonstrated in a single In(Ga)As quantum dot (QD) over a wide range of laser tunings relative to the exciton transition energy to assess the level of robustness for parallel inversion of practical QD systems. We observe high-fidelity excitation over a 20 meV bandwidth at a pulse area of 1.5π, spanning the typical inhomogeneous broadenings of self-assembled QD ensembles. Our findings indicate that ARP is an ideal control protocol for synchronous triggering of quantum light sources for applications in photonic quantum technology.

5.2 Manuscript

Efficient, on-demand sources of single and entangled photons are needed for applications such as linear optical quantum computing [222] and distributed quantum networks [19], which utilize the quantum state of a photon (a so-called flying qubit) for transferring and/or manipulating information. Semiconductor QDs have emerged as a near-ideal solid-state quantum emitter system for these applications [75, 203, 204, 90, 191, 88, 119, 205, 121, 206, 207, 109, 208] owing to their strong optical transitions [200, 178, 153], high optical coherence [19], large internal quantum efficiency enabling a high photon generation rate [19], and the ease with which they may be integrated into photonic structures for efficient photon extraction [223, 65, 66]. The development of scalable networks requires the integration of multiple, synchronous quantum light sources that can be triggered in parallel using a single pulsed laser source [19]. To realize this goal, one must address the intrinsic inhomogeneity in the QD optical transition energies due to the variations in QD size. In recent experimental demonstrations of two-photon interference involving remote QD sources [189, 190, 191, 70], the QDs have either been excited in the wetting layer surrounding the QDs compromising the performance due to multiple carrier capture events [189, 190], or individual QDs with near-identical size and shape have been hand-picked out of the larger ensemble enabling the simultaneous resonant pumping of an excited state transition within both QDs [190, 191, 70]. The latter approach is impractical for a scalable network due to the low yield of useful emitters.

The conventional method for triggering a QD photon source is to carry out a Rabi rotation on the exciton in the QD [178, 153, 155, 154] (or the biexciton for application to entangled photon sources [125, 160]), however unless the laser is strictly resonant with the QD transition energy, the inversion of the quantum state is poor. ARP provides an alternative to a Rabi rotation that is robust to both variations in the optical properties of the emitter (transition energy, dipole moment) and the average power of the driving laser source [216, 49], making this an attractive scheme for parallel quantum state initialization of inequivalent emitters. In ARP, the optically-driven QD system is adiabatically transferred through an anti-crossing between the system dressed states, each of which represents a dynamic admixture

of the bare QD states ($|0\rangle$ and $|1\rangle$, where $|0\rangle$ ($|1\rangle$) represents the absence (presence) of a single exciton in the QD). Robust inversion occurs because, provided the system is initially in the ground state, the dressed state is uniquely identified with the exciton at the end of the laser pulse. ARP has been demonstrated in single QDs for inverting excitons [163, 162, 56, 141] and biexcitons [126], and was recently applied to triggering a single photon source [87]. In the latter work, the suppression of LA-phonon mediated damping through the use of positively-chirped laser pulses [56] led to both high single photon purity and 99.5% photon indistinguishability [87]. Determination of the level of robustness of ARP in practical QD systems would facilitate the extension of this technique to triggering multiple QD emitters.

In experiments on a single In(Ga)As/GaAs QDs, we show here that high-fidelity quantum state inversion is possible over a large laser tuning range of 20 meV. This high bandwidth of accessible detunings, which we find is $\sim$5-fold larger than for Rabi rotations using transform-limited laser pulses under otherwise identical conditions, exploits the intrinsic properties of ARP together with the use of short laser pulses for quantum state control. The high-fidelity inversion we demonstrate here covers the full inhomogeneous linewidth of typical self-assembled QD ensembles [224, 220, 225]. In contrast, recently-developed approaches to off-resonance driving of QDs based on phonon-assisted excitation [121, 127, 175] allow only 1-2 meV of detuning, limited by the width of the phonon spectral density [38, 54]. For applications of single-photon sources requiring photon indistinguishability [65], our experiments remove the simultaneous constraints of equivalent ground-state (GS) emission energies and equal energy separations between the GS and excited state (ES) optical transitions [224, 220, 225] since ARP enables the ES in inequivalent emitters to be driven far from resonance. Our simulations of the quantum state dynamics incorporating coupling to LA-phonons indicate that suppression of phonon-induced transitions between the dressed states of the QD, which unlike the other control schemes is possible for ARP for positive pulse chirp, is essential to maintain the level of robustness we report here.

The dressed states of an optically-driven two level system ($|\Psi_{\pm}\rangle$) are shown in Fig. 5.1. Fig. 5.1(a) [Fig. 5.1(b)] shows the case of a Rabi rotation (ARP) for resonant driving of the two-level system, while Fig. 5.1(c) and Fig. 5.1(d) show

the corresponding state dynamics for a detuned laser pulse. In the general case, the energy splitting between the dressed states is given by $\sqrt{\Omega(t)^2 + \Delta(t)^2}$, where $\Omega(t) = \frac{\mu E_p(t)}{\hbar}$ is the Rabi frequency, μ is the dipole moment of the optical transition, $E_p(t)$ is the pulse envelope, and $\Delta(t)$ is the instantaneous value of the detuning of the laser from the exciton transition. For a Rabi rotation, the control pulse has a constant phase with $\Delta = 0$, while ARP utilizes a frequency-swept laser pulse, given by $E(t) = \frac{1}{2}E_p(t)\exp\left[-i(\omega_l t + \alpha t^2)\right]$, where ω_l is the center frequency, $\Delta(t) = -2\alpha t$, and α is the temporal chirp.

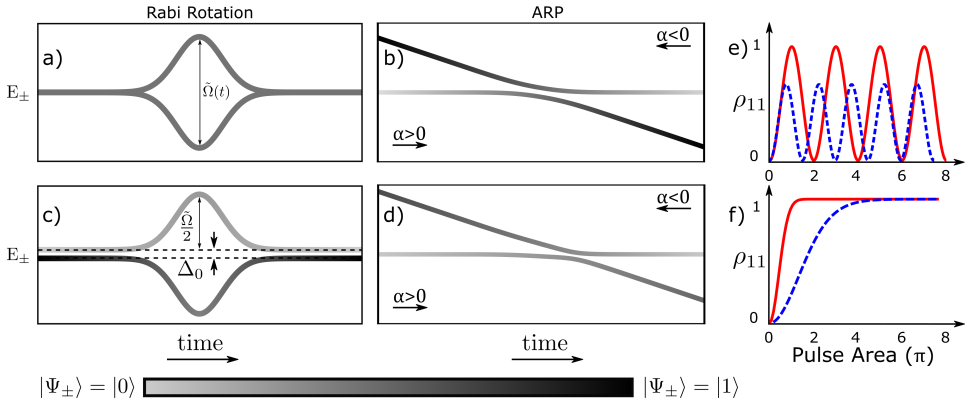

Figure 5.1: (a)-(d): Dressed state energies as a function of time during excitation: (a) Resonant Rabi rotation ($\phi'' = 0$). (b) Resonant ARP. (c) Detuned Rabi rotation with a detuning Δ. (d) Detuned ARP. (e)/(f) Final occupation of the exciton state for a Rabi rotation [(e)] and ARP [(f)] as a function of pulse area for a resonant (red solid curve) and off-resonant (blue dashed curve) laser pulse.

For resonant driving of the system using a Rabi rotation, the system is in an equal superposition of the two dressed states during the control pulse and the relative amplitude of the bare QD states oscillates versus time. The final state of the system is determined by the pulse area, given by $\theta = \int_{-\infty}^{\infty} \frac{\mu E_p(t)}{\hbar} dt$. Only when the pulse area is an odd-multiple of π is the final state of the system $|1\rangle$, a condition determined by the average power of the laser and the dipole moment of the QD. If the laser is detuned from the transition, the superposition of the dressed states is characterized by unequal amplitudes and the exciton occupation never reaches unity (Fig. 5.1(e)). For ARP, the dressed states each correspond to a dynamic admixture of the two bare QD states and the system evolves through an anti-crossing during the control pulse, as shown in Fig. 5.1(b) and Fig. 5.1(d). A positive (negative) value of α leads to state evolution via the higher- (lower-) energy dressed state. If the system starts

in $|0\rangle$, the final state of the system is uniquely identified with $|1\rangle$. This adiabatic evolution occurs provided that $|\Omega(t)| > \frac{d}{dt}|\frac{\Delta(t)}{\Omega(t)}|$, a condition that is satisfied for sufficiently large values of $\Omega(t)$ and α [216, 49]. The final exciton occupation is thus insensitive to the exact values of $\Omega(t)$ beyond the threshold for ARP, corresponding to robust state inversion. Since it is still possible to satisfy the adiabaticity condition for a detuned pulse, unlike Rabi rotations ARP can still invert the two-level system with high fidelity [Fig. 5.1(f)].

Quantum control experiments are carried out on a single InGaAs/GaAs QD with a GS optical transition at 1259 nm [arrow in Fig. 5.2(a)]. A schematic diagram of the experimental apparatus is shown in Fig. 5.2(b). The sample is housed in a liquid-helium flow-through microscopy cryostat equipped with a nanopositioning stage. For all experiments reported here, the sample temperature was 10 K. The laser source is an optical parametric oscillator with a repetition rate of 76 MHz and a pulse bandwidth of 20 meV. For Rabi rotation measurements, a 4f-pulse shaper is used to impose dispersion compensation using multiphoton interference phase scan [226, 140], resulting in a pulse duration at the sample position of $\tau_0 = 100$ fs. For ARP, the same 4f pulse shaper was used to impose spectral chirp (ϕ'', related to the temporal chirp α by $\alpha = 2\phi''/[\tau_0^4/(2\ln(2))^2 + (2\phi'')^2]$). Optical excitation is carried out on the first ES optical transition in the QD at 1162 nm determined using PL excitation measurements. The emission from the GS transition was detected using a 0.75 m monochromator and a liquid nitrogen cooled InGaAs array detector with an overall energy resolution of 30 μeV.

The results of Rabi rotation experiments for laser detunings of $\Delta = 0$ meV, -9 meV, and -15 meV are shown in Fig. 5.2(c). For resonant excitation, a damped Rabi oscillation is observed. The damping is induced by electron-LA phonon coupling, which leads to resonant transitions between the dressed states with a rate governed by the phonon spectral density and the instantaneous value of the splitting [165, 166, 158]. As the laser is detuned from resonance, the amplitude of the Rabi rotation drops rapidly, resulting in poor state inversion. The demonstration of ARP for the same values of Δ are shown in Fig. 5.2(d). Exciton inversion still occurs for a detuned pulse provided $\Omega(t)$ is large enough to reach the adiabatic regime. Notably, the final exciton inversion still reaches a high value for a large detuning from

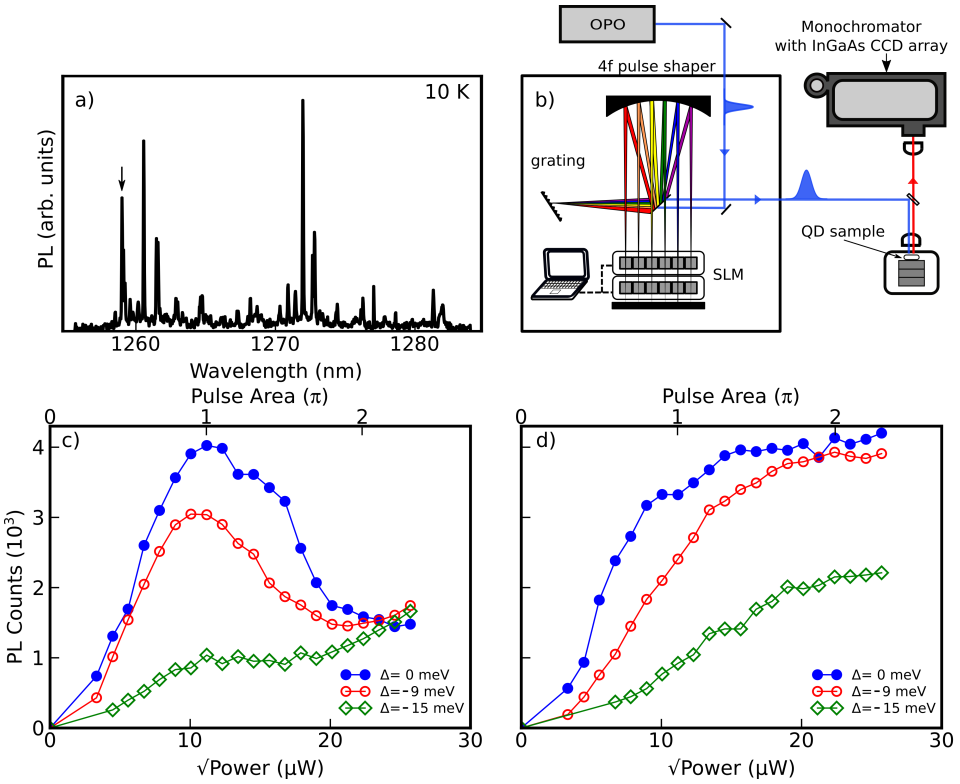

Figure 5.2: (a) Micro-PL showing the GS emission from individual QDs. The QD studied here is marked with an arrow. (b) Schematic diagram of the experimental setup. Pulses from the OPO laser source are dispersion-compensated and chirped using a 4-f pulse shaper. Optical control is carried out on the ES transition within the QD. Pulses are focused onto the sample using a microscope objective and the final quantum state of the exciton is read-out through detected photoluminescence on the GS transition. (c)/(d) PL intensity as a function of square-root of excitation power for Rabi rotation [(c)] and ARP ($\phi'' = 0.3$ ps^2) [(d)] for different detunings.

resonance of 9 meV. Experimental results corresponding to a full range of detunings are shown for a Rabi rotation (ARP) in Fig. 5.3(a) [Fig. 5.3(b)]. For the Rabi rotation, the maximum exciton inversion occurs for detuning values ± 3 meV and for pulse areas over a range of $\sim 0.25\pi$. In contrast, for ARP the inversion is insensitive to changes in pulse area beyond the threshold for adiabatic control. This threshold occurs at larger pulse areas for larger detunings. As a result, the bandwidth of detunings for which maximum inversion occurs increases with pulse area. For a pulse area of 2.5π, maximum exciton inversion for ARP occurs over a range of 20 ± 3 meV.

The results of calculations of the quantum state dynamics [139, 55] are shown

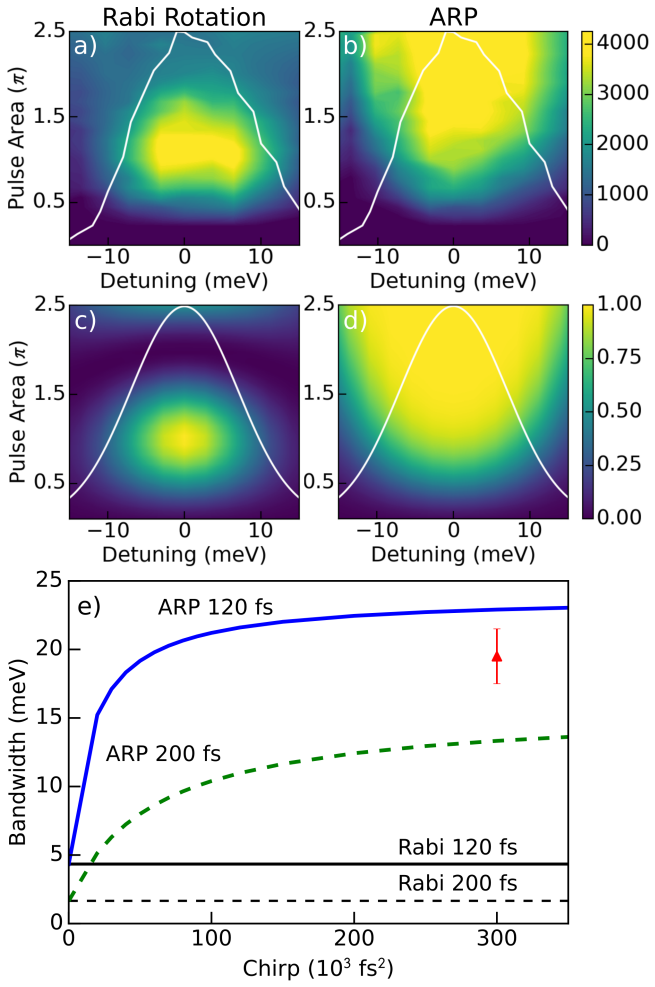

Figure 5.3: (a)/(b) PL intensity as a function of pulse area and detuning for excitation with a TL pulse [(a)] and a chirped pulse with $\phi'' = 0.3$ ps^2 [(b)]. (c)/(d) Calculated exciton occupation for the same conditions used in (a)/(b). The white curves in (a), (b) [(c), (d)] indicate the experimental [calculated] laser spectrum. (e) Calculated bandwidth for state preparation with an exciton occupation ≥ 0.95 as function of chirp for different transform-limited pulse durations (τ_0). The measured bandwidth for excitation with a chirped pulse ($\phi'' = 0.3$ ps^2) is indicated by the red triangle.

in Fig. 5.3(c) and Fig. 5.3(d). The bandwidth for which high-fidelity inversion of the exciton occurs increases with increasing pulse area, in agreement with the experimental results in Fig. 5.3(a)/(b). Assuming a threshold exciton occupation corresponding to acceptable inversion of 0.95, the calculated bandwidth for a pulse area of 2.5π is shown in Fig. 5.3(e) for two different values of τ_0. The bandwidth for ARP exhibits a saturation behavior versus ϕ'', with a value at saturation that

depends on τ_0. The calculated bandwidth is 23 meV for inversion with τ_0 = 120 fs compared to 4.4 meV for Rabi rotations. A large range of detunings may therefore be used for pumping QD single photon sources provided that femtosecond control pulses are used.

The ARP experiments in Fig. 5.2 and Fig. 5.3 utilized a positively-chirped laser pulse. Under these conditions, decoherence tied to phonon-induced transitions between the dressed states is suppressed at low temperatures because the system undergoes evolution through the anti-crossing along the lower-energy dressed state [56]. As the temperature of the sample is increased, phonon absorption processes will start to contribute and reduce the fidelity of quantum state control. In order to investigate the impact of phonons on the bandwidth of the ARP control process, we performed numerical simulations as a function of laser detuning for both positive and negative laser pulse chirps. The results of these calculations are shown in Fig. 5.4(a)-(c). The bandwidth of ARP for both signs of ϕ'' is shown in Fig. 5.4(f), indicating that exciton inversion using a negatively-chirped pulse is not as robust due to the impact of phonons, with a width $\sim$2 $\times$ lower than that for positive chirp. Our results therefore indicate that positive chirp is essential to maintain the level of robustness we demonstrate experimentally. In recent experiments, a complete suppression of phonon-induced decoherence for ARP was observed in the regime of short pulses and large chirps [61, 227]. Under these conditions, the chirp-sign dependence of the bandwidth would be eliminated and robust exciton inversion would persist at elevated temperatures.

The ability to achieve high-fidelity exciton inversion over a wide range of laser detunings would greatly facilitate the simultaneous pumping of multiple single photon sources using the same pulsed laser. The use of a near-resonant pumping scheme in which the ES transition in the QD is excited has been shown to lead to excellent single photon emission properties (single photon purity, brightness, indistinguishability) [190, 191, 70, 65]. The ES transition energies vary over a range of 10-30 meV in typical self-assembled QDs due to variations in QD size and shape, even for QDs possessing the same GS emission wavelength [224, 220, 225, 228, 194]. Our experiments show that ARP provides a robust method for realizing parallel quantum state inversion in distinct QD-based quantum emitters due to the broad

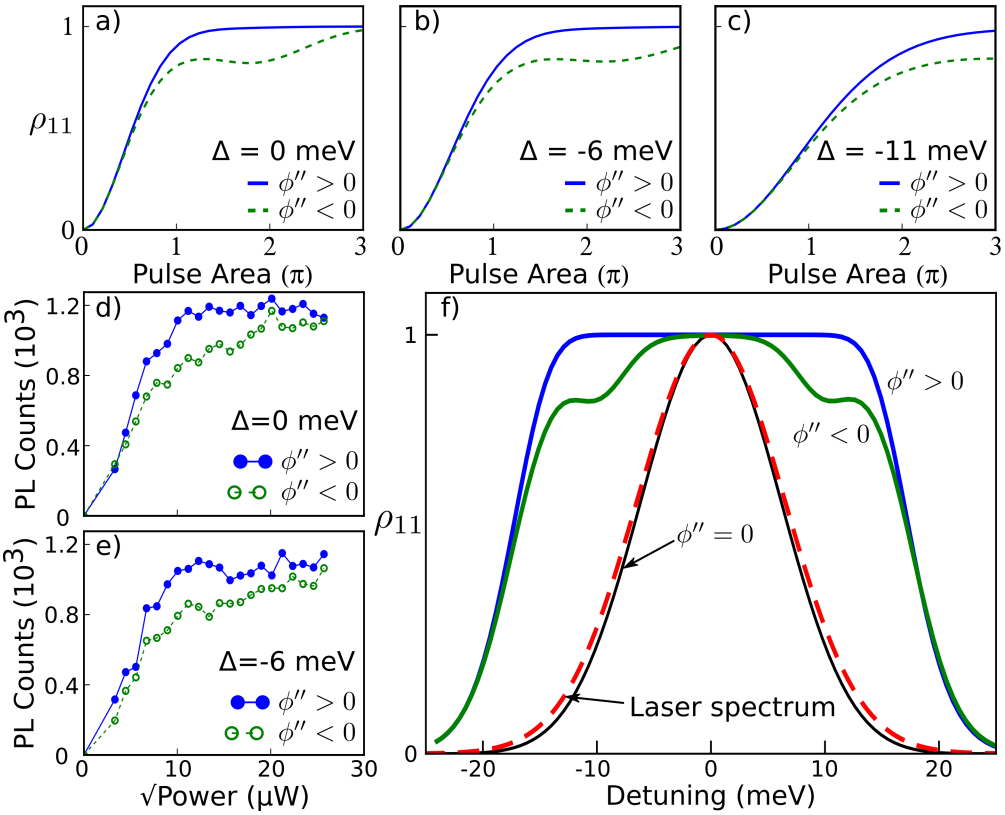

Figure 5.4: (a)-(c) Calculated exciton occupation as a function of pulse area for positively- (blue solid curves) and negatively- (green dashed curves) chirped control pulses for different detunings ($|\phi''| = 0.3$ ps^2). (d) -(e) PL intensity as a function of square-root of excitation power for the same conditions as in (a) and (b). (f) Calculated exciton occupation at a laser pulse area of 2.5π as a function of detuning for $|\phi''| = 0.3$ ps^2 and $|\phi''| = 0$ ps^2. The laser spectrum is also shown for reference. The bandwidths corresponding to 95% inversion are 27 meV (positive chirp), 12 meV (negative chirp), and 4.4 meV (zero chirp).

bandwidth over which high fidelity excitation is possible. Experiments employing phonon-emission-assisted excitation to invert two QD single photon sources using the same laser source have recently been reported [121]. This scheme also exhibits robustness to detuning but over a much smaller spectral range to that reported here (a few meV) due to the limited bandwidth of the phonon spectral density [38, 54].

In summary, we have demonstrated ARP on a single In(Ga)As/InAs QD using a wide range of laser detunings, enabling us to quantify the level of robustness of this control scheme in the context of practical QD systems possessing variations in QD size and shape. Our findings indicate that, in contrast to Rabi rotations for which

the exciton occupation follows the spectrum of the laser pulse and is highly sensitive to pulse area, the use of frequency-swept pulses in ARP enables a dramatic increase in the tolerance to differences between the QDs, with a high exciton inversion efficiency demonstrated over a 20 meV laser tuning bandwidth using control pulses with a transform-limited duration of 100 fs. As this bandwidth is comparable to typical variations in both the GS optical transition energies and the energy separation between the GS and ES transitions in self-assembled QD ensembles, this indicates that ARP is an ideal control scheme for realizing parallel quantum state initialization of multiple QD quantum emitters. Our findings will support the development of quantum networks and linear optical computing platforms utilizing semiconductor QDs.

Chapter 6

Robust Parallel Quantum State Initialization in Inequivalent Solid State Emitters

Authors: A Ramachandran[1], Reuble Mathew[1], Allister Mason[1], S. Freisem[2], D. G. Deppe[2], and K. C. Hall[1]

[1]Department of Physics and Atmospheric Science, Dalhousie University, Halifax, Nova Scotia B3H4R2, Canada
[2]The College of Optics and Photonics, University of Central Florida, Orlando, Florida 32816-2700, USA

This chapter contains a manuscript that is being prepared for submission to the Journal of Applied Physics. Ajan Ramachandran developed the techniques, performed the experiments and the data analysis. Reuble Mathew built the experimental setup and assisted with the numerical calculations. Allister Mason assisted with data collection. Sabine Freisem and Dennis Deppe developed and grew the sample. Kimberley C. Hall and Ajan Ramachandran conceived and designed the experiments. Ajan Ramachandran and Kimberley C. Hall wrote the manuscript with input from all authors.

6.1 Abstract

We demonstrate simultaneous adiabatic rapid passage (ARP) on multiple semiconductor quantum dots (QD) using a chirped laser pulse. State preparation using ARP is shown to be robust against variations in the dipole moments and transition energies of the QDs reflective of realistic self-assembled QD ensembles. Numerical calculations of the exciton occupation in the QD ensemble indicate high fidelity state preparation is possible for experimentally accessible values of chirp and laser

pulse area.

6.2 Manuscript

Adiabatic rapid passage provides an effective scheme for quantum state initialization and inversion in optically-driven two-levels systems. ARP was first demonstrated in atomic systems [48, 161] and later in solid-state quantum emitters in semiconductor QDs [163, 162], including the recent achievement of subpicosecond control times for the inversion of excitons immune to phonon-mediated dephasing [56, 227]. ARP is carried out using a frequency-swept control laser pulse given by $E(t) = \frac{1}{2}E_p(t)\exp\left[-i(\omega_l t + \alpha t^2)\right]$, where ω_l is the center frequency of the laser pulse and α is the rate of the frequency sweep. Such a linearly-chirped pulse may be obtained using standard $4f$ pulse shapers by introducing a spectral chirp ϕ'', where $\alpha = 2\phi''/[\tau_0^4/(2\ln(2))^2 + (2\phi'')^2]$, and τ_0 is the duration of the associated unshaped pulse. In quantum information science applications employing QD-based quantum emitters, ARP would be applicable to quantum state initialization in quantum simulators and memory nodes [19], or for optically triggering quantum light sources exploiting the optical driving of excitonic or biexcitonic resonances [87, 126].

Provided that the characteristics of such a frequency-swept control pulse satisfy the adiabaticity condition $\Omega > \left(\frac{d}{dt}\right)\left|\frac{\Delta}{\Omega}\right|$, where $\Omega(t) = \frac{\vec{\mu}\cdot\vec{E}(t)}{\hbar}$ is the Rabi frequency and $\Delta(t)$ is the detuning between the laser pulse and the transition frequency, ARP will be tolerant to variations in the optical properties of the driven two-level system (dipole moment, transition energy). This tolerance is especially important for semiconductor QD-based emitters because there are intrinsic variations in QD size inherent to the growth process [181, 224]. The robustness of ARP was recently verified experimentally for semiconductor QDs [229], with high fidelity inversion being observed for a detuning of the laser pulse from the QD transition as large as 15 meV, spanning the transition energies in typical self-assembled QD ensembles [224]. This level of robustness points to the potential for triggering multiple quantum emitters in parallel using a single pulsed laser source, essential for the development of scalable quantum systems applicable to distributed quantum networks [19] and linear optical quantum computing [65, 66]. While some progress in the parallel driving of distinct QDs has been made in recent years, including the application of

general pulse shape engineering to arbitrary qubit rotations [139, 140, 141, 142], the implementation of ARP on distinct emitters would enable fault-tolerant parallel quantum state initialization and inversion of QD-based qubits and quantum light sources, adding to the toolkit for coherent optical quantum control in semiconductor QDs.

Here we report the demonstration of adiabatic rapid passage on two QDs with distinct optical characteristics using a single laser pulse. High-fidelity inversion is obtained despite a 25% difference in the dipole moment and exciton transition energies differing by 7 meV, verifying the robustness of the ARP approach for solid state emitters based on semiconductor QDs. We also extend these findings to the application of ARP to more than 20 QDs, revealing robust inversion across the ensemble. These experiments are supported by our theortical simulations showing that high-fidelity exciton control should be possible on QD ensembles with realistic size variations for experimentally accessible values of laser pulse fluence and applied chirp. Our findings will support the development of scalable quantum information systems based on QD emitters and pave the way for controlling QD ensembles [230, 8].

The InAs/GaAs QDs studied in this work were grown using molecular beam epitaxy. A metallic mask with an array of apertures was deposited on the sample surface and used to isolate the individual QD emission lines from the ensemble. The experiments reported here were carried out through excitation of QDs within a $0.6\,\mu\mathrm{m}$ aperture. Laser pulses for optical control were generated using an optical parametric oscillator with a repetition rate of 76 MHz, tunable from 1100 nm to 1600 nm with a dispersion compensated pulse duration of 120 fs. A $4f$ pulse shaper with a 128 pixel spatial light modulator (SLM) in the Fourier plane is used to compensate for dispersion and to apply a chirp to the laser pulse. The temporal duration of the dispersion compensated control pulse was measured to be within 0.5% of that of a transform-limited pulse of the same bandwidth. A high numerical aperture microscope objective (NA 0.7, 100x) was used to focus the excitation beam on the sample. The photoluminescence emission from the QDs was spectrally resolved and detected using a 0.75 m monochromator with a resolution of 30 μeV and an InGaAs array detector. For all experiments, the sample was held at 10 K in

a continuous flow helium cryostat.

Quantum control was carried out on the first excited state optical transition in the QDs, with quantum state readout through detection of the emitted photoluminescence from the ground-state optical transition. For the QDs under study, PL and PL excitation measurements indicated a ground state PL emission peak for the quantum dot ensemble centered at 1294 nm with the first excited state transition centered at 1190 nm. The laser pulses were circularly polarized to suppress biexciton dynamics. The large energy separation between the ground state and first excited state transitions (90 meV) and between the first excited state transition and the wetting layer (310 meV) aided in avoiding unintended excitations.

Fig 6.1(c) and Fig 6.1(d) show the results of quantum control experiments using unshaped optical pulses on two quantum dots from the ensemble with ground state optical transition wavelengths of 1259 nm and 1273 nm, referred to as QD A and QD B. The first excited state transitions for these QDs occur at 1162 nm and 1171 nm, respectively. The detected PL from the ground state optical transition is shown as a function of the square root of the excitation power for control pulses of different detunings. Both QDs exhibit Rabi rotations with a period determined by their dipole moments. As the detuning of the laser pulse increases in either direction, the amplitude of the oscillation decreases, giving way to a linearly increasing background tied to incoherent filling of the QD states. The difference in Rabi periods for resonant excitation indicates that the dipole moment of QD B is 1.25 times larger than that of QD A.

Fig. 6.2(a) and Fig. 6.2(b) show a comparison of the quantum state dynamics in the two QDs for resonant control of the exciton transition using an unshaped pulse (blue circles) and a linearly-chirped pulse with $\phi'' = 0.3$ ps^2 (green pentagons). For these experiments, the spectrum of the control pulse was tuned in between the excited state optical transitions in the two QDs, as shown in Fig 6.1(b). For zero chirp, both QDs exhibit a Rabi rotation; while for the chirped pulse, the PL intensity reaches a plateau after a threshold excitation power. Saturation of the PL intensity from the exciton for pulse areas higher than a threshold is a signature of ARP and robust state inversion. The peak PL emission for the Rabi rotation is lower than that for control with a chirped laser pulse. This lower occupation reflects the fact

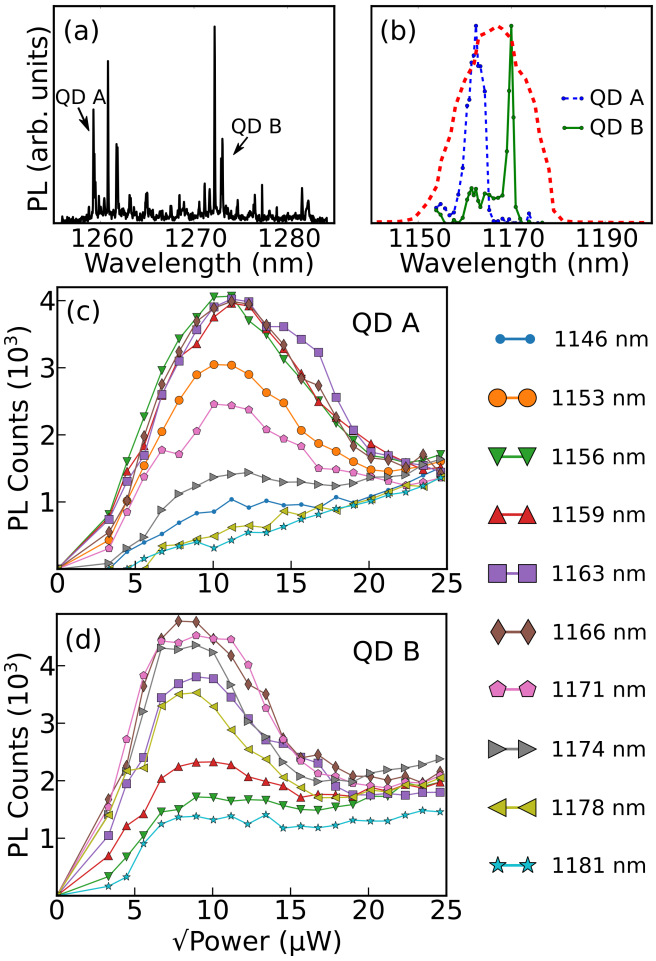

Figure 6.1: (a) Spectrally-resolved PL from the ground state optical transition. The two QDs of interest are indicated with arrows. (b) Photoluminescence excitation spectrum for QD A and QD B, together with the laser spectrum. (c)-(d) PL intensity as a function of the square root of the excitation power for quantum control using an unshaped laser pulse for (a) QD A and (b) QD B. The PL response is shown for different laser detunings from the excited state transition in each QD.

that since the control laser pulse was off-resonant with both QDs, the Rabi rotations do not result in a complete transfer of occupation to the exciton. In contrast, ARP leads to good exciton inversion in both QDs.

Fig. 6.3 shows the results of quantum control on a range of detected QDs within the aperture of interest for the same laser excitation spectrum as in Fig. 6.1(b). Fig. 6.3(a) shows the results for a chirped control pulse and Fig. 6.3(b) for an unshaped pulse. The different maximum PL intensities for different QD emission lines reflect variations in the location of the QDs within the aperture, which determines

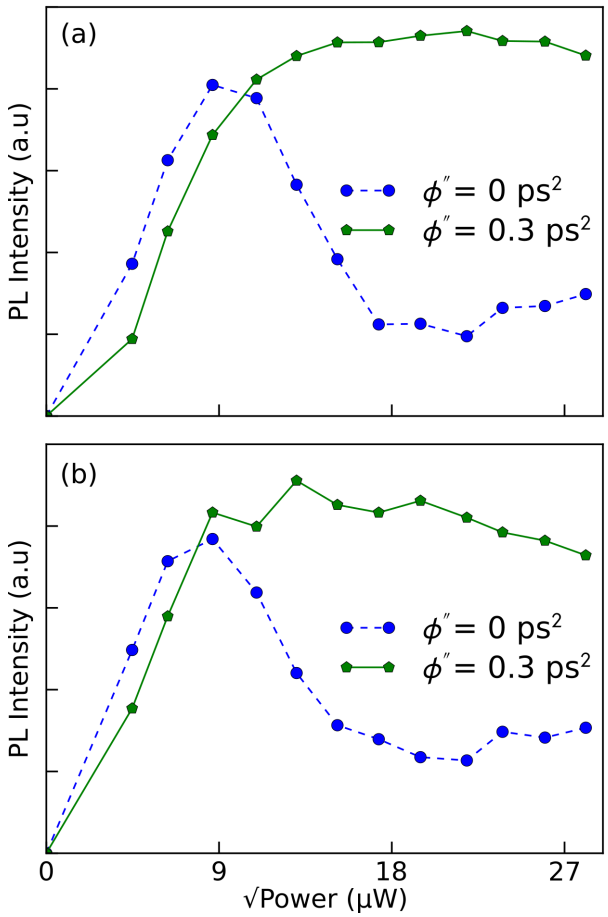

Figure 6.2: PL intensity as a function of square-root of excitation power for (blue dashed, $\phi'' = 0\,\mathrm{ps}^2$; green solid, $\phi'' = +0.3\,\mathrm{ps}^2$) (a) QD A (b) for QD B.

the efficiency of coupling of the optical emission into the objective lens and thus the efficiency of PL detection. The excited state optical transitions of the QDs seen in Fig 6.3(a) and Fig 6.3(b) range from 1162 nm to 1175 nm. Several of the QDs exhibit Rabi rotations, however the quality of rotation varies considerably from QD to QD due to the differing detunings of the control pulse with respect to the excited state transition in each QD, reflecting the high sensitivity of the amplitude of Rabi rotations to the laser detuning (Fig. 6.1(c),(d)). Despite the poor quality of the Rabi rotation for many of the QDs within the aperture, under optical control with a chirped laser pulse, the majority of QDs exhibit the characteristic plateau associated with ARP indicating high-quality inversion. These results show that, unlike Rabi rotations, ARP is insensitive to variations in the dipole moments and optical transition energies in the QDs. These experiments indicate that inversion of a full ensemble of

QDs or a series of QD quantum light sources grown under typical conditions should be possible.

To gain further insight into the level of robustness of the ARP control scheme, we carried out numerical simulations of the quantum state dynamics for a large ensemble of 468 QDs. The results of these calculations are shown in Fig. 6.3(c) and Fig. 6.3(d). For these calculations, the ensemble was chosen to have a Gaussian distribution of transition energies with a full width half maximum (FWHM) that was either 10 meV or 30 meV, corresponding to a width that is larger or smaller than the spectrum of the control pulse (16 meV). For comparison, the transition energies in typical self-assembled QD samples span approximately 25 meV [224]. The distribution of dipole moments in the simulations was taken to have a FWHM of 4 Debyes [192]. For zero pulse chirp, corresponding to the calculated values of the exciton inversion along the x-axis in Fig. 6.3(c)/(d), a damped Rabi oscillation is observed. The maximum inversion for zero chirp is 0.72 in Fig. 6.3(c) and 0.47 in Fig. 6.3(d). The low value of the maximum exciton occupation and the low contrast of the Rabi rotations in Fig. 6.3)c) and Fig. 6.3(d) reflect the high sensitivity of the quality of control via unshaped laser pulses to variations in the QD optical properties, an effect that becomes worse the larger the degree of QD inhomogeneity. As the laser chirp is increased from zero, the exciton occupation increases. The dashed curves in Fig. 6.3(c) and Fig. 6.3(d) indicate a calculated exciton occupation of 0.95, showing that a high exciton inversion is accessible for sufficiently large values of the pulse chirp and pulse area. An occupation of 0.99 occurs above a threshold pulse area of 2.45π (3.74π) and chirp of 0.018 ps^2 (0.026 ps^2) in (c) [(d)]. While similar results were obtained in earlier numerical simulations of optically-controlled QD ensembles [192], a much narrower distribution of transition energies was used (2 meV), in contrast to the realistic QD size distribution considered here.

In summary, we applied frequency-swept optical control pulses to demonstrate ARP on two QDs with distinct optical properties using the same shaped laser pulse, experiments that we then extended to the parallel inversion of more than 20 QDs. Our numerical simulations indicate that QD ensembles with inhomogeneities characteristic of realistic self-assembled QD systems may be inverted with high fidelity with pulse areas below 4π, values that are readily accessible experimentally. These

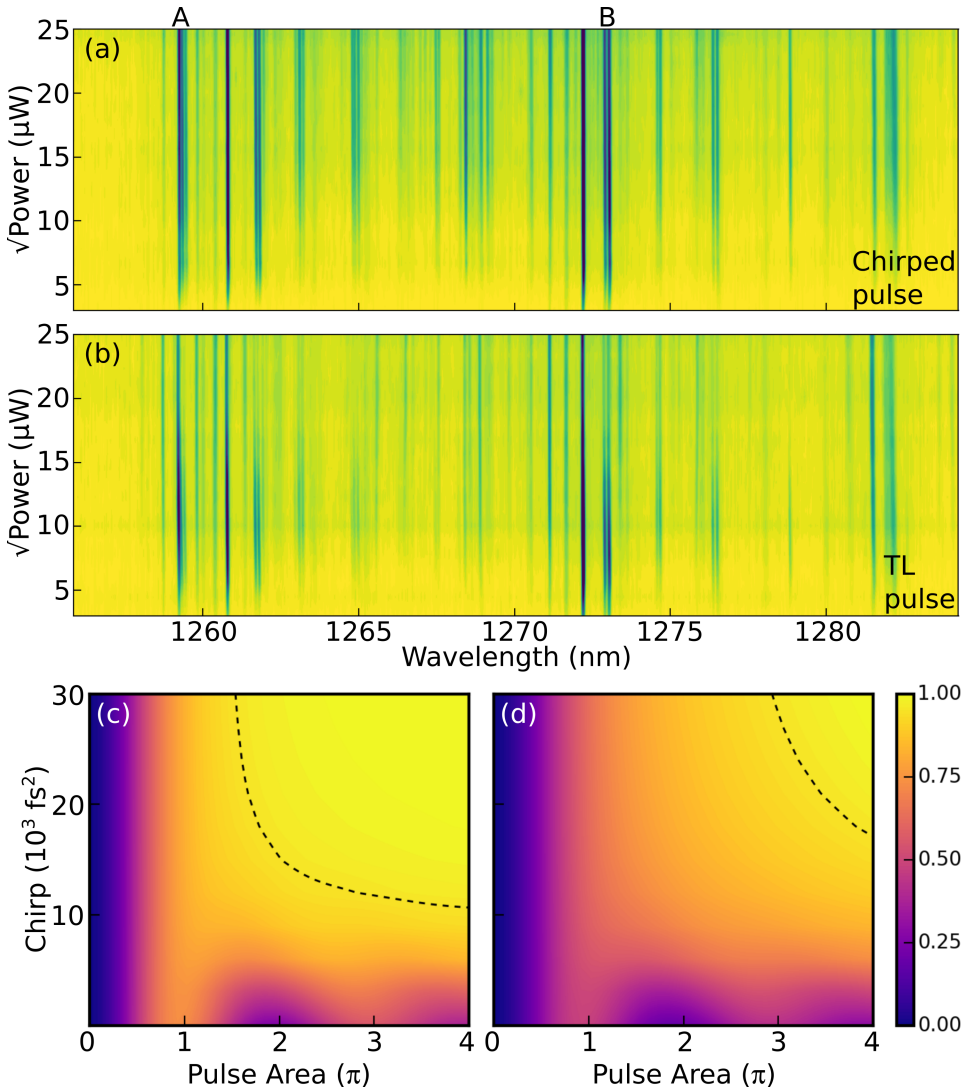

Figure 6.3: PL intensity as a function of pulse area for all QDs within the aperture (a) chirped pulse with $\phi'' = +0.3\,\mathrm{ps}^2$ and (b) unshaped pulse. (c)/(d): Calculated total exciton occupation for an ensemble of QDs as a function of chirp and pulse area. The QD distributions have transition energies that are (c) 10 meV (d) 30 meV wide. The dotted line indicates a threshold of 95% occupation. The pulse area values on the x-axis correspond to the QDs that lie at the mean of the transition energy and dipole moment distributions.

experiments, which build upon recent demonstrations of simultaneous arbitrary qubit rotations in QDs [141, 142], illustrate the tolerance of the ARP control scheme to variations in the QD transition energies and dipole moments, and lay the foundation for parallel quantum state initialization and inversion in applications such as quantum light sources and quantum networks.

Chapter 7

Conclusion

7.1 Summary of the Thesis Work

Semiconductor quantum dots are poised to play an important role in future QIP systems. Their solid-state nature should allow for scalability to a large number of qubits, where the exploitation of a semiconductor-based platform implies that traditional device processing techniques developed for current technologies (CMOS, laser diodes etc.) could be leveraged for QIP technologies as well. For the same reasons, a semiconductor QD QIP system would be easily integrated with classical computing platforms. The size dependent optical properties of QDs enable flexibility in the tuning of their transition energies so that operation in telecommunication bandwidths is possible, furthering their potential integration with classical technologies and benefiting potential applications such as quantum networks. Their ability to host qubits in the form of excitons or carrier spins while also being an excellent emitter of single and entangled photons makes them a promising interface between photonic and material qubits systems. Despite of all these advantages, the progress of QD based QIP systems is hindered by a few remaining roadblocks. These include the inhomogeneity in their optical properties arising from their growth process and dephasing processes tied to their solid state nature. This thesis work has advanced the state of QIP using self-assembled InAs QDs through theoretical calculations and experimental demonstrations of quantum state preparation protocols that are tolerant to inhomogeneities in QD optical properties and immune to phonon mediated dephasing. The additions made by this thesis work to the existing body of knowledge therefore advance the progress of a QD based QIP system by developing experimental strategies that address some of the difficulties associated with them. This work has also provided a better understanding of the state preparation process tied to ARP in a solid state quantum emitter and has laid the foundation for the development of a decoherence free single photon emitter that is

compatible with the current telecommunication infrastructure.

The first component of this thesis work demonstrated a four-fold lower threshold for the suppression of phonon assisted decoherence in QDs designed to work in the telecommunication band. InAs QDs designed to emit in the IR band, owing to their large size and the femtosecond pulses use to excite them, display a much lower threshold for the dynamic suppression of electron-phonon interactions. This result was demonstrated through the convergence of the exciton occupation levels in ARP experiments that use negatively and positively chirped pulses. Our results pave the way for a QD based quantum emitter working at higher temperatures in the critically important telecommunications band. A robust single photon source that works in the telecommunications band is an essential component of long distance quantum encrypted communication networks. Our calculations also explored the dependence of exciton-phonon coupling on the physical dimensions of the QD and the symmetry of the exciton wavefunction. Our results indicate that resonant excitation of the QD could display an even lower threshold for decoherence suppression than those reported in this work.

The second component of this thesis work experimentally quantified the detuning tolerance of ARP. Our findings indicate that, in contrast to Rabi rotations for which the exciton occupation follows the spectrum of the laser pulse and is highly sensitive to the pulse area of the control pulse, the use of chirped control pulses leads to a dramatic increase in the tolerance to variations in the transition frequencies of the QDs. A high exciton inversion efficiency was demonstrated over a 20 meV laser tuning bandwidth using chirped control pulses that correspond to a transform-limited duration of 100 fs. A state preparation process that is tolerant to fluctuations in experimental parameters requires less laser resources because the same laser source could be used to invert a number of single photon sources in parallel. This would be particularly beneficial for applications such as linear optical quantum computing networks that require synchronous quantum light sources. Our findings should support the development of a QD based scalable QIP infrastructure.

A natural extension to quantifying the detuning tolerance of ARP is to use ARP for state preparation in an ensemble of QDs. The final project in this thesis involved the experimental demonstration of ARP in two distinct and dissimilar QDs using

a single laser pulse for the first time. This demonstration, which involved QDs whose transition energies differed by 7 meV and dipole moments that differed by 25%, indicated that ARP can be used for state preparation in an ensemble of QDs. The results of numerical calculations suggest that state preparation through ARP is possible at high chirps and higher pulse areas on an ensemble of QDs with an inhomogeneous broadening comparable to typical QD samples.

7.2 Future Work

An immediate follow up to the decoherence suppression project would be to experimentally verify our prediction of the lower threshold for decoherence suppression for resonant excitation. A single photon source that can operate at higher temperatures (> 80 K) would simplify the deployment and eventual integration of a photonic quantum network with the existing infrastructure. Developing a QD based single photon source capable of working at higher temperatures requires experimental verification of the temperature dependence of the threshold pulse area for decoherence suppression. QDs are often embedded in nanostructures such as as microcavities and nanowires to improve their photon extraction efficiency. Another valuable extension to this work would be studying the influence of such nanostructures on exciton-phonon interactions.

As a next step to the work on parallel ARP in QDs, the state preparation efficiency of ARP on an ensemble of QDs need to be studied experimentally. Such an experiment requires building a transient absorption spectroscopy apparatus for quantum state read-out from an ensemble of QDs. An ensemble of coupled qubits is an essential requirement for applications like quantum memories.

7.3 Outlook

A future general purpose QIP system would include quantum computers capable of running quantum algorithms and a quantum network infrastructure to transfer quantum information between nodes. QDs, with their ability to host qubits and to act as an interface between solid-state and photonic qubits, are poised at play an important role in this development. Incredible efforts over the past few years have

resulted in many exciting experimental demonstrations, such as single and multi-qubit gates [152, 134, 135, 56, 138], spin-photon [211, 212, 213] and spin-spin entanglement [214, 151], quantum teleportation [231] and quantum relays [232]. However significant challenges remain in building a general purpose QIP platform based on QDs. Decoherence times in these systems are significantly lower ($\sim$10 μs for electron spins [19]) when compared to other competing platforms (for example $\sim$1 s in NV centers [19]). However this challenge can be overcome by using faster control pulses for gate operations. Interactions between qubits encoded in QDs are challenging and over the years several proposals have been made towards achieving this goal [147, 148, 20, 149]. With the exception of optical control of QD molecules, which is difficult to scale beyond a few QDs, so far there have been only a few experimental demonstrations of optically mediated conditional dynamics in coupled QD systems [150, 151]. However, all potential QIP platforms have their own strength and weaknesses. Hence any future implementation of QIP will very likely be a hybrid system that combines the strengths of multiple candidate platforms. QDs due to their excellent optical properties, could act as interface nodes between photonic qubits and material qubits. QD based sources with their highest reported indistinguishability [88], high single photon purity [233] and high photon extraction efficiencies [65] are currently the best performing single photon sources [19, 65]. In addition, applications such as sensing and auxiliary quantum technologies like quantum repeaters could work with systems that have a moderate number of qubits [12] and can provide commercial viability as these systems are being scaled up for QIP.

Bibliography

[1] E. Bernstein and U. Vazirani, "Quantum complexity theory," *SIAM Journal on computing*, vol. 26, no. 5, pp. 1411–1473, 1997.

[2] P. W. Shor, "Algorithms for quantum computation: discrete logarithms and factoring," *Proceedings of the 35th Annual Symposium on Foundations of Computer Science*, 1994.

[3] L. K. Grover, "A fast quantum mechanical algorithm for database search," in *Proceedings of the twenty-eighth annual ACM symposium on Theory of computing*, pp. 212–219, 1996.

[4] R. P. Feynman, "Simulating physics with computers," *Int. J. Theor. Phys*, vol. 21, no. 6/7, 1999.

[5] E. Martin-Lopez, A. Laing, T. Lawson, R. Alvarez, X.-Q. Zhou, and J. L. O'brien, "Experimental realization of shor's quantum factoring algorithm using qubit recycling," *Nature photonics*, vol. 6, no. 11, pp. 773–776, 2012.

[6] M. A. Nielsen and I. Chuang, "Quantum computation and quantum information," 2002.

[7] T. Albash and D. A. Lidar, "Adiabatic quantum computation," *Reviews of Modern Physics*, vol. 90, no. 1, p. 015002, 2018.

[8] G. Sanders, K. Kim, and W. Holton, "Quantum computing with complex instruction sets," *Physical Review A*, vol. 59, no. 2, p. 1098, 1999.

[9] H. J. Briegel, D. E. Browne, W. Dür, R. Raussendorf, and M. Van den Nest, "Measurement-based quantum computation," *Nature Physics*, vol. 5, no. 1, pp. 19–26, 2009.

[10] Z. Amitay, R. Kosloff, and S. R. Leone, "Experimental coherent computation of a multiple-input and gate using pure molecular superpositions," *Chemical physics letters*, vol. 359, no. 1-2, pp. 8–14, 2002.

[11] D. P. DiVincenzo, "The physical implementation of quantum computation," *Fortschritte der Physik: Progress of Physics*, vol. 48, no. 9-11, pp. 771–783, 2000.

[12] E. National Academies of Sciences, Medicine, *et al.*, *Quantum computing: progress and prospects*. National Academies Press, 2019.

[13] C. Monroe, D. Meekhof, B. King, W. M. Itano, and D. J. Wineland, "Demonstration of a fundamental quantum logic gate," *Physical review letters*, vol. 75, no. 25, p. 4714, 1995.

[14] K. R. Brown, J. Kim, and C. Monroe, "Co-designing a scalable quantum computer with trapped atomic ions," *npj Quantum Information*, vol. 2, no. 1, pp. 1–10, 2016.

[15] J. M. Gambetta, J. M. Chow, and M. Steffen, "Building logical qubits in a superconducting quantum computing system," *npj Quantum Information*, vol. 3, no. 1, pp. 1–7, 2017.

[16] G. Wendin and V. Shumeiko, "Quantum bits with josephson junctions," *Low Temperature Physics*, vol. 33, no. 9, pp. 724–744, 2007.

[17] D. D. Awschalom, L. C. Bassett, A. S. Dzurak, E. L. Hu, and J. R. Petta, "Quantum spintronics: engineering and manipulating atom-like spins in semiconductors," *Science*, vol. 339, no. 6124, pp. 1174–1179, 2013.

[18] F. A. Zwanenburg, A. S. Dzurak, A. Morello, M. Y. Simmons, L. C. Hollenberg, G. Klimeck, S. Rogge, S. N. Coppersmith, and M. A. Eriksson, "Silicon quantum electronics," *Reviews of modern physics*, vol. 85, no. 3, p. 961, 2013.

[19] M. Atatüre, D. Englund, N. Vamivakas, S.-Y. Lee, and J. Wrachtrup, "Material platforms for spin-based photonic quantum technologies," *Nature Reviews Materials*, vol. 3, no. 5, pp. 38–51, 2018.

[20] A. Imamog, D. D. Awschalom, G. Burkard, D. P. DiVincenzo, D. Loss, M. Sherwin, A. Small, *et al.*, "Quantum information processing using quantum dot spins and cavity qed," *Physical review letters*, vol. 83, no. 20, p. 4204, 1999.

[21] J. L. O'brien, "Optical quantum computing," *Science*, vol. 318, no. 5856, pp. 1567–1570, 2007.

[22] N. Treps, N. Grosse, W. P. Bowen, C. Fabre, H.-A. Bachor, and P. K. Lam, "A quantum laser pointer," *Science*, vol. 301, no. 5635, pp. 940–943, 2003.

[23] G. B. Lemos, V. Borish, G. D. Cole, S. Ramelow, R. Lapkiewicz, and A. Zeilinger, "Quantum imaging with undetected photons," *Nature*, vol. 512, no. 7515, pp. 409–412, 2014.

[24] N. Samantaray, I. Ruo-Berchera, A. Meda, and M. Genovese, "Realization of the first sub-shot-noise wide field microscope," *Light: Science & Applications*, vol. 6, no. 7, pp. e17005–e17005, 2017.

[25] D. Budker and M. Romalis, "Optical magnetometry," *Nature physics*, vol. 3, no. 4, pp. 227–234, 2007.

[26] G. Balasubramanian, I. Chan, R. Kolesov, M. Al-Hmoud, J. Tisler, C. Shin, C. Kim, A. Wojcik, P. R. Hemmer, A. Krueger, *et al.*, "Nanoscale imaging magnetometry with diamond spins under ambient conditions," *Nature*, vol. 455, no. 7213, pp. 648–651, 2008.

[27] M. Müller, H. Vural, C. Schneider, A. Rastelli, O. Schmidt, S. Höfling, and P. Michler, "Quantum-dot single-photon sources for entanglement enhanced interferometry," *Physical review letters*, vol. 118, no. 25, p. 257402, 2017.

[28] C. L. Degen, F. Reinhard, and P. Cappellaro, "Quantum sensing," *Reviews of modern physics*, vol. 89, no. 3, p. 035002, 2017.

[29] C. Elliott, "Building the quantum network," *New Journal of Physics*, vol. 4, no. 1, p. 46, 2002.

[30] S. Ritter, C. Nölleke, C. Hahn, A. Reiserer, A. Neuzner, M. Uphoff, M. Mücke, E. Figueroa, J. Bochmann, and G. Rempe, "An elementary quantum network of single atoms in optical cavities," *Nature*, vol. 484, no. 7393, p. 195, 2012.

[31] M. Gilaberte Basset, F. Setzpfandt, F. Steinlechner, E. Beckert, T. Pertsch, and M. Gräfe, "Perspectives for applications of quantum imaging," *Laser & Photonics Reviews*, vol. 13, no. 10, p. 1900097, 2019.

[32] L. A. Lugiato, A. Gatti, and E. Brambilla, "An introduction to quantum imaging," in *Quantum Communication and Information Technologies* (A. S. Shumovsky and V. I. Rupasov, eds.), (Dordrecht), pp. 85–99, Springer Netherlands, 2003.

[33] I. Kominis, T. Kornack, J. Allred, and M. V. Romalis, "A subfemtotesla multichannel atomic magnetometer," *Nature*, vol. 422, no. 6932, pp. 596–599, 2003.

[34] J. R. Maze, P. L. Stanwix, J. S. Hodges, S. Hong, J. M. Taylor, P. Cappellaro, L. Jiang, M. G. Dutt, E. Togan, A. Zibrov, *et al.*, "Nanoscale magnetic sensing with an individual electronic spin in diamond," *Nature*, vol. 455, no. 7213, pp. 644–647, 2008.

[35] M. W. Doherty, V. V. Struzhkin, D. A. Simpson, L. P. McGuinness, Y. Meng, A. Stacey, T. J. Karle, R. J. Hemley, N. B. Manson, L. C. Hollenberg, *et al.*, "Electronic properties and metrology applications of the diamond nv- center under pressure," *Physical review letters*, vol. 112, no. 4, p. 047601, 2014.

[36] G. Kucsko, P. C. Maurer, N. Y. Yao, M. Kubo, H. J. Noh, P. K. Lo, H. Park, and M. D. Lukin, "Nanometre-scale thermometry in a living cell," *Nature*, vol. 500, no. 7460, pp. 54–58, 2013.

[37] Y.-H. Deng, H. Wang, X. Ding, Z.-C. Duan, J. Qin, M.-C. Chen, Y. He, Y.-M. He, J.-P. Li, Y.-H. Li, *et al.*, "Quantum interference between light sources separated by 150 million kilometers," *Physical review letters*, vol. 123, no. 8, p. 080401, 2019.

[38] A. J. Ramsay, "A review of the coherent optical control of the exciton and spin states of semiconductor quantum dots," *Semicond. Sci. Technol.*, vol. 25, no. 10, p. 103001, 2010.

[39] D. Bruls, J. Vugs, P. Koenraad, H. Salemink, J. Wolter, M. Hopkinson, M. Skolnick, F. Long, and S. Gill, "Determination of the shape and indium distribution of low-growth-rate InAs quantum dots by cross-sectional scanning tunneling microscopy," *Applied physics letters*, vol. 81, no. 9, pp. 1708–1710, 2002.

[40] F. Troiani, U. Hohenester, and E. Molinari, "Exploiting exciton-exciton interactions in semiconductor quantum dots for quantum-information processing," *Physical Review B*, vol. 62, no. 4, p. R2263, 2000.

[41] P. Chen, C. Piermarocchi, and L. Sham, "Control of exciton dynamics in nanodots for quantum operations," *Physical review letters*, vol. 87, no. 6, p. 067401, 2001.

[42] C. Piermarocchi, P. Chen, L. Sham, and D. Steel, "Optical rkky interaction between charged semiconductor quantum dots," *Physical review letters*, vol. 89, no. 16, p. 167402, 2002.

[43] D. Loss and D. P. DiVincenzo, "Quantum computation with quantum dots," *Physical Review A*, vol. 57, no. 1, p. 120, 1998.

[44] P. Chen, C. Piermarocchi, L. Sham, D. Gammon, and D. Steel, "Theory of quantum optical control of a single spin in a quantum dot," *Physical Review B*, vol. 69, no. 7, p. 075320, 2004.

[45] S. E. Economou, L. Sham, Y. Wu, and D. Steel, "Proposal for optical u (1) rotations of electron spin trapped in a quantum dot," *Physical Review B*, vol. 74, no. 20, p. 205415, 2006.

[46] S. M. Clark, K.-M. C. Fu, T. D. Ladd, and Y. Yamamoto, "Quantum computers based on electron spins controlled by ultrafast off-resonant single optical pulses," *Physical review letters*, vol. 99, no. 4, p. 040501, 2007.

[47] T. E. Hodgson, L. Viola, and I. D'Amico, "Decoherence-protected storage of exciton qubits through ultrafast multipulse control," *Physical Review B*, vol. 78, no. 16, p. 165311, 2008.

[48] J. Melinger, S. R. Gandhi, A. Hariharan, D. Goswami, and W. Warren, "Adiabatic population transfer with frequency-swept laser pulses," *The Journal of chemical physics*, vol. 101, no. 8, pp. 6439–6454, 1994.

[49] V. Malinovsky and J. Krause, "General theory of population transfer by adiabatic rapid passage with intense, chirped laser pulses," *The European Physical Journal D-Atomic, Molecular, Optical and Plasma Physics*, vol. 14, no. 2, pp. 147–155, 2001.

[50] P. Borri, W. Langbein, S. Schneider, U. Woggon, R. L. Sellin, D. Ouyang, and D. Bimberg, "Ultralong dephasing time in InGaAs quantum dots," *Physical Review Letters*, vol. 87, no. 15, p. 157401, 2001.

[51] P. Borri, W. Langbein, U. Woggon, V. Stavarache, D. Reuter, and A. Wieck, "Exciton dephasing via phonon interactions in InAs quantum dots: Dependence on quantum confinement," *Physical Review B*, vol. 71, no. 11, p. 115328, 2005.

[52] A. J. Ramsay, A. V. Gopal, E. M. Gauger, A. Nazir, B. W. Lovett, a. M. Fox, and M. S. Skolnick, "Damping of Exciton Rabi Rotations by Acoustic Phonons in Optically Excited InGaAs/GaAs Quantum Dots," *Phys. Rev. Lett.*, vol. 104, no. 1, pp. 20–23, 2010.

[53] D. Reiter, T. Kuhn, M. Glässl, and V. M. Axt, "The role of phonons for exciton and biexciton generation in an optically driven quantum dot," *Journal of Physics: Condensed Matter*, vol. 26, no. 42, p. 423203, 2014.

[54] S. Lüker and D. E. Reiter, "A review on optical excitation of semiconductor quantum dots under the influence of phonons," *Semiconductor Science and Technology*, vol. 34, no. 6, p. 063002, 2019.

[55] A. Ramsay, T. Godden, S. Boyle, E. Gauger, A. Nazir, B. Lovett, A. V. Gopal, A. Fox, and M. Skolnick, "Effect of detuning on the phonon induced dephasing of optically driven InGaAs/GaAs quantum dots," *Journal of Applied Physics*, vol. 109, no. 10, p. 102415, 2011.

[56] R. Mathew, E. Dilcher, A. Gamouras, A. Ramachandran, H. Y. S. Yang, S. Freisem, D. Deppe, and K. C. Hall, "Subpicosecond adiabatic rapid passage on a single semiconductor quantum dot: Phonon-mediated dephasing in the strong-driving regime," *Phys. Rev. B*, vol. 90, no. 3, pp. 1–6, 2014.

[57] A. Debnath, C. Meier, B. Chatel, and T. Amand, "Chirped laser excitation of quantum dot excitons coupled to a phonon bath," *Phys. Rev. B*, vol. 86, no. 16, p. 161304, 2012.

[58] S. Lüker, K. Gawarecki, D. Reiter, A. Grodecka-Grad, V. M. Axt, P. Machnikowski, and T. Kuhn, "Influence of acoustic phonons on the optical control of quantum dots driven by adiabatic rapid passage," *Physical Review B*, vol. 85, no. 12, p. 121302, 2012.

[59] A. Vagov, M. D. Croitoru, V. M. Axt, T. Kuhn, and F. Peeters, "Nonmonotonic field dependence of damping and reappearance of rabi oscillations in quantum dots," *Physical review letters*, vol. 98, no. 22, p. 227403, 2007.

[60] M. Glässl, M. D. Croitoru, A. Vagov, V. M. Axt, and T. Kuhn, "Influence of the pulse shape and the dot size on the decay and reappearance of rabi rotations in laser driven quantum dots," *Physical Review B*, vol. 84, no. 12, p. 125304, 2011.

[61] T. Kaldewey, S. Lüker, A. V. Kuhlmann, S. R. Valentin, J. M. Chauveau, A. Ludwig, A. D. Wieck, D. E. Reiter, T. Kuhn, and R. J. Warburton, "Demonstrating the decoupling regime of the electron-phonon interaction in a quantum dot using chirped optical excitation," *Phys. Rev. B*, vol. 95, no. 24, pp. 1–5, 2017.

[62] E. A. Muljarov and R. Zimmermann, "Dephasing in quantum dots: Quadratic coupling to acoustic phonons," *Physical review letters*, vol. 93, no. 23, p. 237401, 2004.

[63] A. Reigue, J. Iles-Smith, F. Lux, L. Monniello, M. Bernard, F. Margaillan, A. Lemaitre, A. Martinez, D. P. Mccutcheon, J. Mørk, *et al.*, "Probing electron-phonon interaction through two-photon interference in resonantly driven semiconductor quantum dots," *Physical Review Letters*, vol. 118, no. 23, p. 233602, 2017.

[64] S. Gerhardt, J. Iles-Smith, D. P. McCutcheon, Y.-M. He, S. Unsleber, S. Betzold, N. Gregersen, J. Mørk, S. Höfling, and C. Schneider, "Intrinsic and environmental effects on the interference properties of a high-performance quantum dot single-photon source," *Physical Review B*, vol. 97, no. 19, p. 195432, 2018.

[65] P. Senellart, G. Solomon, and A. White, "High-performance semiconductor quantum-dot single-photon sources," *Nature nanotechnology*, vol. 12, no. 11, p. 1026, 2017.

[66] D. Huber, M. Reindl, J. Aberl, A. Rastelli, and R. Trotta, "Semiconductor quantum dots as an ideal source of polarization-entangled photon pairs on-demand: a review," *Journal of Optics*, vol. 20, no. 7, p. 073002, 2018.

[67] P. W. Shor, "Algorithms for quantum computation: discrete logarithms and factoring," in *Proceedings 35th annual symposium on foundations of computer science*, pp. 124–134, Ieee, 1994.

[68] C. H. Bennett and G. Brassard, "Quantum cryptography: Public key distribution and con tos5," in *Proceedings of the International Conference on Computers, Systems and Signal Processing*, 1984.

[69] A. K. Ekert, "Quantum cryptography based on bell's theorem," *Physical review letters*, vol. 67, no. 6, p. 661, 1991.

[70] A. Thoma, P. Schnauber, J. Böhm, M. Gschrey, J.-H. Schulze, A. Strittmatter, S. Rodt, T. Heindel, and S. Reitzenstein, "Two-photon interference from remote deterministic quantum dot microlenses," *Applied Physics Letters*, vol. 110, no. 1, p. 011104, 2017.

[71] F. Olbrich, J. Höschele, M. Müller, J. Kettler, S. Luca Portalupi, M. Paul, M. Jetter, and P. Michler, "Polarization-entangled photons from an InGaAs-based quantum dot emitting in the telecom c-band," *Applied Physics Letters*, vol. 111, no. 13, p. 133106, 2017.

[72] R. Keil, M. Zopf, Y. Chen, B. Höfer, J. Zhang, F. Ding, and O. G. Schmidt, "Solid-state ensemble of highly entangled photon sources at rubidium atomic transitions," *Nature communications*, vol. 8, no. 1, pp. 1–8, 2017.

[73] J.-Y. Marzin, J.-M. Gérard, A. Izraël, D. Barrier, and G. Bastard, "Photoluminescence of single InAs quantum dots obtained by self-organized growth on GaAs," *Physical review letters*, vol. 73, no. 5, p. 716, 1994.

[74] S. Fafard, D. Leonard, J. Merz, and P. Petroff, "Selective excitation of the photoluminescence and the energy levels of ultrasmall InGaAs/GaAs quantum dots," *Applied physics letters*, vol. 65, no. 11, pp. 1388–1390, 1994.

[75] P. Michler, A. Kiraz, C. Becher, W. Schoenfeld, P. Petroff, L. Zhang, E. Hu, and A. Imamoglu, "A quantum dot single-photon turnstile device," *science*, vol. 290, no. 5500, pp. 2282–2285, 2000.

[76] Z. Yuan, B. E. Kardynal, R. M. Stevenson, A. J. Shields, C. J. Lobo, K. Cooper, N. S. Beattie, D. A. Ritchie, and M. Pepper, "Electrically driven single-photon source," *science*, vol. 295, no. 5552, pp. 102–105, 2002.

[77] T. Miyazawa, K. Takemoto, Y. Nambu, S. Miki, T. Yamashita, H. Terai, M. Fujiwara, M. Sasaki, Y. Sakuma, M. Takatsu, *et al.*, "Single-photon emission at 1.5 μ m from an InAs/InP quantum dot with highly suppressed multi-photon emission probabilities," *Applied Physics Letters*, vol. 109, no. 13, p. 132106, 2016.

[78] L. Schweickert, K. D. Jöns, K. D. Zeuner, S. F. Covre da Silva, H. Huang, T. Lettner, M. Reindl, J. Zichi, R. Trotta, A. Rastelli, *et al.*, "On-demand generation of background-free single photons from a solid-state source," *Applied Physics Letters*, vol. 112, no. 9, p. 093106, 2018.

[79] A. Thoma, P. Schnauber, M. Gschrey, M. Seifried, J. Wolters, J.-H. Schulze, A. Strittmatter, S. Rodt, A. Carmele, A. Knorr, *et al.*, "Exploring dephasing of a solid-state quantum emitter via time-and temperature-dependent hong-ou-mandel experiments," *Physical review letters*, vol. 116, no. 3, p. 033601, 2016.

[80] I. Favero, G. Cassabois, R. Ferreira, D. Darson, C. Voisin, J. Tignon, C. Delalande, G. Bastard, P. Roussignol, and J. Gérard, "Acoustic phonon sidebands in the emission line of single InAs/GaAs quantum dots," *Physical Review B*, vol. 68, no. 23, p. 233301, 2003.

[81] L. Besombes, K. Kheng, L. Marsal, and H. Mariette, "Acoustic phonon broadening mechanism in single quantum dot emission," *Physical Review B*, vol. 63, no. 15, p. 155307, 2001.

[82] E. B. Flagg, S. V. Polyakov, T. Thomay, and G. S. Solomon, "Dynamics of nonclassical light from a single solid-state quantum emitter," *Physical review letters*, vol. 109, no. 16, p. 163601, 2012.

[83] S. Varoutsis, S. Laurent, P. Kramper, A. Lemaître, I. Sagnes, I. Robert-Philip, and I. Abram, "Restoration of photon indistinguishability in the emission of a semiconductor quantum dot," *Physical Review B*, vol. 72, no. 4, p. 041303, 2005.

[84] T. Grange, N. Somaschi, C. Antón, L. De Santis, G. Coppola, V. Giesz, A. Lemaître, I. Sagnes, A. Auffèves, and P. Senellart, "Reducing phonon-induced decoherence in solid-state single-photon sources with cavity quantum electrodynamics," *Physical review letters*, vol. 118, no. 25, p. 253602, 2017.

[85] P. Kaer and J. Mørk, "Decoherence in semiconductor cavity qed systems due to phonon couplings," *Physical Review B*, vol. 90, no. 3, p. 035312, 2014.

[86] S. L. Portalupi, M. Jetter, and P. Michler, "InAs quantum dots grown on metamorphic buffers as non-classical light sources at telecom c-band: a review," *Semiconductor Science and Technology*, vol. 34, no. 5, p. 053001, 2019.

[87] Y.-j. Wei, Y.-M. He, M.-c. Chen, Y.-n. Hu, Y.-M. He, D. Wu, C. Schneider, M. Kamp, S. Höfling, C.-Y. Lu, and J.-W. Pan, "Deterministic and Robust Generation of Single Photons On a Chip with 99.5% Indistinguishability Using Rapid Adiabatic Passage," *Nano Lett.*, vol. 14, p. 6515, 2014.

[88] N. Somaschi, V. Giesz, L. De Santis, J. Loredo, M. P. Almeida, G. Hornecker, S. L. Portalupi, T. Grange, C. Antón, J. Demory, *et al.*, "Near-optimal single-photon sources in the solid state," *Nature Photonics*, vol. 10, no. 5, p. 340, 2016.

[89] S. L. Portalupi, G. Hornecker, V. Giesz, T. Grange, A. Lemaître, J. Demory, I. Sagnes, N. D. Lanzillotti-Kimura, L. Lanco, A. Auffèves, *et al.*, "Bright phonon-tuned single-photon source," *Nano letters*, vol. 15, no. 10, pp. 6290–6294, 2015.

[90] O. Gazzano, S. M. De Vasconcellos, C. Arnold, A. Nowak, E. Galopin, I. Sagnes, L. Lanco, A. Lemaître, and P. Senellart, "Bright solid-state sources of indistinguishable single photons," *Nature communications*, vol. 4, no. 1, pp. 1–6, 2013.

[91] J. Claudon, J. Bleuse, N. S. Malik, M. Bazin, P. Jaffrennou, N. Gregersen, C. Sauvan, P. Lalanne, and J.-M. Gérard, "A highly efficient single-photon source based on a quantum dot in a photonic nanowire," *Nature Photonics*, vol. 4, no. 3, pp. 174–177, 2010.

[92] M. Munsch, N. S. Malik, E. Dupuy, A. Delga, J. Bleuse, J.-M. Gérard, J. Claudon, N. Gregersen, and J. Mørk, "Dielectric GaAs antenna ensuring an efficient broadband coupling between an InAs quantum dot and a gaussian optical beam," *Physical Review Letters*, vol. 110, no. 17, p. 177402, 2013.

[93] M. Gschrey, A. Thoma, P. Schnauber, M. Seifried, R. Schmidt, B. Wohlfeil, L. Krüger, J.-H. Schulze, T. Heindel, S. Burger, *et al.*, "Highly indistinguishable photons from deterministic quantum-dot microlenses utilizing three-dimensional in situ electron-beam lithography," *Nature communications*, vol. 6, no. 1, pp. 1–8, 2015.

[94] U. Sinha, S. N. Sahoo, A. Singh, K. Joarder, R. Chatterjee, and S. Chakraborti, "Single-photon sources," *Optics and Photonics News*, vol. 30, no. 9, pp. 32–39, 2019.

[95] I. Aharonovich, D. Englund, and M. Toth, "Solid-state single-photon emitters," *Nature Photonics*, vol. 10, no. 10, p. 631, 2016.

[96] P. Aboussouan, O. Alibart, D. B. Ostrowsky, P. Baldi, and S. Tanzilli, "High-visibility two-photon interference at a telecom wavelength using picosecond-regime separated sources," *Physical Review A*, vol. 81, no. 2, p. 021801, 2010.

[97] V. Leong, S. Kosen, B. Srivathsan, G. K. Gulati, A. Cere, and C. Kurtsiefer, "Hong-ou-mandel interference between triggered and heralded single photons from separate atomic systems," *Physical Review A*, vol. 91, no. 6, p. 063829, 2015.

[98] H. Bernien, L. Childress, L. Robledo, M. Markham, D. Twitchen, and R. Hanson, "Two-photon quantum interference from separate nitrogen vacancy centers in diamond," *Physical Review Letters*, vol. 108, no. 4, p. 043604, 2012.

[99] F. Massa, A. Moqanaki, Ä. Baumeler, F. Del Santo, J. A. Kettlewell, B. Dakić, and P. Walther, "Experimental two-way communication with one photon," *Advanced Quantum Technologies*, vol. 2, no. 11, p. 1900050, 2019.

[100] D. B. Higginbottom, L. Slodička, G. Araneda, L. Lachman, R. Filip, M. Hennrich, and R. Blatt, "Pure single photons from a trapped atom source," *New Journal of Physics*, vol. 18, no. 9, p. 093038, 2016.

[101] A. Beveratos, R. Brouri, T. Gacoin, A. Villing, J.-P. Poizat, and P. Grangier, "Single photon quantum cryptography," *Physical review letters*, vol. 89, no. 18, p. 187901, 2002.

[102] M. D. C. Pereira, F. E. Becerra, B. L. Glebov, J. Fan, S. W. Nam, and A. Migdall, "Demonstrating highly symmetric single-mode, single-photon heralding efficiency in spontaneous parametric downconversion," *Optics letters*, vol. 38, no. 10, pp. 1609–1611, 2013.

[103] H. Barros, A. Stute, T. Northup, C. Russo, P. Schmidt, and R. Blatt, "Deterministic single-photon source from a single ion," *New Journal of Physics*, vol. 11, no. 10, p. 103004, 2009.

[104] D. Press, S. Götzinger, S. Reitzenstein, C. Hofmann, A. Löffler, M. Kamp, A. Forchel, and Y. Yamamoto, "Photon antibunching from a single quantum-dot-microcavity system in the strong coupling regime," *Physical Review Letters*, vol. 98, no. 11, p. 117402, 2007.

[105] S. K. Andersen, S. Kumar, and S. I. Bozhevolnyi, "Ultrabright linearly polarized photon generation from a nitrogen vacancy center in a nanocube dimer antenna," *Nano letters*, vol. 17, no. 6, pp. 3889–3895, 2017.

[106] B. J. Smith, P. Mahou, O. Cohen, J. Lundeen, and I. Walmsley, "Photon pair generation in birefringent optical fibers," *Optics express*, vol. 17, no. 26, pp. 23589–23602, 2009.

[107] J. B. Altepeter, E. R. Jeffrey, and P. G. Kwiat, "Phase-compensated ultra-bright source of entangled photons," *Optics Express*, vol. 13, no. 22, pp. 8951–8959, 2005.

[108] F. Diedrich and H. Walther, "Nonclassical radiation of a single stored ion," *Physical review letters*, vol. 58, no. 3, p. 203, 1987.

[109] Y. Chen, M. Zopf, R. Keil, F. Ding, and O. G. Schmidt, "Highly-efficient extraction of entangled photons from quantum dots using a broadband optical antenna," *Nature communications*, vol. 9, no. 1, pp. 1–7, 2018.

[110] W. C. Jiang, X. Lu, J. Zhang, O. Painter, and Q. Lin, "Silicon-chip source of bright photon pairs," *Optics express*, vol. 23, no. 16, pp. 20884–20904, 2015.

[111] A. Fedrizzi, T. Herbst, A. Poppe, T. Jennewein, and A. Zeilinger, "A wavelength-tunable fiber-coupled source of narrowband entangled photons," *Optics Express*, vol. 15, no. 23, pp. 15377–15386, 2007.

[112] B. Weber, H. P. Specht, T. Müller, J. Bochmann, M. Mücke, D. L. Moehring, and G. Rempe, "Photon-photon entanglement with a single trapped atom," *Physical review letters*, vol. 102, no. 3, p. 030501, 2009.

[113] D. Huber, M. Reindl, S. F. C. Da Silva, C. Schimpf, J. Martín-Sánchez, H. Huang, G. Piredda, J. Edlinger, A. Rastelli, and R. Trotta, "Strain-tunable GaAs quantum dot: A nearly dephasing-free source of entangled photon pairs on demand," *Physical review letters*, vol. 121, no. 3, p. 033902, 2018.

[114] M. Medic, J. B. Altepeter, M. A. Hall, M. Patel, and P. Kumar, "Fiber-based telecommunication-band source of degenerate entangled photons," *Optics letters*, vol. 35, no. 6, pp. 802–804, 2010.

[115] P. Kok, C. P. Williams, and J. P. Dowling, "Construction of a quantum repeater with linear optics," *Physical Review A*, vol. 68, no. 2, p. 022301, 2003.

[116] S. C. Benjamin, B. W. Lovett, and J. M. Smith, "Prospects for measurement-based quantum computing with solid state spins," *Laser & Photonics Reviews*, vol. 3, no. 6, pp. 556–574, 2009.

[117] T. Ono, R. Okamoto, and S. Takeuchi, "An entanglement-enhanced microscope," *Nature communications*, vol. 4, no. 1, pp. 1–7, 2013.

[118] O. Benson, C. Santori, M. Pelton, and Y. Yamamoto, "Regulated and entangled photons from a single quantum dot," *Physical review letters*, vol. 84, no. 11, p. 2513, 2000.

[119] N. Akopian, N. Lindner, E. Poem, Y. Berlatzky, J. Avron, D. Gershoni, B. Gerardot, and P. Petroff, "Entangled photon pairs from semiconductor quantum dots," *Physical review letters*, vol. 96, no. 13, p. 130501, 2006.

[120] M. Müller, S. Bounouar, K. D. Jöns, M. Glässl, and P. Michler, "On-demand generation of indistinguishable polarization-entangled photon pairs," *Nature Photonics*, vol. 8, no. 3, p. 224, 2014.

[121] M. Reindl, K. D. Jöns, D. Huber, C. Schimpf, Y. Huo, V. Zwiller, A. Rastelli, and R. Trotta, "Phonon-Assisted Two-Photon Interference from Remote Quantum Emitters," *Nano Lett.*, vol. 17, no. 7, pp. 4090–4095, 2017.

[122] D. Huber, M. Reindl, Y. Huo, H. Huang, J. S. Wildmann, O. G. Schmidt, A. Rastelli, and R. Trotta, "Highly indistinguishable and strongly entangled photons from symmetric GaAs quantum dots," *Nature communications*, vol. 8, no. 1, pp. 1–7, 2017.

[123] T. Müller, J. Skiba-Szymanska, A. Krysa, J. Huwer, M. Felle, M. Anderson, R. Stevenson, J. Heffernan, D. Ritchie, and A. Shields, "A quantum light-emitting diode for the standard telecom window around 1,550 nm," *Nature communications*, vol. 9, no. 1, pp. 1–6, 2018.

[124] A. Fognini, A. Ahmadi, M. Zeeshan, J. T. Fokkens, S. J. Gibson, N. Sherlekar, S. J. Daley, D. Dalacu, P. J. Poole, K. Jöns, *et al.*, "Dephasing free photon entanglement with a quantum dot," *ACS Photonics*, vol. 6, no. 7, pp. 1656–1663, 2019.

[125] S. Stufler, P. Machnikowski, P. Ester, M. Bichler, V. M. Axt, T. Kuhn, and A. Zrenner, "Two-photon rabi oscillations in a single $In_xGa_{1-x}As$/GaAs quantum dot," *Physical Review B*, vol. 73, no. 12, p. 125304, 2006.

[126] T. Kaldewey, S. Lüker, A. V. Kuhlmann, S. R. Valentin, A. Ludwig, A. D. Wieck, D. E. Reiter, T. Kuhn, and R. J. Warburton, "Coherent and robust high-fidelity generation of a biexciton in a quantum dot by rapid adiabatic passage," *Phys. Rev. B*, vol. 95, no. 16, pp. 1–5, 2017.

[127] P. L. Ardelt, L. Hanschke, K. A. Fischer, K. Müller, A. Kleinkauf, M. Koller, A. Bechtold, T. Simmet, J. Wierzbowski, H. Riedl, G. Abstreiter, and J. J. Finley, "Dissipative preparation of the exciton and biexciton in self-assembled quantum dots on picosecond time scales," *Phys. Rev. B*, vol. 90, no. 24, pp. 1–5, 2014.

[128] H. Jayakumar, A. Predojević, T. Kauten, T. Huber, G. S. Solomon, and G. Weihs, "Time-bin entangled photons from a quantum dot," *Nature communications*, vol. 5, no. 1, pp. 1–5, 2014.

[129] A. Freschi and J. Frejlich, "Adjustable phase control in stabilized interferometry," *Optics letters*, vol. 20, no. 6, pp. 635–637, 1995.

[130] T. Okada, K. Komori, K. Goshima, S. Yamauchi, I. Morohashi, T. Sugaya, M. Ogura, and N. Tsurumachi, "Development of high resolution michelson interferometer for stable phase-locked ultrashort pulse pair generation," *Review of Scientific Instruments*, vol. 79, no. 10, p. 103101, 2008.

[131] N. H. Bonadeo, J. Erland, D. Gammon, D. Park, D. Katzer, and D. Steel, "Coherent optical control of the quantum state of a single quantum dot," *Science*, vol. 282, no. 5393, pp. 1473–1476, 1998.

[132] L. Besombes, J. Baumberg, and J. Motohisa, "Coherent spectroscopy of optically gated charged single InGaAs quantum dots," *Physical review letters*, vol. 90, no. 25, p. 257402, 2003.

[133] S. Stufler, P. Ester, A. Zrenner, and M. Bichler, "Quantum optical properties of a single $In_xGa_{1-x}As$ - GaAs quantum dot two-level system," *Physical Review B*, vol. 72, no. 12, p. 121301, 2005.

[134] R. Kolodka, A. Ramsay, J. Skiba-Szymanska, P. Fry, H. Liu, A. Fox, and M. Skolnick, "Inversion recovery of single quantum-dot exciton based qubit," *Physical Review B*, vol. 75, no. 19, p. 193306, 2007.

[135] J. Lee, A. Bennett, J. Skiba-Szymanska, D. Ellis, I. Farrer, D. Ritchie, and A. Shields, "Ramsey interference in a multilevel quantum system," *Physical Review B*, vol. 93, no. 8, p. 085407, 2016.

[136] T. Unold, K. Mueller, C. Lienau, T. Elsaesser, and A. D. Wieck, "Optical stark effect in a quantum dot: Ultrafast control of single exciton polarizations," *Physical review letters*, vol. 92, no. 15, p. 157401, 2004.

[137] X. Li, Y. Wu, D. Steel, D. Gammon, T. Stievater, D. Katzer, D. Park, C. Piermarocchi, and L. Sham, "An all-optical quantum gate in a semiconductor quantum dot," *Science*, vol. 301, no. 5634, pp. 809–811, 2003.

[138] S. Boyle, A. Ramsay, F. Bello, H. Liu, M. Hopkinson, A. Fox, and M. Skolnick, "Two-qubit conditional quantum-logic operation in a single self-assembled quantum dot," *Physical Review B*, vol. 78, no. 7, p. 075301, 2008.

[139] R. Mathew, C. E. Pryor, M. E. Flatté, and K. C. Hall, "Optimal quantum control for conditional rotation of exciton qubits in semiconductor quantum dots," *Physical Review B*, vol. 84, no. 20, p. 205322, 2011.

[140] A. Gamouras, R. Mathew, and K. C. Hall, "Optically engineered ultrafast pulses for controlled rotations of exciton qubits in semiconductor quantum dots," *Journal of Applied Physics*, vol. 112, no. 1, p. 014313, 2012.

[141] A. Gamouras, R. Mathew, S. Freisem, D. G. Deppe, and K. C. Hall, "Simultaneous deterministic control of distant qubits in two semiconductor quantum dots.," *Nano Lett.*, vol. 13, no. 10, pp. 4666–70, 2013.

[142] R. Mathew, H. Y. S. Yang, and K. C. Hall, "Simultaneous SU(2) rotations on multiple quantum dot exciton qubits using a single shaped pulse," *Phys. Rev. B*, vol. 92, no. 15, pp. 1–8, 2015.

[143] K. Müller, G. Reithmaier, E. C. Clark, V. Jovanov, M. Bichler, H. J. Krenner, M. Betz, G. Abstreiter, and J. J. Finley, "Excited state quantum couplings and optical switching of an artificial molecule," *Physical Review B*, vol. 84, no. 8, p. 081302, 2011.

[144] D. Kim, S. G. Carter, A. Greilich, A. S. Bracker, and D. Gammon, "Ultrafast optical control of entanglement between two quantum-dot spins," *Nature Physics*, vol. 7, no. 3, pp. 223–229, 2011.

[145] R. Brunner, Y.-S. Shin, T. Obata, M. Pioro-Ladrière, T. Kubo, K. Yoshida, T. Taniyama, Y. Tokura, and S. Tarucha, "Two-qubit gate of combined single-spin rotation and interdot spin exchange in a double quantum dot," *Physical review letters*, vol. 107, no. 14, p. 146801, 2011.

[146] A. Greilich, S. G. Carter, D. Kim, A. S. Bracker, and D. Gammon, "Optical control of one and two hole spins in interacting quantum dots," *Nature Photonics*, vol. 5, no. 11, p. 702, 2011.

[147] A. Barenco, D. Deutsch, A. Ekert, and R. Jozsa, "Conditional quantum dynamics and logic gates," *Physical Review Letters*, vol. 74, no. 20, p. 4083, 1995.

[148] L. Quiroga and N. F. Johnson, "Entangled bell and greenberger-horne-zeilinger states of excitons in coupled quantum dots," *Physical review letters*, vol. 83, no. 11, p. 2270, 1999.

[149] T. A. Brun and H. Wang, "Coupling nanocrystals to a high-q silica microsphere: entanglement in quantum dots via photon exchange," *Physical Review A*, vol. 61, no. 3, p. 032307, 2000.

[150] A. Delteil, Z. Sun, W.-b. Gao, E. Togan, S. Faelt, and A. Imamoğlu, "Generation of heralded entanglement between distant hole spins," *Nature Physics*, vol. 12, no. 3, pp. 218–223, 2016.

[151] R. Stockill, M. Stanley, L. Huthmacher, E. Clarke, M. Hugues, A. Miller, C. Matthiesen, C. Le Gall, and M. Atatüre, "Phase-tuned entangled state generation between distant spin qubits," *Physical review letters*, vol. 119, no. 1, p. 010503, 2017.

[152] T. H. Stievater, X. Li, D. G. Steel, D. Gammon, D. S. Katzer, D. Park, C. Piermarocchi, and L. J. Sham, "Rabi oscillations of excitons in single quantum dots," *Phys. Rev. Lett.*, vol. 87, p. 133603, Sep 2001.

[153] H. Kamada, H. Gotoh, J. Temmyo, T. Takagahara, and H. Ando, "Exciton rabi oscillation in a single quantum dot," *Phys. Rev. Lett.*, vol. 87, p. 246401, Nov 2001.

[154] H. Htoon, T. Takagahara, D. Kulik, O. Baklenov, A. L. Holmes, and C. K. Shih, "Interplay of rabi oscillations and quantum interference in semiconductor quantum dots," *Phys. Rev. Lett.*, vol. 88, p. 087401, Feb 2002.

[155] A. Zrenner, E. Beham, S. Stufler, F. Findeis, M. Bichler, and G. Abstreiter, "Coherent properties of a two-level system based on a quantum-dot photodiode," *Nature*, vol. 418, no. 6898, pp. 612–614, 2002.

[156] R. Melet, V. Voliotis, A. Enderlin, D. Roditchev, X. Wang, T. Guillet, and R. Grousson, "Resonant excitonic emission of a single quantum dot in the rabi regime," *Physical Review B*, vol. 78, no. 7, p. 073301, 2008.

[157] A. Ramsay, T. Godden, S. Boyle, E. M. Gauger, A. Nazir, B. W. Lovett, A. Fox, and M. Skolnick, "Phonon-induced rabi-frequency renormalization of optically driven single InGaAs/GaAs quantum dots," *Physical review letters*, vol. 105, no. 17, p. 177402, 2010.

[158] A. Ramsay, A. V. Gopal, E. Gauger, A. Nazir, B. W. Lovett, A. Fox, and M. Skolnick, "Damping of exciton rabi rotations by acoustic phonons in optically excited InGaAs/GaAs quantum dots," *Physical review letters*, vol. 104, no. 1, p. 017402, 2010.

[159] H. Wang, Z.-C. Duan, Y.-H. Li, S. Chen, J.-P. Li, Y.-M. He, M.-C. Chen, Y. He, X. Ding, C.-Z. Peng, C. Schneider, M. Kamp, S. Höfling, C.-Y. Lu, and J.-W. Pan, "Near-transform-limited single photons from an efficient solid-state quantum emitter," *Phys. Rev. Lett.*, vol. 116, p. 213601, May 2016.

[160] H. Jayakumar, A. Predojević, T. Huber, T. Kauten, G. S. Solomon, and G. Weihs, "Deterministic photon pairs and coherent optical control of a single quantum dot," *Physical review letters*, vol. 110, no. 13, p. 135505, 2013.

[161] N. V. Vitanov, T. Halfmann, B. W. Shore, and K. Bergmann, "Laser-induced population transfer by adiabatic passage techniques," *Annual review of physical chemistry*, vol. 52, no. 1, pp. 763–809, 2001.

[162] Y. Wu, I. Piper, M. Ediger, P. Brereton, E. Schmidgall, P. Eastham, M. Hugues, M. Hopkinson, and R. Phillips, "Population Inversion in a Single InGaAs Quantum Dot Using the Method of Adiabatic Rapid Passage," *Phys. Rev. Lett.*, vol. 106, no. 6, pp. 1–4, 2011.

[163] C.-M. Simon, T. Belhadj, B. Chatel, T. Amand, P. Renucci, a. Lemaitre, O. Krebs, P. a. Dalgarno, R. J. Warburton, X. Marie, and B. Urbaszek, "Robust Quantum Dot Exciton Generation via Adiabatic Passage with Frequency-Swept Optical Pulses," *Phys. Rev. Lett.*, vol. 106, no. 16, pp. 1–4, 2011.

[164] T. Kaldewey, A. V. Kuhlmann, S. R. Valentin, A. Ludwig, A. D. Wieck, and R. J. Warburton, "Far-field nanoscopy on a semiconductor quantum dot via a rapid-adiabatic-passage-based switch," *Nature Photonics*, vol. 12, no. 2, pp. 68–72, 2018.

[165] J. Förstner, C. Weber, J. Danckwerts, and A. Knorr, "Phonon-assisted damping of rabi oscillations in semiconductor quantum dots," *Physical review letters*, vol. 91, no. 12, p. 127401, 2003.

[166] A. Krügel, V. M. Axt, T. Kuhn, P. Machnikowski, and A. Vagov, "The role of acoustic phonons for rabi oscillations in semiconductor quantum dots," *Applied Physics B*, vol. 81, no. 7, pp. 897–904, 2005.

[167] P. Machnikowski and L. Jacak, "Resonant nature of phonon-induced damping of rabi oscillations in quantum dots," *Physical Review B*, vol. 69, no. 19, p. 193302, 2004.

[168] A. Vagov, M. D. Croitoru, M. Glässl, V. M. Axt, and T. Kuhn, "Real-time path integrals for quantum dots: Quantum dissipative dynamics with superohmic environment coupling," *Physical Review B*, vol. 83, no. 9, p. 094303, 2011.

[169] D. P. McCutcheon and A. Nazir, "Quantum dot rabi rotations beyond the weak exciton–phonon coupling regime," *New Journal of Physics*, vol. 12, no. 11, p. 113042, 2010.

[170] D. P. McCutcheon, N. S. Dattani, E. M. Gauger, B. W. Lovett, and A. Nazir, "A general approach to quantum dynamics using a variational master equation: Application to phonon-damped rabi rotations in quantum dots," *Physical Review B*, vol. 84, no. 8, p. 081305, 2011.

[171] S. Weiler, A. Ulhaq, S. Ulrich, D. Richter, M. Jetter, P. Michler, C. Roy, and S. Hughes, "Phonon-assisted incoherent excitation of a quantum dot and its emission properties," *Physical Review B*, vol. 86, no. 24, p. 241304, 2012.

[172] P. Eastham, A. Spracklen, and J. Keeling, "Lindblad theory of dynamical decoherence of quantum-dot excitons," *Physical Review B*, vol. 87, no. 19, p. 195306, 2013.

[173] J. Villas-Bôas, S. E. Ulloa, and A. Govorov, "Decoherence of rabi oscillations in a single quantum dot," *Physical review letters*, vol. 94, no. 5, p. 057404, 2005.

[174] S. Bounouar, M. Müller, A. M. Barth, M. Glässl, V. M. Axt, and P. Michler, "Phonon-assisted robust and deterministic two-photon biexciton preparation in a quantum dot," *Phys. Rev. B*, vol. 91, no. 16, pp. 1–5, 2015.

[175] J. H. Quilter, A. J. Brash, F. Liu, M. Glässl, A. M. Barth, V. M. Axt, A. J. Ramsay, M. S. Skolnick, and A. M. Fox, "Phonon-Assisted Population Inversion of a Single InGaAs/GaAs Quantum Dot by Pulsed Laser Excitation," *Phys. Rev. Lett.*, vol. 114, no. 13, pp. 1–5, 2015.

[176] F. Liu, L. Martins, A. Brash, A. M. Barth, J. H. Quilter, V. M. Axt, M. Skolnick, and A. Fox, "Ultrafast depopulation of a quantum dot by la-phonon-assisted stimulated emission," *Physical Review B*, vol. 93, no. 16, p. 161407, 2016.

[177] M. Glässl, A. M. Barth, and V. M. Axt, "Proposed robust and high-fidelity preparation of excitons and biexcitons in semiconductor quantum dots making active use of phonons," *Physical review letters*, vol. 110, no. 14, p. 147401, 2013.

[178] T. Stievater, X. Li, D. G. Steel, D. Gammon, D. Katzer, D. Park, C. Piermarocchi, and L. Sham, "Rabi oscillations of excitons in single quantum dots," *Physical Review Letters*, vol. 87, no. 13, p. 133603, 2001.

[179] Y. Wu, X. Li, L. Duan, D. Steel, and D. Gammon, "Density matrix tomography through sequential coherent optical rotations of an exciton qubit in a single quantum dot," *Physical review letters*, vol. 96, no. 8, p. 087402, 2006.

[180] B. Patton, U. Woggon, and W. Langbein, "Coherent control and polarization readout of individual excitonic states," *Physical review letters*, vol. 95, no. 26, p. 266401, 2005.

[181] D. Hufiaker, G. Park, Z. Zou, O. Shchekin, and D. Deppe, "Continuous-wave low-threshold performance of 1.3-/um InGaAs-GaAs quantum-dot lasers," *IEEE J. Select. Topics Quantum Electron*, vol. 6, pp. 452–461, 2000.

[182] A. Rastelli, A. Ulhaq, S. Kiravittaya, L. Wang, A. Zrenner, and O. Schmidt, "In situ laser microprocessing of single self-assembled quantum dots and optical microcavities," *Applied physics letters*, vol. 90, no. 7, p. 073120, 2007.

[183] D. Ellis, R. Stevenson, R. Young, A. Shields, P. Atkinson, and D. Ritchie, "Control of fine-structure splitting of individual InAs quantum dots by rapid thermal annealing," *Applied Physics Letters*, vol. 90, no. 1, p. 011907, 2007.

[184] D. Chithrani, R. Williams, J. Lefebvre, P. Poole, and G. Aers, "Optical spectroscopy of single, site-selected, InAs/InP self-assembled quantum dots," *Applied physics letters*, vol. 84, no. 6, pp. 978–980, 2004.

[185] Q. Wang, A. Muller, P. Bianucci, E. Rossi, Q. Xue, T. Takagahara, C. Piermarocchi, A. H. MacDonald, and C.-K. Shih, "Decoherence processes during optical manipulation of excitonic qubits in semiconductor quantum dots," *Physical Review B*, vol. 72, no. 3, p. 035306, 2005.

[186] J.-H. Kim, T. Cai, C. J. Richardson, R. P. Leavitt, and E. Waks, "Two-photon interference from a bright single-photon source at telecom wavelengths," *Optica*, vol. 3, no. 6, pp. 577–584, 2016.

[187] Ł. Dusanowski, P. Holewa, A. Maryński, A. Musiał, T. Heuser, N. Srocka, D. Quandt, A. Strittmatter, S. Rodt, J. Misiewicz, S. Reitzenstein, and G. Sęk, "Triggered high-purity telecom-wavelength single-photon generation from p-shell-driven InGaAs/GaAs quantum dot," *Optics express*, vol. 25, no. 25, pp. 31122–31129, 2017.

[188] N. Sangouard, C. Simon, H. De Riedmatten, and N. Gisin, "Quantum repeaters based on atomic ensembles and linear optics," *Reviews of Modern Physics*, vol. 83, no. 1, p. 33, 2011.

[189] E. B. Flagg, A. Muller, S. V. Polyakov, A. Ling, A. Migdall, and G. S. Solomon, "Interference of single photons from two separate semiconductor quantum dots," *Physical Review Letters*, vol. 104, no. 13, p. 137401, 2010.

[190] P. Gold, A. Thoma, S. Maier, S. Reitzenstein, C. Schneider, S. Höfling, and M. Kamp, "Two-photon interference from remote quantum dots with inhomogeneously broadened linewidths," *Physical Review B*, vol. 89, no. 3, p. 035313, 2014.

[191] V. Giesz, S. Portalupi, T. Grange, C. Antón, L. De Santis, J. Demory, N. Somaschi, I. Sagnes, A. Lemaître, L. Lanco, *et al.*, "Cavity-enhanced two-photon interference using remote quantum dot sources," *Physical Review B*, vol. 92, no. 16, p. 161302, 2015.

[192] E. R. Schmidgall, P. R. Eastham, and R. T. Phillips, "Population inversion in quantum dot ensembles via adiabatic rapid passage," *Phys. Rev. B*, vol. 81, no. 19, pp. 1–5, 2010.

[193] S. Lüker, T. Kuhn, and D. Reiter, "Phonon impact on optical control schemes of quantum dots: role of quantum dot geometry and symmetry," *Physical Review B*, vol. 96, no. 24, p. 245306, 2017.

[194] H. Htoon, D. Kulik, O. Baklenov, A. Holmes Jr, T. Takagahara, and C.-K. Shih, "Carrier relaxation and quantum decoherence of excited states in self-assembled quantum dots," *Physical Review B*, vol. 63, no. 24, p. 241303, 2001.

[195] A. Zrenner, E. Beham, S. Stufler, F. Findeis, M. Bichler, and G. Abstreiter, "Coherent properties of a two-level system based on a quantum-dot photodiode," *Nature*, vol. 418, no. 6898, pp. 612–614, 2002.

[196] A. V. Kuhlmann, J. Houel, D. Brunner, A. Ludwig, D. Reuter, A. D. Wieck, and R. J. Warburton, "A dark-field microscope for background-free detection of resonance fluorescence from single semiconductor quantum dots operating in a set-and-forget mode," *Review of scientific instruments*, vol. 84, no. 7, p. 073905, 2013.

[197] D. Wigger, C. Schneider, S. Gerhardt, M. Kamp, S. Höfling, T. Kuhn, and J. Kasprzak, "Rabi oscillations of a quantum dot exciton coupled to acoustic phonons: coherence and population readout," *Optica*, vol. 5, no. 11, pp. 1442–1450, 2018.

[198] K. Kuroda, T. Kuroda, K. Watanabe, T. Mano, K. Sakoda, G. Kido, and N. Koguchi, "Final-state readout of exciton qubits by observing resonantly excited photoluminescence in quantum dots," *Applied Physics Letters*, vol. 90, no. 5, p. 051909, 2007.

[199] M. Kujiraoka, J. Ishi-Hayase, K. Akahane, N. Yamamoto, K. Ema, and M. Sasaki, "Optical rabi oscillations in a quantum dot ensemble," *Applied Physics Express*, vol. 3, no. 9, p. 092801, 2010.

[200] P. Eliseev, H. Li, A. Stintz, G. Liu, T. Newell, K. Malloy, and L. Lester, "Transition dipole moment of InAs/InGaAs quantum dots from experiments on ultralow-threshold laser diodes," *Applied Physics Letters*, vol. 77, no. 2, pp. 262–264, 2000.

[201] G. Park, O. B. Shchekin, D. L. Huffaker, and D. G. Deppe, "Low-threshold oxide-confined 1.3-μm quantum-dot laser," *IEEE Photonics Technology Letters*, vol. 12, no. 3, pp. 230–232, 2000.

[202] S. Haffouz, K. D. Zeuner, D. Dalacu, P. J. Poole, J. Lapointe, D. Poitras, K. Mnaymneh, X. Wu, M. Couillard, M. Korkusinski, *et al.*, "Bright single InAsP quantum dots at telecom wavelengths in position-controlled InP nanowires: the role of the photonic waveguide," *Nano letters*, vol. 18, no. 5, pp. 3047–3052, 2018.

[203] C. Santori, D. Fattal, J. Vučković, G. S. Solomon, and Y. Yamamoto, "Indistinguishable photons from a single-photon device," *nature*, vol. 419, no. 6907, pp. 594–597, 2002.

[204] S. Ates, S. Ulrich, S. Reitzenstein, A. Löffler, A. Forchel, and P. Michler, "Post-selected indistinguishable photons from the resonance fluorescence of a single quantum dot in a microcavity," *Physical Review Letters*, vol. 103, no. 16, p. 167402, 2009.

[205] T. Heindel, A. Thoma, M. von Helversen, M. Schmidt, A. Schlehahn, M. Gschrey, P. Schnauber, J.-H. Schulze, A. Strittmatter, J. Beyer, *et al.*, "A bright triggered twin-photon source in the solid state," *Nature communications*, vol. 8, no. 1, pp. 1–7, 2017.

[206] S. Bounouar, M. Strauß, A. Carmele, P. Schnauber, A. Thoma, M. Gschrey, J.-H. Schulze, A. Strittmatter, S. Rodt, A. Knorr, *et al.*, "Path-controlled time reordering of paired photons in a dressed three-level cascade," *Physical review letters*, vol. 118, no. 23, p. 233601, 2017.

[207] R. Winik, D. Cogan, Y. Don, I. Schwartz, L. Gantz, E. Schmidgall, N. Livneh, R. Rapaport, E. Buks, and D. Gershoni, "On-demand source of maximally entangled photon pairs using the biexciton-exciton radiative cascade," *Physical Review B*, vol. 95, no. 23, p. 235435, 2017.

[208] C. Gustin and S. Hughes, "Influence of electron-phonon scattering for an on-demand quantum dot single-photon source using cavity-assisted adiabatic passage," *Physical Review B*, vol. 96, no. 8, p. 085305, 2017.

[209] S. M. De Vasconcellos, S. Gordon, M. Bichler, T. Meier, and A. Zrenner, "Coherent control of a single exciton qubit by optoelectronic manipulation," *Nature Photonics*, vol. 4, no. 8, p. 545, 2010.

[210] A. Widhalm, A. Mukherjee, S. Krehs, N. Sharma, P. Kölling, A. Thiede, D. Reuter, J. Förstner, and A. Zrenner, "Ultrafast electric phase control of a single exciton qubit," *Applied Physics Letters*, vol. 112, no. 11, p. 111105, 2018.

[211] K. De Greve, L. Yu, P. L. McMahon, J. S. Pelc, C. M. Natarajan, N. Y. Kim, E. Abe, S. Maier, C. Schneider, M. Kamp, *et al.*, "Quantum-dot spin–photon entanglement via frequency downconversion to telecom wavelength," *Nature*, vol. 491, no. 7424, pp. 421–425, 2012.

[212] W. Gao, P. Fallahi, E. Togan, J. Miguel-Sánchez, and A. Imamoglu, "Observation of entanglement between a quantum dot spin and a single photon," *Nature*, vol. 491, no. 7424, pp. 426–430, 2012.

[213] J. Schaibley, A. Burgers, G. McCracken, L.-M. Duan, P. Berman, D. Steel, A. Bracker, D. Gammon, and L. Sham, "Demonstration of quantum entanglement between a single electron spin confined to an InAs quantum dot and a photon," *Physical review letters*, vol. 110, no. 16, p. 167401, 2013.

[214] A. Delteil, Z. Sun, S. Fält, and A. Imamoğlu, "Realization of a cascaded quantum system: Heralded absorption of a single photon qubit by a single-electron charged quantum dot," *Physical review letters*, vol. 118, no. 17, p. 177401, 2017.

[215] Y. He, Y.-M. He, Y.-J. Wei, X. Jiang, K. Chen, C.-Y. Lu, J.-W. Pan, C. Schneider, M. Kamp, and S. Höfling, "Quantum state transfer from a single photon to a distant quantum-dot electron spin," *Physical review letters*, vol. 119, no. 6, p. 060501, 2017.

[216] M. M. Loy, "Observation of population inversion by optical adiabatic rapid passage," *Physical Review Letters*, vol. 32, no. 15, p. 814, 1974.

[217] E. Stock, M.-R. Dachner, T. Warming, A. Schliwa, A. Lochmann, A. Hoffmann, A. I. Toropov, A. K. Bakarov, I. A. Derebezov, M. Richter, *et al.*, "Acoustic and optical phonon scattering in a single In(Ga)As quantum dot," *Physical Review B*, vol. 83, no. 4, p. 041304, 2011.

[218] K. C. Hall, K. Gundogdu, T. F. Boggess, O. B. Shchekin, and D. G. Deppe, "Carrier and spin dynamics in charged quantum dots," in *Quantum Dots, Nanoparticles, and Nanoclusters*, vol. 5361, pp. 76–87, International Society for Optics and Photonics, 2004.

[219] K. Gündoğdu, K. Hall, T. F. Boggess, D. Deppe, and O. Shchekin, "Efficient electron spin detection with positively charged quantum dots," *Applied physics letters*, vol. 84, no. 15, pp. 2793–2795, 2004.

[220] J. Robb, Y. Chen, A. Timmons, K. Hall, O. Shchekin, and D. Deppe, "Time-resolved faraday rotation measurements of spin relaxation in InGaAs/GaAs quantum dots: Role of excess energy," *Applied physics letters*, vol. 90, no. 15, p. 153118, 2007.

[221] D. Wigger, S. Lüker, D. Reiter, V. M. Axt, P. Machnikowski, and T. Kuhn, "Energy transport and coherence properties of acoustic phonons generated by optical excitation of a quantum dot," *Journal of Physics: Condensed Matter*, vol. 26, no. 35, p. 355802, 2014.

[222] E. Knill, R. Laflamme, and G. J. Milburn, "A scheme for efficient quantum computation with linear optics," *nature*, vol. 409, no. 6816, pp. 46–52, 2001.

[223] D. Dalacu, P. J. Poole, and R. L. Williams, "Nanowire-based sources of non-classical light," *Nanotechnology*, vol. 30, no. 23, p. 232001, 2019.

[224] T. F. Boggess, L. Zhang, D. Deppe, D. Huffaker, and C. Cao, "Spectral engineering of carrier dynamics in In(Ga)As self-assembled quantum dots," *Applied Physics Letters*, vol. 78, no. 3, pp. 276–278, 2001.

[225] A. Mohan, P. Gallo, M. Felici, B. Dwir, A. Rudra, J. Faist, and E. Kapon, "Record-low inhomogeneous broadening of site-controlled quantum dots for nanophotonics," *Small*, vol. 6, no. 12, pp. 1268–1272, 2010.

[226] V. V. Lozovoy, I. Pastirk, and M. Dantus, "Multiphoton intrapulse interference. iv. ultrashort laser pulse spectral phase characterization and compensation," *Optics letters*, vol. 29, no. 7, pp. 775–777, 2004.

[227] A. Ramachandran, G. R. Wilbur, S. Freisem, D. Deppe, and K. C. Hall, "Low threshold suppression of decoherence tied to exciton-phonon coupling in telecom-compatible quantum dots," *Unpublished*, 2020.

[228] A. Gamouras, M. Britton, M. Khairy, R. Mathew, D. Dalacu, P. Poole, D. Poitras, R. Williams, and K. Hall, "Energy-selective optical excitation and detection in InAs/InP quantum dot ensembles using a one-dimensional optical microcavity," *Applied Physics Letters*, vol. 103, no. 25, p. 253109, 2013.

[229] A. Ramachandran, J. Fraser-Leach, S. Freisem, D. Deppe, and K. C. Hall, "Quantification of the robustness of adiabatic rapid passage for quantum state inversion in semiconductor quantum dots," *Unpublished*, 2020.

[230] P. R. Eastham and R. T. Phillips, "Quantum condensation from a tailored exciton population in a microcavity," *Phys. Rev. B*, vol. 79, no. 16, pp. 1–5, 2009.

[231] W. Gao, P. Fallahi, E. Togan, A. Delteil, Y. Chin, J. Miguel-Sanchez, and A. Imamoğlu, "Quantum teleportation from a propagating photon to a solid-state spin qubit," *Nature communications*, vol. 4, no. 1, pp. 1–8, 2013.

[232] C. Varnava, R. M. Stevenson, J. Nilsson, J. Skiba-Szymanska, B. Dzurňák, M. Lucamarini, R. V. Penty, I. Farrer, D. A. Ritchie, and A. J. Shields, "An entangled-led-driven quantum relay over 1 km," *Npj Quantum Information*, vol. 2, no. 1, pp. 1–7, 2016.

[233] L. Schweickert, K. D. Jöns, K. D. Zeuner, S. F. C. da Silva, H. Huang, T. Lettner, M. Reindl, J. Zichi, R. Trotta, A. Rastelli, *et al.*, "On–demand solid–state single–photon source with 99.99% purity," *arXiv preprint arXiv:1712.06937*, 2017.

Appendix A

Copyright Permission

SPRINGER NATURE LICENSE
TERMS AND CONDITIONS

Apr 17, 2020

This Agreement between Dalhousie University -- Ajan Ramachandran ("You") and Springer Nature ("Springer Nature") consists of your license details and the terms and conditions provided by Springer Nature and Copyright Clearance Center.

License Number	4811450563372
License date	Apr 17, 2020
Licensed Content Publisher	Springer Nature
Licensed Content Publication	Nature Reviews Materials
Licensed Content Title	Material platforms for spin-based photonic quantum technologies
Licensed Content Author	Mete Atatüre et al
Licensed Content Date	Apr 30, 2018
Type of Use	Thesis/Dissertation
Requestor type	academic/university or research institute
Format	electronic
Portion	figures/tables/illustrations

Number of figures/tables /illustrations	1
High-res required	no
Will you be translating?	no
Circulation/distribution	1 - 29
Author of this Springer Nature content	no
Title	Quantum State Preparation Using Chirped Laser Pulses in Semiconductor Quantum Dots
Institution name	Dalhousie University
Expected presentation date	Apr 2020
Portions	Figure 1 Quantum network
Requestor Location	Dalhousie University 6310 Coburg Road Department of Physics Halifax, NS B3H 4R2 Canada Attn: Dalhousie University
Total	0.00 CAD

Terms and Conditions

Springer Nature Customer Service Centre GmbH
Terms and Conditions

This agreement sets out the terms and conditions of the licence (the **Licence**) between you and **Springer Nature Customer Service Centre GmbH** (the **Licensor**). By clicking 'accept' and completing the transaction for the material (**Licensed Material**), you also confirm your acceptance of these terms and conditions.

1. Grant of License

1. 1. The Licensor grants you a personal, non-exclusive, non-transferable, world-wide licence to reproduce the Licensed Material for the purpose specified in your order only. Licences are granted for the specific use requested in the order and for no other use, subject to the conditions below.

1. 2. The Licensor warrants that it has, to the best of its knowledge, the rights to license reuse of the Licensed Material. However, you should ensure that the material you are requesting is original to the Licensor and does not carry the copyright of another entity (as credited in the published version).

1. 3. If the credit line on any part of the material you have requested indicates that it was reprinted or adapted with permission from another source, then you should also seek permission from that source to reuse the material.

2. Scope of Licence

2. 1. You may only use the Licensed Content in the manner and to the extent permitted by these Ts&Cs and any applicable laws.

2. 2. A separate licence may be required for any additional use of the Licensed Material, e.g. where a licence has been purchased for print only use, separate permission must be obtained for electronic re-use. Similarly, a licence is only valid in the language selected and does not apply for editions in other languages unless additional translation rights have been granted separately in the licence. Any content owned by third parties are expressly excluded from the licence.

2. 3. Similarly, rights for additional components such as custom editions and derivatives require additional permission and may be subject to an additional fee. Please apply to Journalpermissions@springernature.com/bookpermissions@springernature.com for these rights.

2. 4. Where permission has been granted **free of charge** for material in print, permission may also be granted for any electronic version of that work, provided that the material is incidental to your work as a whole and that the electronic version is essentially equivalent to, or substitutes for, the print

version.

2. 5. An alternative scope of licence may apply to signatories of the STM Permissions Guidelines, as amended from time to time.

3. Duration of Licence

3. 1. A licence for is valid from the date of purchase ('Licence Date') at the end of the relevant period in the below table:

Scope of Licence	**Duration of Licence**
Post on a website	12 months
Presentations	12 months
Books and journals	Lifetime of the edition in the language purchased

4. Acknowledgement

4. 1. The Licensor's permission must be acknowledged next to the Licenced Material in print. In electronic form, this acknowledgement must be visible at the same time as the figures/tables/illustrations or abstract, and must be hyperlinked to the journal/book's homepage. Our required acknowledgement format is in the Appendix below.

5. Restrictions on use

5. 1. Use of the Licensed Material may be permitted for incidental promotional use and minor editing privileges e.g. minor adaptations of single figures, changes of format, colour and/or style where the adaptation is credited as set out in Appendix 1 below. Any other changes including but not limited to, cropping, adapting, omitting material that affect the meaning, intention or moral rights of the author are strictly prohibited.

5. 2. You must not use any Licensed Material as part of any design or trademark.

5. 3. Licensed Material may be used in Open Access Publications (OAP) before publication by Springer Nature, but any Licensed Material must be removed from OAP sites prior to final publication.

6. Ownership of Rights

6. 1. Licensed Material remains the property of either Licensor or the relevant third party and any rights not explicitly granted herein are expressly reserved.

7. Warranty

IN NO EVENT SHALL LICENSOR BE LIABLE TO YOU OR ANY OTHER PARTY OR ANY OTHER PERSON OR FOR ANY SPECIAL, CONSEQUENTIAL, INCIDENTAL OR INDIRECT DAMAGES, HOWEVER CAUSED, ARISING OUT OF OR IN CONNECTION WITH THE DOWNLOADING, VIEWING OR USE OF THE MATERIALS REGARDLESS OF THE FORM OF ACTION, WHETHER FOR BREACH OF CONTRACT, BREACH OF WARRANTY, TORT, NEGLIGENCE, INFRINGEMENT OR OTHERWISE (INCLUDING, WITHOUT LIMITATION, DAMAGES BASED ON LOSS OF PROFITS, DATA, FILES, USE, BUSINESS OPPORTUNITY OR CLAIMS OF THIRD PARTIES), AND
WHETHER OR NOT THE PARTY HAS BEEN ADVISED OF THE POSSIBILITY OF SUCH DAMAGES. THIS LIMITATION SHALL APPLY NOTWITHSTANDING ANY FAILURE OF ESSENTIAL PURPOSE OF ANY LIMITED REMEDY PROVIDED HEREIN.

8. Limitations

8. 1. ***BOOKS ONLY:*** Where **'reuse in a dissertation/thesis'** has been selected the following terms apply: Print rights of the final author's accepted manuscript (for clarity, NOT the published version) for up to 100 copies, electronic rights for use only on a personal website or institutional repository as defined by the Sherpa guideline (www.sherpa.ac.uk/romeo/).

9. Termination and Cancellation

9. 1. Licences will expire after the period shown in Clause 3 (above).

9. 2. Licensee reserves the right to terminate the Licence in the event that payment is not received in full or if there has been a breach of this agreement by you.

Appendix 1 — Acknowledgements:

For Journal Content:

Reprinted by permission from [**the Licensor**]: [**Journal Publisher** (e.g. Nature/Springer/Palgrave)] [**JOURNAL NAME**] [**REFERENCE CITATION** (Article name, Author(s) Name), [**COPYRIGHT**] (year of publication)

For **Advance Online Publication papers:**
Reprinted by permission from [**the Licensor**]: [**Journal Publisher** (e.g. Nature/Springer/Palgrave)] [**JOURNAL NAME**] [**REFERENCE CITATION** (Article name, Author(s) Name), [**COPYRIGHT**] (year of publication), advance online publication, day month year (doi: 10.1038/sj.[JOURNAL ACRONYM].)

For Adaptations/Translations:
Adapted/Translated by permission from [**the Licensor**]: [**Journal Publisher** (e.g. Nature/Springer/Palgrave)] [**JOURNAL NAME**] [**REFERENCE CITATION** (Article name, Author(s) Name), [**COPYRIGHT**] (year of publication)

Note: For any republication from the British Journal of Cancer, the following credit line style applies:

Reprinted/adapted/translated by permission from [**the Licensor**]: on behalf of Cancer Research UK: : [**Journal Publisher** (e.g. Nature/Springer/Palgrave)] [**JOURNAL NAME**] [**REFERENCE CITATION** (Article name, Author(s) Name), [**COPYRIGHT]** (year of publication)

For **Advance Online Publication** papers:
Reprinted by permission from The [**the Licensor**]: on behalf of Cancer Research UK: [**Journal Publisher** (e.g. Nature/Springer/Palgrave)] [**JOURNAL NAME**] [**REFERENCE CITATION** (Article name, Author(s) Name), [**COPYRIGHT**] (year of publication), advance online publication, day month year (doi: 10.1038/sj.[JOURNAL ACRONYM])

For Book content:
Reprinted/adapted by permission from [**the Licensor**]: [**Book Publisher** (e.g. Palgrave Macmillan, Springer etc) [**Book Title**] by [**Book author**(s)] [**COPYRIGHT**] (year of publication)

Other Conditions:

Version 1.2

Questions? customercare@copyright.com or +1-855-239-3415 (toll free in the US) or +1-978-646-2777.

AIP PUBLISHING LICENSE
TERMS AND CONDITIONS

Apr 17, 2020

This Agreement between Dalhousie University -- Ajan Ramachandran ("You") and AIP Publishing ("AIP Publishing") consists of your license details and the terms and conditions provided by AIP Publishing and Copyright Clearance Center.

License Number	4811451028488
License date	Apr 17, 2020
Licensed Content Publisher	AIP Publishing
Licensed Content Publication	Applied Physics Letters
Licensed Content Title	Determination of the shape and indium distribution of low-growth-rate InAs quantum dots by cross-sectional scanning tunneling microscopy
Licensed Content Author	D. M. Bruls, J. W. A. M. Vugs, P. M. Koenraad, et al
Licensed Content Date	Aug 26, 2002
Licensed Content Volume	81

Licensed Content Issue	9
Type of Use	Thesis/Dissertation
Requestor type	Student
Format	Electronic
Portion	Figure/Table
Number of figures/tables	1
Title	Quantum State Preparation Using Chirped Laser Pulses in Semiconductor Quantum Dots
Institution name	Dalhousie University
Expected presentation date	Apr 2020
Portions	Figure 1
Requestor Location	Dalhousie University 6310 Coburg Road Department of Physics Halifax, NS B3H 4R2 Canada Attn: Dalhousie University
Total	0.00 CAD

Terms and Conditions

AIP Publishing -- Terms and Conditions: Permissions Uses

AIP Publishing hereby grants to you the non-exclusive right and license to use and/or distribute the Material according to the use specified in your order, on a one-time basis, for the specified term, with a maximum distribution equal to the number that you have ordered. Any links or other content accompanying the Material are not the subject of this license.

1. You agree to include the following copyright and permission notice with the reproduction of the Material:"Reprinted from [FULL CITATION], with the permission of AIP Publishing." For an article, the credit line and permission notice must be printed on the first page of the article or book chapter. For photographs, covers, or tables, the notice may appear with the Material, in a footnote, or in the reference list.
2. If you have licensed reuse of a figure, photograph, cover, or table, it is your responsibility to ensure that the material is original to AIP Publishing and does not contain the copyright of another entity, and that the copyright notice of the figure, photograph, cover, or table does not indicate that it was reprinted by AIP Publishing, with permission, from another source. Under no circumstances does AIP Publishing purport or intend to grant permission to reuse material to which it does not hold appropriate rights.
   You may not alter or modify the Material in any manner. You may translate the Material into another language only if you have licensed translation rights. You may not use the Material for promotional purposes.
3. The foregoing license shall not take effect unless and until AIP Publishing or its agent, Copyright Clearance Center, receives the Payment in accordance with Copyright Clearance Center Billing and Payment Terms and Conditions, which are incorporated herein by reference.
4. AIP Publishing or Copyright Clearance Center may, within two business days of granting this license, revoke the license for any reason whatsoever, with a full refund payable to you. Should you violate the terms of this license at any time, AIP Publishing, or Copyright Clearance Center may revoke the license with no refund to you. Notice of such revocation will be made using the contact information provided by you. Failure to receive such notice will not

nullify the revocation.

5. AIP Publishing makes no representations or warranties with respect to the Material. You agree to indemnify and hold harmless AIP Publishing, and their officers, directors, employees or agents from and against any and all claims arising out of your use of the Material other than as specifically authorized herein.
6. The permission granted herein is personal to you and is not transferable or assignable without the prior written permission of AIP Publishing. This license may not be amended except in a writing signed by the party to be charged.
7. If purchase orders, acknowledgments or check endorsements are issued on any forms containing terms and conditions which are inconsistent with these provisions, such inconsistent terms and conditions shall be of no force and effect. This document, including the CCC Billing and Payment Terms and Conditions, shall be the entire agreement between the parties relating to the subject matter hereof.

This Agreement shall be governed by and construed in accordance with the laws of the State of New York. Both parties hereby submit to the jurisdiction of the courts of New York County for purposes of resolving any disputes that may arise hereunder.

V1.2

Questions? customercare@copyright.com or +1-855-239-3415 (toll free in the US) or +1-978-646-2777.

Copyright Clearance Center Marketplace™

Order Confirmation

Thank you, your order has been placed. An email confirmation has been sent to you. Your order license details printable licenses will be available within 24 hours. Please access Manage Account for final order deta

This is not an invoice. Please go to manage account to access your order history and invoices.

CUSTOMER INFORMATION

Payment by invoice: You can cancel your order until the invoice is generated by contacting customer serv

Billing Address

Ajan Ramachandran
Dalhousie University
6310 Coburg Road
Department of Physics
Halifax, NS B3H 4R2
Canada

+1 (902) 293-4151
ajanpr@dal.ca

Customer Location

Ajan Ramachandran
Dalhousie University
6310 Coburg Road
Department of Physics
Halifax, NS B3H 4R2
Canada

PO Number (optional)

N/A

Payment options

Invoice

PENDING ORDER CONFIRMATION

Confirmation Number: Pending

Order Date: 17-Apr-2020

1. Semiconductor Science and Technology

0.00 CAD

Order license ID	Pending	**Publisher**	IOP Publishing
ISSN	0268-1242	**Portion**	Chart/graph/table /figure
Type of Use	Republish in a thesis/dissertation		

LICENSED CONTENT

Publication Title	Semiconductor Science and Technology	**Country**	United Kingdom of Great Britain and Northern Ireland
Author/Editor	Institute of Physics (Great Britain), American Institute of Physics.	**Rightsholder**	IOP Publishing, Ltd
		Publication Type	Journal
Date	01/01/1986		
Language	English		

REQUEST DETAILS

Portion Type	Chart/graph/table/figur	**Distribution**	Canada
Number of charts / graphs / tables / figures requested	1	**Translation**	Original language of publication
		Copies for the disabled?	No
Format (select all that apply)	Electronic	**Minor editing privileges?**	No
Who will republish the content?	Academic institution	**Incidental promotional use?**	No
Duration of Use	Life of current editior	**Currency**	CAD
Lifetime Unit Quantity	Up to 499		
Rights Requested	Main product		

NEW WORK DETAILS

Title	QUANTUM STATE PREPARATION USING CHIRPED LASER PULSES IN SEMICONDUCTOR QUANTUM DOTS	**Institution name**	Dalhousie University
		Expected presentation date	2020-05-21
Instructor name	Ajan Ramachandran		

ADDITIONAL DETAILS

Order reference number	N/A	**The requesting person / organization to appear on the license**	Ajan Ramachandran

REUSE CONTENT DETAILS

Title, description or numeric reference of the portion(s)	Figure 11	**Title of the article/chapter the portion is from**	A review of the coherent optical control ofthe exciton and spin states ofsemiconductor quantum dots
Editor of portion(s)	N/A		
Volume of serial or monograph	Semicond. Sci. Technol.25 103001	**Author of portion(s)**	A J Ramsay
Page or page range of portion	10	**Issue, if republishing an article from a serial**	N/A

Publication date of portion 2010-08-06

PUBLISHER TERMS AND CONDITIONS

These special terms and conditions are in addition to the standard terms and conditions for CCC's Republication Ser and, together with those standard terms and conditions, govern the use of the Works. As the User you will mak reasonable efforts to contact the author(s) of the article which the Work is to be reused from, to seek consent for intended use. Contacting one author who is acting expressly as authorised agent for their co-author(s) is acceptable. U will reproduce the following wording prominently alongside the Work: the source of the Work, including author, articl title of journal, volume number, issue number (if relevant), page range (or first page if this is the only information avail and date of first publication. This information can be contained in a footnote or reference note; and a link back t article (via DOI); and if practicable, and IN ALL CASES for new works published under any of the Creative Commor licences, the words "© IOP Publishing. Reproduced with permission. All rights reserved" Without the express permiss of the author(s) and the Rightsholder of the article from which the Work is to be reused, User shall not use it in any which, in the opinion of the Rightsholder, could: (i) distort or alter the author(s)' original intention(s) and meaning; (i prejudicial to the honour or reputation of the author(s); and/or (iii) imply endorsement by the author(s) and/ Rightsholder. This licence does not apply to any article which is credited to another source and which does not have copyright line '© IOP Publishing Ltd'. User must check the copyright line of the article from which the Work is to be reu to check that IOP Publishing Ltd has all the necessary rights to be able to grant permission. User is solely responsible identifying and obtaining separate licences and permissions from the copyright owner for reuse of any such third material/figures which the Rightsholder is not the copyright owner of. The Rightsholder shall not reimburse any fees w User pays for a republication license for such third party content. This licence does not apply to any material/figure w is credited to another source in the Rightsholder's publication or has been obtained from a third party. User must c the Version of Record of the article from which the Work is to be reused, to check whether any of the material in the V is third party material. Third party citations and/or copyright notices and/or permissions statements may not be inclu any other version of the article from which the Work is to be reused and so cannot be relied upon by the User. Us solely responsible for identifying and obtaining separate licences and permissions from the copyright owner for reu any such third party material/figures where the Rightsholder is not the copyright owner. The Rightsholder sha reimburse any fees which User pays for a republication license for such third party content. User and CCC acknowle that the Rightsholder may, from time to time, make changes or additions to these special terms and conditions wi express notification, provided that these shall not apply to permissions already secured and paid for by User prior to change or addition. User acknowledges that the Rightsholder (which includes companies within its group and third pa for whom it publishes its titles) may make use of personal data collected through the service in the course of business. If User is the author of the Work, User may automatically have the right to reuse it under the rights granted when User transferred the copyright in the article to the Rightsholder. User should check the copyright form an relevant author rights policy to check whether permission is required. If User is the author of the Work and does re permission for proposed reuse of the Work, User should select 'Author of requested content' as the Requestor Type. Rightsholder shall not reimburse any fees which User pays for a republication license. If User is the author of the ar which User wishes to reuse in User's thesis or dissertation, the republication licence covers the right to include Accepted Manuscript version (not the Version of Record) of the article. User must include citation details and, for or use, a link to the Version of Record of the article on the Rightsholder's website. User may need to obtain separ permission for any third party content included within the article. User must check this with the copyright owner of third party content. User may not include the article in a thesis or dissertation which is published by ProQuest. Any c commercial use of User's thesis or dissertation containing the article would also need to be expressly notified in writi the Rightsholder at the time of request and would require separate written permission from the Rightsholder. User not need to request permission for Work which has been published under a CC BY licence. User must check the Vers of Record of the CC BY article from which the Work is to be reused, to check whether any of the material in the Wor third party material and so not published under the CC BY licence. User is solely responsible for identifying and obtai separate licences and permissions from the copyright owner for reuse of any such third party material/figures Rightsholder shall not reimburse any fees which User pays for such licences and permissions. As well as CCC, th Rightsholder shall have the right to bring any legal action that it deems necessary to enforce its rights should it cons that the Work infringes those rights in any way. For STM Signatories ONLY (as agreed as part of the STM Guidelines) Ar licence granted for a particular edition of a Work will apply also to subsequent editions of it and for editions in languages, provided such editions are for the Work as a whole in situ and do not involve the separate exploitation o permitted illustrations or excerpt

Total Due: 0.00 CAD

American Physical Society
Reuse and Permissions License

19-Apr-2020

This license agreement between the American Physical Society ("APS") and Ajan Ramachandran ("You") consists of your license details and the terms and conditions provided by the American Physical Society and SciPris.

Licensed Content Information

License Number:	**RNP/20/APR/024949**
License date:	19-Apr-2020
DOI:	10.1103/PhysRevB.85.121302
Title:	Influence of acoustic phonons on the optical control of quantum dots driven by adiabatic rapid passage
Author:	S. Lüker et al.
Publication:	Physical Review B
Publisher:	American Physical Society
Cost:	USD $ 0.00

Request Details

Does your reuse require significant modifications: No

Specify intended distribution locations:	Canada
Reuse Category:	Reuse in a thesis/dissertation
Requestor Type:	Student
Items for Reuse:	Figures/Tables
Number of Figure/Tables:	1
Figure/Tables Details:	Figure 3 (a)
Format for Reuse:	Electronic

Information about New Publication:

University/Publisher:	Dalhousie University
Title of dissertation/thesis:	QUANTUM STATE PREPARATION USING CHIRPED LASER PULSES IN SEMICONDUCTOR QUANTUM DOTS
Author(s):	Ajan Ramachandran
Expected completion date:	May. 2020

License Requestor Information

Name:	Ajan Ramachandran
Affiliation:	Individual
Email Id:	ajanpr@dal.ca
Country:	Canada

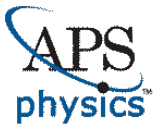

American Physical Society
Reuse and Permissions License

TERMS AND CONDITIONS

The American Physical Society (APS) is pleased to grant the Requestor of this license a non-exclusive, non-transferable permission, limited to Electronic format, provided all criteria outlined below are followed.

1. You must also obtain permission from at least one of the lead authors for each separate work, if you haven't done so already. The author's name and affiliation can be found on the first page of the published Article.
2. For electronic format permissions, Requestor agrees to provide a hyperlink from the reprinted APS material using the source material's DOI on the web page where the work appears. The hyperlink should use the standard DOI resolution URL, http://dx.doi.org/{DOI}. The hyperlink may be embedded in the copyright credit line.
3. For print format permissions, Requestor agrees to print the required copyright credit line on the first page where the material appears: "Reprinted (abstract/excerpt/figure) with permission from [(FULL REFERENCE CITATION) as follows: Author's Names, APS Journal Title, Volume Number, Page Number and Year of Publication.] Copyright (YEAR) by the American Physical Society."
4. Permission granted in this license is for a one-time use and does not include permission for any future editions, updates, databases, formats or other matters. Permission must be sought for any additional use.
5. Use of the material does not and must not imply any endorsement by APS.
6. APS does not imply, purport or intend to grant permission to reuse materials to which it does not hold copyright. It is the requestor's sole responsibility to ensure the licensed material is original to APS and does not contain the copyright of another entity, and that the copyright notice of the figure, photograph, cover or table does not indicate it was reprinted by APS with permission from another source.
7. The permission granted herein is personal to the Requestor for the use specified and is not transferable or assignable without express written permission of APS. This license may not be amended except in writing by APS.
8. You may not alter, edit or modify the material in any manner.
9. You may translate the materials only when translation rights have been granted.
10. APS is not responsible for any errors or omissions due to translation.
11. You may not use the material for promotional, sales, advertising or marketing purposes.
12. The foregoing license shall not take effect unless and until APS or its agent, Aptara, receives payment in full in accordance with Aptara Billing and Payment Terms and Conditions, which are incorporated herein by reference.
13. Should the terms of this license be violated at any time, APS or Aptara may revoke the license with no refund to you and seek relief to the fullest extent of the laws of the USA. Official written notice will be made using the contact information provided with the permission request. Failure to receive such notice will not nullify revocation of the permission.
14. APS reserves all rights not specifically granted herein.
15. This document, including the Aptara Billing and Payment Terms and Conditions, shall be the entire agreement between the parties relating to the subject matter hereof.

American Physical Society
Reuse and Permissions License

17-Apr-2020

This license agreement between the American Physical Society ("APS") and Ajan Ramachandran ("You") consists of your license details and the terms and conditions provided by the American Physical Society and SciPris.

Licensed Content Information

License Number:	**RNP/20/APR/024896**
License date:	17-Apr-2020
DOI:	10.1103/PhysRevB.90.035316
Title:	Subpicosecond adiabatic rapid passage on a single semiconductor quantum dot: Phonon-mediated dephasing in the strong-driving regime
Author:	Reuble Mathew et al.
Publication:	Physical Review B
Publisher:	American Physical Society
Cost:	USD $ 0.00

Request Details

Does your reuse require significant modifications: No

Specify intended distribution locations:	Canada
Reuse Category:	Reuse in a thesis/dissertation
Requestor Type:	Student
Items for Reuse:	Figures/Tables
Number of Figure/Tables:	1
Figure/Tables Details:	Figure 2
Format for Reuse:	Electronic

Information about New Publication:

University/Publisher:	Dalhousie University
Title of dissertation/thesis:	QUANTUM STATE PREPARATION USING CHIRPED LASER PULSES IN SEMICONDUCTOR QUANTUM DOTS
Author(s):	Ajan Ramachandran
Expected completion date:	May. 2020

License Requestor Information

Name:	Ajan Ramachandran
Affiliation:	Individual
Email Id:	ajanpr@dal.ca
Country:	Canada

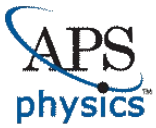

American Physical Society
Reuse and Permissions License

TERMS AND CONDITIONS

The American Physical Society (APS) is pleased to grant the Requestor of this license a non-exclusive, non-transferable permission, limited to Electronic format, provided all criteria outlined below are followed.

1. You must also obtain permission from at least one of the lead authors for each separate work, if you haven't done so already. The author's name and affiliation can be found on the first page of the published Article.
2. For electronic format permissions, Requestor agrees to provide a hyperlink from the reprinted APS material using the source material's DOI on the web page where the work appears. The hyperlink should use the standard DOI resolution URL, http://dx.doi.org/{DOI}. The hyperlink may be embedded in the copyright credit line.
3. For print format permissions, Requestor agrees to print the required copyright credit line on the first page where the material appears: "Reprinted (abstract/excerpt/figure) with permission from [(FULL REFERENCE CITATION) as follows: Author's Names, APS Journal Title, Volume Number, Page Number and Year of Publication.] Copyright (YEAR) by the American Physical Society."
4. Permission granted in this license is for a one-time use and does not include permission for any future editions, updates, databases, formats or other matters. Permission must be sought for any additional use.
5. Use of the material does not and must not imply any endorsement by APS.
6. APS does not imply, purport or intend to grant permission to reuse materials to which it does not hold copyright. It is the requestor's sole responsibility to ensure the licensed material is original to APS and does not contain the copyright of another entity, and that the copyright notice of the figure, photograph, cover or table does not indicate it was reprinted by APS with permission from another source.
7. The permission granted herein is personal to the Requestor for the use specified and is not transferable or assignable without express written permission of APS. This license may not be amended except in writing by APS.
8. You may not alter, edit or modify the material in any manner.
9. You may translate the materials only when translation rights have been granted.
10. APS is not responsible for any errors or omissions due to translation.
11. You may not use the material for promotional, sales, advertising or marketing purposes.
12. The foregoing license shall not take effect unless and until APS or its agent, Aptara, receives payment in full in accordance with Aptara Billing and Payment Terms and Conditions, which are incorporated herein by reference.
13. Should the terms of this license be violated at any time, APS or Aptara may revoke the license with no refund to you and seek relief to the fullest extent of the laws of the USA. Official written notice will be made using the contact information provided with the permission request. Failure to receive such notice will not nullify revocation of the permission.
14. APS reserves all rights not specifically granted herein.
15. This document, including the Aptara Billing and Payment Terms and Conditions, shall be the entire agreement between the parties relating to the subject matter hereof.

Re: Permission to reuse the table from "Single-Photon Sources," Optics & Photonics News 30(9), 32-39 (2019)

Urbasi Sinha <usinha@rri.res.in>
Mon 20-04-2020 14:24
To: Ajan Ramachandran <ajanpr@Dal.Ca>

CAUTION: The Sender of this email is not from within Dalhousie.

Dear Ajan,

Yes that should be fine provided proper citation is given to our work.

All the best.

--
Prof. Urbasi Sinha
Raman Research Institute
C. V. Raman Avenue
Sadashivanagar
Bangalore - 560 080
INDIA. Editorial Board Member, New Journal of Physics.
[Personal website: http://www.rri.res.in/~usinha/Lab website: http://www.rri.res.in/quic/]

----- Original Message -----
From: Ajan Ramachandran <ajanpr@Dal.Ca>
To: usinha@rri.res.in
Sent: Mon, 20 Apr 2020 21:27:13 +0530 (IST)
Subject: Permission to reuse the table from "Single-Photon Sources," Optics & Photonics News 30(9), 32-39 (2019)

Hello Prof. Sinha,

I am Ajan Ramachandran, a PhD student in Dalhousie University Halifax, N.S., Canada.

I would like to get permission to reuse the table at the end of the article "Single-Photon Sources," Optics & Photonics News 30(9), 32-39 (2019) " by Sinha et al in my doctoral thesis titled "Quantum State Preparation Using Chirped Laser Pulses in Semiconductor Quantum Dots".

The table will be used in a section comparing different single photon emitter technologies.

Thank you very much for your time.

Regards
Ajan Ramachandran

American Physical Society
Reuse and Permissions License

04-Mar-2020

This license agreement between the American Physical Society ("APS") and Ajan Ramachandran ("You") consists of your license details and the terms and conditions provided by the American Physical Society and SciPris.

Licensed Content Information

License Number:	**RNP/20/MAR/023408**
License date:	04-Mar-2020
DOI:	10.1103/PhysRevB.93.085407
Title:	Ramsey interference in a multilevel quantum system
Author:	J. P. Lee et al.
Publication:	Physical Review B
Publisher:	American Physical Society
Cost:	USD $ 0.00

Request Details

Does your reuse require significant modifications: No

Specify intended distribution locations:	Worldwide
Reuse Category:	Reuse in a thesis/dissertation
Requestor Type:	Student
Items for Reuse:	Figures/Tables
Number of Figure/Tables:	1
Figure/Tables Details:	Figure 2
Format for Reuse:	Electronic

Information about New Publication:

University/Publisher:	Dalhousie University
Title of dissertation/thesis:	Quantum State Preparation Using Chirped Laser Pulses in Semiconductor Quantum Dots
Author(s):	Ajan Ramachandran
Expected completion date:	Apr. 2020

License Requestor Information

Name:	Ajan Ramachandran
Affiliation:	Individual
Email Id:	ajanpr@gmail.com
Country:	Canada

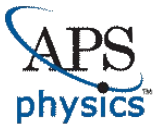

American Physical Society
Reuse and Permissions License

TERMS AND CONDITIONS

The American Physical Society (APS) is pleased to grant the Requestor of this license a non-exclusive, non-transferable permission, limited to Electronic format, provided all criteria outlined below are followed.

1. You must also obtain permission from at least one of the lead authors for each separate work, if you haven't done so already. The author's name and affiliation can be found on the first page of the published Article.
2. For electronic format permissions, Requestor agrees to provide a hyperlink from the reprinted APS material using the source material's DOI on the web page where the work appears. The hyperlink should use the standard DOI resolution URL, http://dx.doi.org/{DOI}. The hyperlink may be embedded in the copyright credit line.
3. For print format permissions, Requestor agrees to print the required copyright credit line on the first page where the material appears: "Reprinted (abstract/excerpt/figure) with permission from [(FULL REFERENCE CITATION) as follows: Author's Names, APS Journal Title, Volume Number, Page Number and Year of Publication.] Copyright (YEAR) by the American Physical Society."
4. Permission granted in this license is for a one-time use and does not include permission for any future editions, updates, databases, formats or other matters. Permission must be sought for any additional use.
5. Use of the material does not and must not imply any endorsement by APS.
6. APS does not imply, purport or intend to grant permission to reuse materials to which it does not hold copyright. It is the requestor's sole responsibility to ensure the licensed material is original to APS and does not contain the copyright of another entity, and that the copyright notice of the figure, photograph, cover or table does not indicate it was reprinted by APS with permission from another source.
7. The permission granted herein is personal to the Requestor for the use specified and is not transferable or assignable without express written permission of APS. This license may not be amended except in writing by APS.
8. You may not alter, edit or modify the material in any manner.
9. You may translate the materials only when translation rights have been granted.
10. APS is not responsible for any errors or omissions due to translation.
11. You may not use the material for promotional, sales, advertising or marketing purposes.
12. The foregoing license shall not take effect unless and until APS or its agent, Aptara, receives payment in full in accordance with Aptara Billing and Payment Terms and Conditions, which are incorporated herein by reference.
13. Should the terms of this license be violated at any time, APS or Aptara may revoke the license with no refund to you and seek relief to the fullest extent of the laws of the USA. Official written notice will be made using the contact information provided with the permission request. Failure to receive such notice will not nullify revocation of the permission.
14. APS reserves all rights not specifically granted herein.
15. This document, including the Aptara Billing and Payment Terms and Conditions, shall be the entire agreement between the parties relating to the subject matter hereof.

American Physical Society
Reuse and Permissions License

04-Mar-2020

This license agreement between the American Physical Society ("APS") and Ajan Ramachandran ("You") consists of your license details and the terms and conditions provided by the American Physical Society and SciPris.

Licensed Content Information

License Number:	**RNP/20/MAR/023409**
License date:	04-Mar-2020
DOI:	10.1103/PhysRevB.78.075301
Title:	Two-qubit conditional quantum-logic operation in a single self-assembled quantum dot
Author:	S. J. Boyle et al.
Publication:	Physical Review B
Publisher:	American Physical Society
Cost:	USD $ 0.00

Request Details

Does your reuse require significant modifications: No

Specify intended distribution locations:	Worldwide
Reuse Category:	Reuse in a thesis/dissertation
Requestor Type:	Student
Items for Reuse:	Figures/Tables
Number of Figure/Tables:	2
Figure/Tables Details:	Figure 2 and Figure 3
Format for Reuse:	Electronic

Information about New Publication:

University/Publisher:	Dalhousie University
Title of dissertation/thesis:	Quantum State Preparation Using Chirped Laser Pulses in Semiconductor Quantum Dots
Author(s):	Ajan Ramachandran
Expected completion date:	Apr. 2020

License Requestor Information

Name:	Ajan Ramachandran
Affiliation:	Individual
Email Id:	ajanpr@gmail.com
Country:	Canada

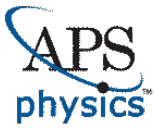

American Physical Society
Reuse and Permissions License

TERMS AND CONDITIONS

The American Physical Society (APS) is pleased to grant the Requestor of this license a non-exclusive, non-transferable permission, limited to Electronic format, provided all criteria outlined below are followed.

1. You must also obtain permission from at least one of the lead authors for each separate work, if you haven't done so already. The author's name and affiliation can be found on the first page of the published Article.
2. For electronic format permissions, Requestor agrees to provide a hyperlink from the reprinted APS material using the source material's DOI on the web page where the work appears. The hyperlink should use the standard DOI resolution URL, http://dx.doi.org/{DOI}. The hyperlink may be embedded in the copyright credit line.
3. For print format permissions, Requestor agrees to print the required copyright credit line on the first page where the material appears: "Reprinted (abstract/excerpt/figure) with permission from [(FULL REFERENCE CITATION) as follows: Author's Names, APS Journal Title, Volume Number, Page Number and Year of Publication.] Copyright (YEAR) by the American Physical Society."
4. Permission granted in this license is for a one-time use and does not include permission for any future editions, updates, databases, formats or other matters. Permission must be sought for any additional use.
5. Use of the material does not and must not imply any endorsement by APS.
6. APS does not imply, purport or intend to grant permission to reuse materials to which it does not hold copyright. It is the requestor's sole responsibility to ensure the licensed material is original to APS and does not contain the copyright of another entity, and that the copyright notice of the figure, photograph, cover or table does not indicate it was reprinted by APS with permission from another source.
7. The permission granted herein is personal to the Requestor for the use specified and is not transferable or assignable without express written permission of APS. This license may not be amended except in writing by APS.
8. You may not alter, edit or modify the material in any manner.
9. You may translate the materials only when translation rights have been granted.
10. APS is not responsible for any errors or omissions due to translation.
11. You may not use the material for promotional, sales, advertising or marketing purposes.
12. The foregoing license shall not take effect unless and until APS or its agent, Aptara, receives payment in full in accordance with Aptara Billing and Payment Terms and Conditions, which are incorporated herein by reference.
13. Should the terms of this license be violated at any time, APS or Aptara may revoke the license with no refund to you and seek relief to the fullest extent of the laws of the USA. Official written notice will be made using the contact information provided with the permission request. Failure to receive such notice will not nullify revocation of the permission.
14. APS reserves all rights not specifically granted herein.
15. This document, including the Aptara Billing and Payment Terms and Conditions, shall be the entire agreement between the parties relating to the subject matter hereof.

American Physical Society
Reuse and Permissions License

19-Apr-2020

This license agreement between the American Physical Society ("APS") and Ajan Ramachandran ("You") consists of your license details and the terms and conditions provided by the American Physical Society and SciPris.

Licensed Content Information

License Number:	**RNP/20/APR/024952**
License date:	19-Apr-2020
DOI:	10.1103/PhysRevB.73.125304
Title:	Two-photon Rabi oscillations in a single $ {\mathrm{In}}_{x} {\mathrm{Ga}}_{1-x}\mathrm{As}/\mathrm{Ga}\mathrm{As}$ quantum dot
Author:	S. Stufler et al.
Publication:	Physical Review B
Publisher:	American Physical Society
Cost:	USD $ 0.00

Request Details

Does your reuse require significant modifications: No

Specify intended distribution locations:	Canada
Reuse Category:	Reuse in a thesis/dissertation
Requestor Type:	Student
Items for Reuse:	Figures/Tables
Number of Figure/Tables:	1
Figure/Tables Details:	Figure 4
Format for Reuse:	Electronic

Information about New Publication:

University/Publisher:	Dalhousie University
Title of dissertation/thesis:	Quantum State Preparation Using Chirped Laser Pulses in Semiconductor Quantum Dots
Author(s):	Ajan Ramachandran
Expected completion date:	May. 2020

License Requestor Information

Name:	Ajan Ramachandran
Affiliation:	Individual
Email Id:	ajanpr@dal.ca
Country:	Canada

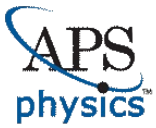

American Physical Society
Reuse and Permissions License

TERMS AND CONDITIONS

The American Physical Society (APS) is pleased to grant the Requestor of this license a non-exclusive, non-transferable permission, limited to Electronic format, provided all criteria outlined below are followed.

1. You must also obtain permission from at least one of the lead authors for each separate work, if you haven't done so already. The author's name and affiliation can be found on the first page of the published Article.
2. For electronic format permissions, Requestor agrees to provide a hyperlink from the reprinted APS material using the source material's DOI on the web page where the work appears. The hyperlink should use the standard DOI resolution URL, http://dx.doi.org/{DOI}. The hyperlink may be embedded in the copyright credit line.
3. For print format permissions, Requestor agrees to print the required copyright credit line on the first page where the material appears: "Reprinted (abstract/excerpt/figure) with permission from [(FULL REFERENCE CITATION) as follows: Author's Names, APS Journal Title, Volume Number, Page Number and Year of Publication.] Copyright (YEAR) by the American Physical Society."
4. Permission granted in this license is for a one-time use and does not include permission for any future editions, updates, databases, formats or other matters. Permission must be sought for any additional use.
5. Use of the material does not and must not imply any endorsement by APS.
6. APS does not imply, purport or intend to grant permission to reuse materials to which it does not hold copyright. It is the requestor's sole responsibility to ensure the licensed material is original to APS and does not contain the copyright of another entity, and that the copyright notice of the figure, photograph, cover or table does not indicate it was reprinted by APS with permission from another source.
7. The permission granted herein is personal to the Requestor for the use specified and is not transferable or assignable without express written permission of APS. This license may not be amended except in writing by APS.
8. You may not alter, edit or modify the material in any manner.
9. You may translate the materials only when translation rights have been granted.
10. APS is not responsible for any errors or omissions due to translation.
11. You may not use the material for promotional, sales, advertising or marketing purposes.
12. The foregoing license shall not take effect unless and until APS or its agent, Aptara, receives payment in full in accordance with Aptara Billing and Payment Terms and Conditions, which are incorporated herein by reference.
13. Should the terms of this license be violated at any time, APS or Aptara may revoke the license with no refund to you and seek relief to the fullest extent of the laws of the USA. Official written notice will be made using the contact information provided with the permission request. Failure to receive such notice will not nullify revocation of the permission.
14. APS reserves all rights not specifically granted herein.
15. This document, including the Aptara Billing and Payment Terms and Conditions, shall be the entire agreement between the parties relating to the subject matter hereof.

American Physical Society
Reuse and Permissions License

04-Mar-2020

This license agreement between the American Physical Society ("APS") and Ajan Ramachandran ("You") consists of your license details and the terms and conditions provided by the American Physical Society and SciPris.

Licensed Content Information

License Number:	**RNP/20/MAR/023407**
License date:	04-Mar-2020
DOI:	10.1103/PhysRevB.95.241306
Title:	Demonstrating the decoupling regime of the electron-phonon interaction in a quantum dot using chirped optical excitation
Author:	Timo Kaldewey et al.
Publication:	Physical Review B
Publisher:	American Physical Society
Cost:	USD $ 0.00

Request Details

Does your reuse require significant modifications: No

Specify intended distribution locations:	Worldwide
Reuse Category:	Reuse in a thesis/dissertation
Requestor Type:	Student
Items for Reuse:	Figures/Tables
Number of Figure/Tables:	1
Figure/Tables Details:	Figure 2
Format for Reuse:	Electronic

Information about New Publication:

University/Publisher:	Dalhousie University
Title of dissertation/thesis:	Quantum State Preparation Using Chirped Laser Pulses in Semiconductor Quantum Dots
Author(s):	Ajan Ramachandran
Expected completion date:	Apr. 2020

License Requestor Information

Name:	Ajan Ramachandran
Affiliation:	Individual
Email Id:	ajanpr@gmail.com
Country:	Canada

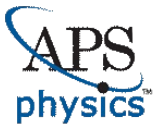

American Physical Society
Reuse and Permissions License

TERMS AND CONDITIONS

The American Physical Society (APS) is pleased to grant the Requestor of this license a non-exclusive, non-transferable permission, limited to Electronic format, provided all criteria outlined below are followed.

1. You must also obtain permission from at least one of the lead authors for each separate work, if you haven't done so already. The author's name and affiliation can be found on the first page of the published Article.
2. For electronic format permissions, Requestor agrees to provide a hyperlink from the reprinted APS material using the source material's DOI on the web page where the work appears. The hyperlink should use the standard DOI resolution URL, http://dx.doi.org/{DOI}. The hyperlink may be embedded in the copyright credit line.
3. For print format permissions, Requestor agrees to print the required copyright credit line on the first page where the material appears: "Reprinted (abstract/excerpt/figure) with permission from [(FULL REFERENCE CITATION) as follows: Author's Names, APS Journal Title, Volume Number, Page Number and Year of Publication.] Copyright (YEAR) by the American Physical Society."
4. Permission granted in this license is for a one-time use and does not include permission for any future editions, updates, databases, formats or other matters. Permission must be sought for any additional use.
5. Use of the material does not and must not imply any endorsement by APS.
6. APS does not imply, purport or intend to grant permission to reuse materials to which it does not hold copyright. It is the requestor's sole responsibility to ensure the licensed material is original to APS and does not contain the copyright of another entity, and that the copyright notice of the figure, photograph, cover or table does not indicate it was reprinted by APS with permission from another source.
7. The permission granted herein is personal to the Requestor for the use specified and is not transferable or assignable without express written permission of APS. This license may not be amended except in writing by APS.
8. You may not alter, edit or modify the material in any manner.
9. You may translate the materials only when translation rights have been granted.
10. APS is not responsible for any errors or omissions due to translation.
11. You may not use the material for promotional, sales, advertising or marketing purposes.
12. The foregoing license shall not take effect unless and until APS or its agent, Aptara, receives payment in full in accordance with Aptara Billing and Payment Terms and Conditions, which are incorporated herein by reference.
13. Should the terms of this license be violated at any time, APS or Aptara may revoke the license with no refund to you and seek relief to the fullest extent of the laws of the USA. Official written notice will be made using the contact information provided with the permission request. Failure to receive such notice will not nullify revocation of the permission.
14. APS reserves all rights not specifically granted herein.
15. This document, including the Aptara Billing and Payment Terms and Conditions, shall be the entire agreement between the parties relating to the subject matter hereof.